UNIVERSITEIT VAN PRETORIA
UNIVERSITY OF PRETORIA
YUNIBESITHI YA PRETORIA
Denkleiers • Leading Minds • Dikgopolo tša Dihlalefi

Investigating the anti-inflammatory properties of epigallocatechin gallate from green tea *Camellia sinensis* (L) O.Kuntze in mammalian innate immunity

by

Nolwando Babalwa Nyide

Submitted in fulfilment for the degree Master of Science in Biochemistry

Department of Biochemistry, Genetics and Microbiology

Faculty of Natural and Agricultural Sciences

University of Pretoria

Contents

LIST OF FIGURES

LIST OF TABLES

PLAGIARISM DECLARATION

Full name

Nolwando Babalwa Nyide

Student number

17311706

Title of dissertation

Investigating the anti-inflammatory properties of epigallocatechin gallate from green tea *Camellia sinensis* (L) O.Kuntze in mammalian innate immunity

Declaration

1. I understand what plagiarism entails and I am aware of the University policy in this regard.
2. I declare that this proposal is my own work. Where someone else work was used (either from a printed source, internet or any other source) due acknowledgement was given and references were given according to departmental requirements.
3. I did not make use of another student's previous work and submit it as my own.
4. I did not allow and will not allow anyone to copy my work with the intention of presenting it his or her own work.

Signature: 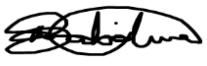

Date: 02 December 2020

ACKNOWLEDGEMENTS

I would like to thank my supervisor, Dr Precious Motshwene, and my co-supervisor, Prof Zeno Apostolides, for the amazing opportunities and the broad exposure afforded to me throughout this journey. My appreciation is also extended to Dr June Serem- a teacher and mentor at heart. Thank you to Prof Nicholas Gay (University of Cambridge, UK), for a wonderful collaboration and the grand opportunity to expand my horizons. I would also like to acknowledge and thank Prof Clare Bryant, Mrs Heather Brooks and Dr Lee Hopkins (University of Cambridge, UK) for their great contributions towards the TLR4 signalling studies, as part of our collaboration. What a privilege it has been working with you and thank you all for your gracious contributions to this work.

I would also like to thank my colleagues, friends, and staff at the Biochemistry division (University of Pretoria) and the Biosciences unit (CSIR) for their assistance and support. I would like to extend a special thank you to Mr Christopher Nyarukowa, Dr Robert Koech and Ms Faith Otukpa from the CAM research group (University of Pretoria). My immense gratitude goes to the NRF for financial support towards this degree and this study.

I would like to thank my parents, siblings and family for inspiring confidence in me and supporting me in this endeavour. A special thank you is extended to those who have made great sacrifices to make these opportunities available and accessible to me. I would also like to thank the *amaNdabase* and *amaNcobela* clans at large who have consistently been a source of strength and encouragement throughout this journey. Lastly, I would like to thank myself for persevering through the challenges.

To God be the glory.

SUMMARY

Humans are hypersensitive to lipopolysaccharide, a gram-negative bacterial endotoxin that stimulates an inflammatory response by binding to the extracellular domain of TLR4 of innate immune cells. Through the MyD88-dependent pathway, NO (a signalling molecule) mediates the inflammatory response to clear pathogenic infection and promote wound healing. This pathway involves the activation of transcription factors, AP-1 and NF-κB, which promote the production of pro-inflammatory cytokines such as TNFα. However, dysregulated inflammation leads to chronic inflammation, causing autoimmune diseases including rheumatoid arthritis and asthma, among others. Considering the shortfalls of currently available treatments such as NSAIDs, there is a growing need for novel treatment strategies. Studies suggest that EGCG, a phenolic compound found abundantly in green tea (*C. sinensis*), possesses anti-inflammatory activity. This study sought to test this hypothesis.

Firstly, 70% methanol was used to extract phenolic compounds and caffeine from three commercial green tea brands (Lipton, Tetley and BST) available on the South African market. Then the EGCG and caffeine contents of these green tea products were measured using UPLC analysis. Additionally, the total phenolic contents (TPCs) were measured for comparison using the Folin-Ciocalteu method. Secondly, the anti-inflammatory properties of EGCG were investigated in an acellular system and in RAW 264.7 cells using the Griess assay to test for NO production. Thereafter, MTT assays were conducted on the macrophages to determine cell viability after exposure to EGCG. Lastly, the role of EGCG on TLR4 signalling during inflammation was tested in the context of the MyD88-dependent pathway. To do this, NF-κB expression was measured using luciferase activity assays in LPS-stimulated HEK 293 cells treated with EGCG. Additionally, ELISAs were performed on stimulated wild-type immortalised bone marrow-derived macrophages (iBMDMs) to monitor the expression of TNFα in response to treatment with EGCG.

This study determined the average total phenolic content of Lipton, Tetley and BST to be 18%, which falls within the range of 15 – 20% reported in previous literature. Lipton contained a significantly ($P < 0.05$) higher %TPC than each of the other brands. Furthermore, it was established that these brands contain between 0.8 – 0.9% caffeine

and approximately 1% EGCG by dry weight. Although the literature indicated that the caffeine content was only slightly lower that the reported range of 1.1 – 2.0%, it was noted that the observed EGCG content was much lower than the expected value of 3%. Furthermore, EGCG exhibited the highest NO-scavenging activity at concentrations of 100 μM in an acellular system, and 200 μM in RAW 264.7 cells. Minimal cytotoxicity towards the cells was observed at a concentration of 200 μM, although previous literature showed that such a high concentration of EGCG was toxic to human astrocytoma U373MG cells. Moreover, TLR4 signalling assays revealed that 10 μM EGCG significantly down-regulated NF-κB expression in LPS-stimulated HEK 293 cells, however, EGCG had no significant effect on the expression levels of TNFα in LPS-stimulated iBMDMs. Hence, it was concluded that further study was required before a sound conclusion can be drawn regarding the role of EGCG in inflammation since the evidence was inconclusive.

LIST OF ABBREVIATIONS

Abbreviation	Meaning
AP-1	Activator protein 1
BBB	Blood brain barrier
C	Catechin
CLR	C-type lectin-like receptors
COX	Cyclo-oxygenase
DAD	Diode array detector
DAMP	Damage-associated molecular patterns
DD	Death domain
DMARD	Disease-modifying antirheumatic drug
DMEM	Dulbecco’s modified eagle medium
DMSO	Dimethyl sulfoxide
DPA	Docosapentaenoic acid
EC	Epicatechin
ECG	Epicatechin gallate
EDTA	Ethylenediaminetetraacetic acid
EGC	Epigallocatechin
EGCG	Epigallocatechin gallate
ELISA	Enzyme-linked immunosorbent assay
eNOS	Endothelial nitric oxide synthase
ESI	Electrospray ionisation
FBS	Foetal bovine serum
FC	Folin-Ciocalteu
GPI	Glycosylphosphatidylinositol
HEK	Human embryonic kidney
hTLR	Human toll-like receptor
iBMDM	Immortalised bone marrow-derived macrophage
IFN	Interferon
IL	Interleukin
IL-1	Interleukin 1

iNOS	Inducible nitric oxide synthase
IRAK	Interleukin-1 receptor associated kinase
IRF3	Interferon regulatory factor 3
ISO	International Standards Organisation
LAL	*Limulus* amoebocyte lysate
LBP	Lipopolysaccharide binding protein
LPS	Lipopolysaccharide
LRR	Leucine-rich repeat
MAPK	Mitogen-activated kinase
MS	Mass spectrometry
MTT	3-[4,5-dimethylthiazole-2-yl]-2,5-diphenyltetrazolium bromide
MyD88	Myeloid differentiation factor 88
NED	N-1-napthylethylenediamine dihydrochloride
NF-κB	Nuclear factor kappa-light-chain-enhancer of activated B cells
NLR	Nucleotide-binding oligomerization domain-like receptors
nNOS	Neuronal nitric oxide synthase
NO	Nitric oxide
NOS	Nitric oxide synthase
NSAID	Non-steroidal anti-inflammatory drug
PAMP	Pathogen-associated molecular patterns
PBS	Phosphate buffered saline
PGE_2	Prostaglandin E_2
PIP_2	Phosphatidylinositol 4,5-biphosphate
PRR	Pathogen recognition receptor
RLR	Retinoic acid-inducible gene-1-like receptors
RNS	Reactive nitrogen species
ROS	Reactive oxygen species
SLE	Systemic lupus erythematosus
SNP	Sodium nitroprusside
TIR	Toll Interleukin-1 receptor
TIRAP	TIR domain-containing adapter protein
TLR	Toll-like receptor

TM	Transmembrane
TNF	Tumour necrosis factor
TPC	Total phenolic content
TRAM	TRIF-related adapter molecule
TRIF	TIR domain-containing adapter inducing interferon β
UPLC	Ultra-performance liquid chromatography

CHAPTER 1: INTRODUCTION

1.1. LITERATURE REVIEW

1.1.1. Innate immunity

Living organisms are constantly challenged with threats from a myriad of pathogens such as bacteria, viruses, fungi, protozoa and worms, which seek to invade their cells with potentially deadly consequences. This invasion often causes illness due to infection of host cells by these virulent pathogens. To counter this, these organisms are equipped with an immune system comprised of a complement of cells, tissues and organs that function co-operatively to protect against pathogenic infection (Warrington et al., 2011).

The human immune system is sub-divided into two categories; the innate immune system, which is also referred to as the body's first line of defence, and the adaptive immune system (Warrington et al., 2011). Some of the distinguishing features between these two sub-categories of immunity are the response times and the longevity of each system's response. The innate immune system is rapidly triggered through the recognition of conserved microbial features using germline-encoded receptors from a small subset of cells (Akira et al., 2006). The adaptive immune system is only activated at a later stage, executing its functions through a growing repertoire of cells adept to facilitating pathogen-specific counterattacks to manage infection. This adaptability is achieved through genetic recombination events, which allow the host's adaptive immune system to co-evolve with pathogens (Flajnik and Kasahara, 2010). In this study, the innate immune system was the primary focus.

Innate immunity is facilitated by many biological barriers, including the blood-brain barrier (BBB), skin, epithelial linings, mucous layers, pulsating cilia, and tight junctions between adjacent cells (Turvey and Broide, 2010, Wesselingh et al., 2019). These structures use various strategies to hinder pathogens physically from invading host cells. They are also complemented by innate immune cells such as macrophages and neutrophils, and enzymatic glandular secretions such as lysozyme in tears and saliva (Turvey and Broide, 2010).

1.1.1.1. The biomolecular interface between host and pathogen

The biomolecular interface where “host meets pathogen” is modulated by pathogen recognition receptors (PRRs) which recognise pathogen-associated molecular patterns (PAMPs) (Akira et al., 2006). PAMPs are conserved pathogen-derived molecules such as microbial nucleic acids, peptides, metabolites, cell wall or membrane constituents, virulence factors and toxins. They serve as markers of pathogenic infection in host cells that stimulate the host immune system to neutralise or eliminate the threat. PAMPs are recognised by various PRRs such as toll-like receptors (TLRs), C-type lectin-like receptors (CLRs), nucleotide-binding oligomerization domain-like receptors (NLRs), retinoic acid-inducible gene-1-like receptors (RLRs), and other cytosolic DNA sensing receptors (Hoving et al., 2014, Kumar et al., 2011, Swidergall, 2019). PRRs also recognise host molecules such as damage-associated molecular patterns (DAMPs) that serve as indicators of cellular damage to trigger an immune response and initiate wound healing (Tang et al., 2012).

1.1.1.2. Toll-like receptors (TLRs)

Toll receptor was discovered in 1985 in the fruit fly, *Drosophila melanogaster*, where its involvement in the establishment of the dorsoventral patterning in developing embryos was shown (Anderson et al., 1985). However, in 1996 the role of Toll in innate immunity was established through *Toll*-knockout studies in adult *Drosophila* flies challenged with fungal infection (Lemaitre et al., 1996). Interestingly, this study showed that components of the dorsoventral pathway, including Toll, control the expression of the gene encoding an antifungal peptide called drosomycin (*Drs*) in fruit flies (Lemaitre et al., 1996).

Wild-type *Drosophila* flies and *Toll*-deficient variants were infected with the fungus, *A. fumigatus*, which is a weak insect pathogen. Astonishingly, only one third mortality was observed for the wild-type flies, while 100% mortality was observed for *Toll*-deficient flies after 2 – 3 days. The high mortality rate of *Toll*-deficient variants was attributed to uncontrolled fungal development due to impaired expression of *Drs* (Lemaitre et al., 1996). Thereafter, the functional characterisation of Toll in *Drosophila* flies pioneered further research into innate immunity receptors. This research led to

the identification of several mammalian homologues of Toll, which were subsequently named TLRs (Takeda and Akira, 2004).

TLRs are a class of PRRs consisting of thirteen family members, denoted TLR1 to TLR13. These proteins are Type 1 transmembrane receptors that are distributed abundantly on the membranes or endosomes of leukocytes and epithelial cell tissues (Kawasaki and Kawai, 2014, Tang et al., 2012). Of the thirteen known TLR family members, only ten (i.e. TLR1 to TLR10) are found in humans (Kawasaki and Kawai, 2014). Of this ten, TLRs 1, 2, 4, 5 and 6 traffic to the plasma membrane after translation, where they recognise PAMPs and DAMPs as ligands (Gay et al., 2014) and trigger signal transduction cascades that lead to the production of pro-inflammatory molecules, as further discussed later.

In contrast, TLRs 3, 7, 8 and 9 are typically found in endosomal compartments (Kawai and Akira, 2010). Their primary role is to sense microbial nucleic acids and initiate the production of Type 1 interferons (IFNs), which play an integral mediatory role in innate immunity (Botos et al., 2011). Although TLR10 was found to be non-functional in mice due to a disruptive retroviral insertion in the gene, its role as a negative regulator of innate immunity pathways in humans was only recently elucidated (Jiang et al., 2016, Oosting et al., 2014).

The recognition of immunostimulants such as PAMPs and DAMPs by TLRs initiates signal transduction cascades that trigger innate immune responses such as inflammation (Tang et al., 2012). The ligands that activate the different TLRs are depicted in **Table 1.1**. Here, it is important to note that activation of TLRs, which is discussed in further detail later, involves the association of two TLR monomers.

Table 1.1: Toll-like receptors and their ligands.
(Fuchs et al., 2018, Gay and Gangloff, 2007, Kumar et al., 2011, Netea et al., 2006)

TLR(s)	Ligand(s)
TLR1/2	Triacyl lipopeptides (Mycobacteria), OspA (*B. burgdorferi*), Porin PorB (*N. meningitidis*)
TLR2	Peptidoglycan, Lipoprotein, Diacyl lipopeptides, Zymosan, Chitin, Hemagglutinin, Lipoteichoic acids
TLR2/6	Diacyl lipopeptides
TLR2/10	Bacterial constituents of *Listeria*
TLR3	Viral dsRNA
TLR4	Lipopolysaccharide (gram-negative bacteria), Flavolipin (*F. meningosepticum)*, Fusion protein (Respiratory syncytial virus), Taxol (plants), O-linked mannosyl chains (*C. albicans*)
TLR5	Bacterial flagellin
TLR7	Imidazoquinolines (synthetic anti-viral compounds)
TLR8	R-848 (a synthetic compound), Guanosine- or uridine-rich HIV ssRNA
TLR9	Unmethylated CpG DNA (bacteria, viruses, yeast, insects)
TLR11	Bacterial flagellin
TLR12	Profilin (*T. gondii*)
TLR13	23S RNA

1.1.1.3. TLR domains and structure

Each TLR is made up of three domains, namely the ectodomain which contains leucine-rich repeats (LRR) found on the N-terminus, a transmembrane (TM) domain which contains a single alpha-helix, and an intracellular Toll Interleukin-1 receptor (TIR) domain (Kawai and Akira, 2010, Medzhitov, 2001). The structures of these domains can be seen in **Figure 1.1**. The LRR domain is a versatile ligand-binding domain comprising tandem repeats of leucine-rich motifs. These motifs are made up of approximately 22-29 hydrophobic residues interspersed by leucine residues at regular intervals (Pålsson-Mcdermott and O'neill, 2007). Together these tandem repeats coalesce to form an alpha-beta tertiary structure that resembles a solenoid horse-shoe shape. In this solenoid horse-shoe form, the mostly helical elements on the convex side of the horse-shoe structure are connected to the beta strands on the concave side by beta turns or short loop sequences (Matsushima et al., 2010). The

higher packing density of the beta-strands on the concave face, in comparison to the non-beta elements of the LRR domain, is the main cause of the convergence of the LRR domain into the characteristic horseshoe shape (Bella et al., 2008, Botos et al., 2011, Kajava, 1998).

The TLR TM domain is the shortest of the three domains, comprising approximately 20 predominantly hydrophobic uncharged residues (Botos et al., 2011). The TIR domain, which derives its name from the homology it shares with the signalling domains of the Interleukin 1 (IL-1) receptor family, is found in the cytoplasmic space (O'neill and Bowie, 2007). This is also illustrated in **Figure 1.1**. The TIR domain is a common feature of adapter proteins involved in TLR and IL-1 cell signalling pathways, where they can associate in a homotypic fashion with TIR domains of other proteins. Through this association, signals from the ligand-bound LRR domain of the TLR are conveyed to designated effectors in the cell to initiate appropriate immunological processes (Botos et al., 2011).

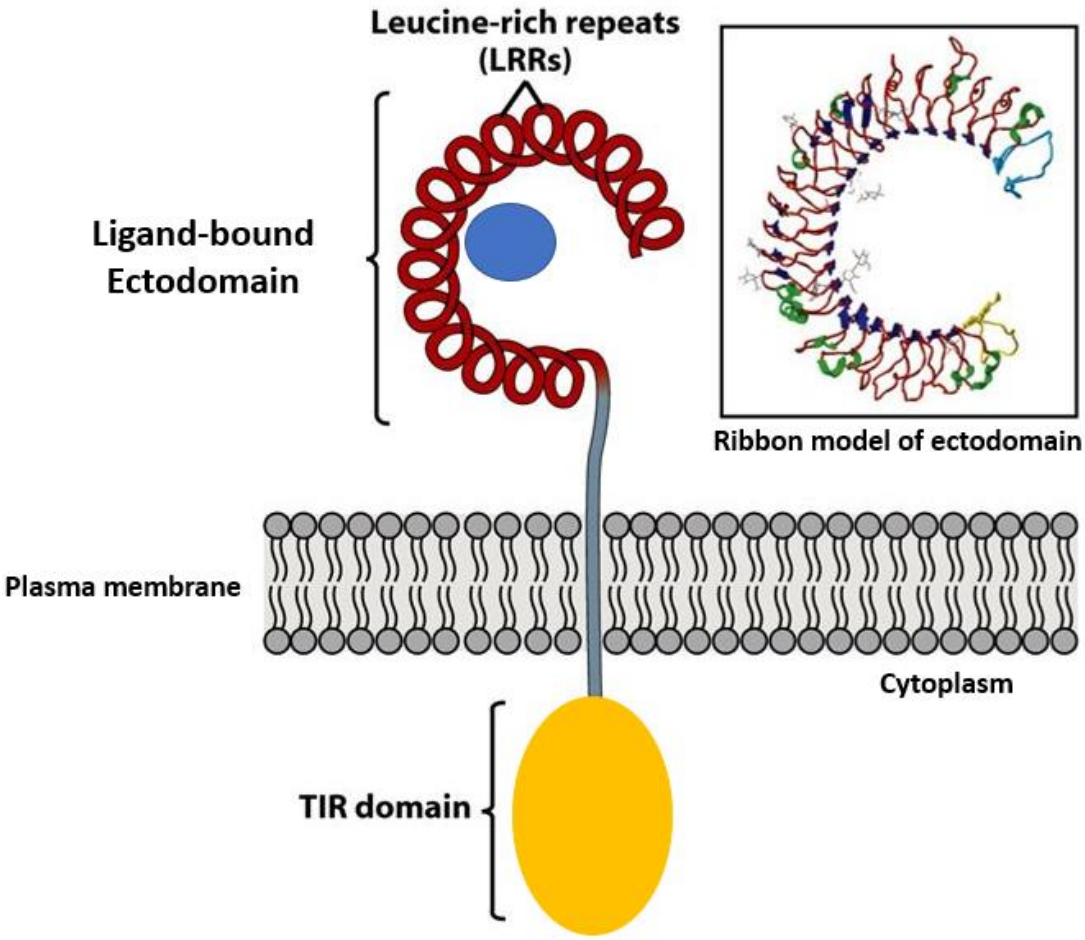

Figure 1.1: Structure of a TLR monomer.
TLRs are made up of three domains, namely the ectodomain, the transmembrane (TM) domain and the TIR domain. In this figure, the TLR is bound to a ligand (represented as a blue circle). The ectodomain is composed of tandem repeats of a leucine-rich motif. The concave surface of this domain, which is typically used as a ligand-binding site, is made up of densely packed parallel beta sheets (seen in the ribbon model). This higher packing density results in the solenoid horse-shoe shape that is characteristic of all TLRs. The TM domain (shown in grey) is a short helical structure mostly comprising hydrophobic residues that anchor it to the plasma membrane. Lastly, the TIR domain, which is represented in yellow, is found on the cytoplasmic side of the membrane. This is a highly conserved domain that is also found in adaptor molecules. It plays an integral role in signal transduction after ligand-induced activation of TLRs. Adapted (Kindt et al., 2007)

1.1.1.4. Activation of TLRs

As previously mentioned in **Table 1.1**, TLR signalling is tightly regulated by specific ligand-binding events. The ligand-binding site of LRR family proteins such as TLRs are located in the concave region of the horse-shoe shaped ectodomain (Kim et al., 2007a, Pancer and Cooper, 2006), as shown in **Figure 1.1**. However, **Figure 1.2** demonstrates that not all TLRs subscribe to this norm (Jin et al., 2007).

Binding of the substrate at the active site induces ligand dimerization of two TLR monomers, leading to TLR signalling. An example of ligand-induced dimerization is illustrated in **Figure 1.2**, where the binding of the ligand, Pam_3CSK_4, activates the TLR1/2 heterodimer, thereby leading to cell signalling events (Jin et al., 2007). Importantly, in their active states, TLRs can function as either homo- or heterodimers. It has been proposed that the monomeric state of TLRs is inactive, and that dimerization is used as a TLR activation mechanism (Ohto and Shimizu, 2016, Reuven et al., 2014). However, this does not hold entirely true for TLR9, which exists as a pre-formed homodimer. In this case, ligand-binding induces a rearrangement of the subunits instead, which then activates cell signalling (Latz et al., 2007).

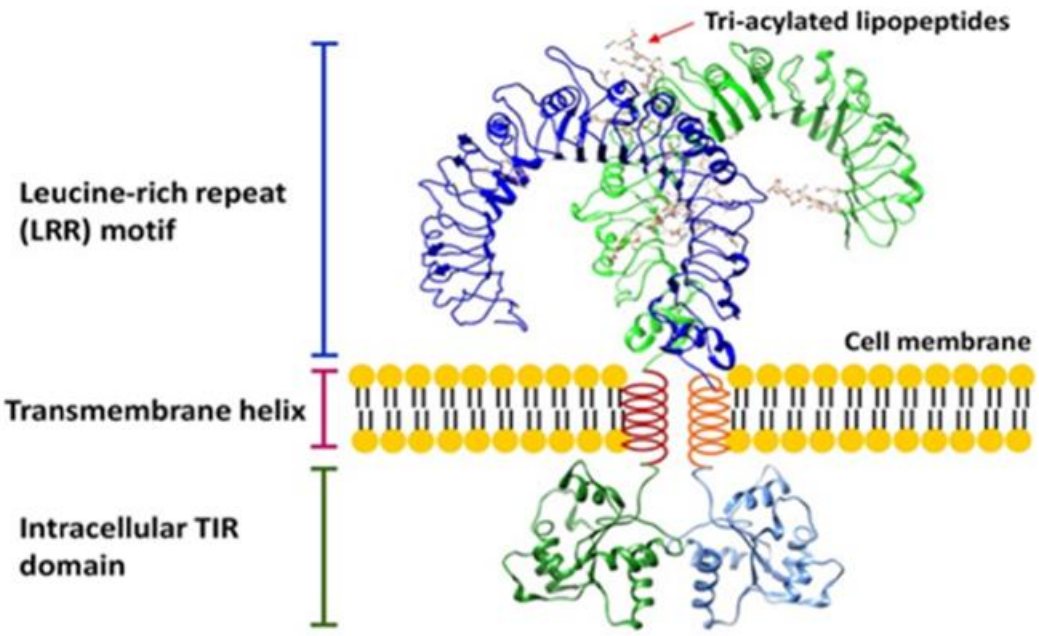

Figure 1.2: Dimerization of TLR1/2 induced by the Pam_3CSK_4 lipopeptide ligand.
The formation of the TLR1/2 heterodimer is induced by the binding of the ligand, a tri-acylated lipopeptide called Pam_3CSK_4. The ectodomain structure of human TLR2 (hTLR2) is shown in blue, whereas the ectodomain structure of human TLR1 (hTLR1) is shown in green. Between them, the ligand is show in red. The parallel beta strands on the concave surfaces of the TLR monomers hold the characteristic solenoid horses-shoe shape of the ectodomains. Notably, not all TLRs have their ligand-binding sites on the concave face of the ectodomain. In the case of the TLR1/2 dimer, the two ester-bound lipid chains of Pam_3CSK_4 are inserted into a pocket on the convex surface of the TLR2 ectodomain. The unbound amide-bound lipid chain and the peptide group remain exposed to the outside of the pocket, where they TLR1 and other residues at the dimer interface. (El-Zayat et al., 2019, Jin et al., 2007)

Upon formation of the dimeric TLR complex, a homotypic interaction is established between the TIR domains of the two TLR monomers involved (Gay et al., 2014, Kawai and Akira, 2010, Kawasaki and Kawai, 2014). This association of the TIR domains typically generates a signal that recruits TIR domain-containing adaptor proteins in the cytoplasm. These adaptor proteins associate in a similar homotypic manner with the TIR domain of TLR, thereby initiating cell signalling events in the cytoplasmic space. In the scope of this study, TLR4 cell signalling was the primary focus.

1.1.1.5. TLR4 cell signalling

TLR4 is a cell-surface mediator of cell signalling, which triggers the production of pro-inflammatory molecules that play a critical role in initiating potent immune responses (Lu et al., 2008). TLR4 is the known receptor for lipopolysaccharide (LPS), also known as endotoxin, which is a structural constituent of the outer membrane of gram-negative bacteria (Kajiwara et al., 2014). Structurally, LPS comprises of three components, namely an O side chain moiety, a core oligosaccharide, and a lipid A component that was identified as the main immunogen (Beutler and Rietschel, 2003, Raetz and Whitfield, 2002). LPS is known to induce septic shock that is caused by overwhelming signalling events in humans, who are hypersensitive to it (Lu et al., 2008). **Figure 1.3** shows the binding of LPS to TLR4, which is facilitated by a protein known as MD-2 that is non-covalently complexed to TLR4. As demonstrated by **Figure 1.3**, the binding of LPS induces dimerization of TLR4.

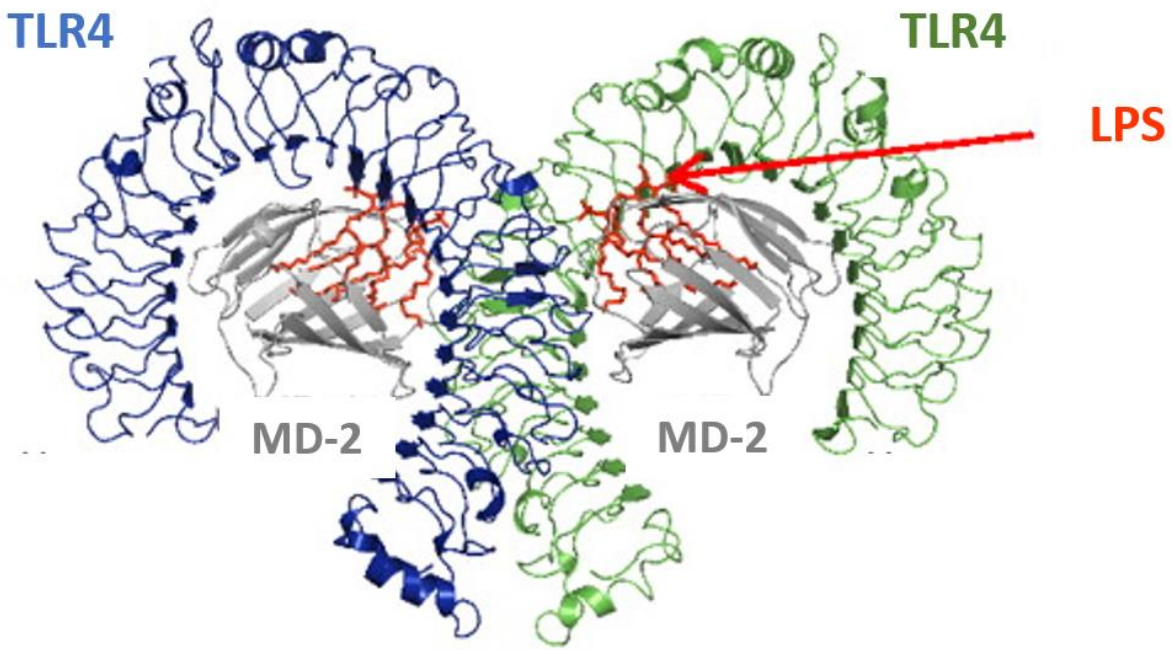

Figure 1.3: TLR4/MD-2/LPS complex.

Activation of TLR4 is initiated by the binding of LPS, which is the known ligand for TLR4. This process is facilitated by MD-2, a protein that is covalently bound to the ectodomain of TLR4 where the LRRs are found. In the case of TLR4, the binding site is located on the concave surface of the LRR domain. In this image, LPS is shown in orange, whereas MD-2 is shown in grey. The two TLR monomers which form this dimer are distinguished in blue and green. Adapted (Ohto et al., 2012)

TLR4 signalling begins in the extracellular environment when LPS binds to a soluble shuttle protein molecule known as LPS-binding protein (LBP), as shown in **Figure 1.4**. In the case of TLR4, ligand-binding occurs on the concave surface of the ectodomain (Lu et al., 2008). LBP then shuttles LPS to a soluble glycosylphosphatidylinositol (GPI)-linked protein called CD14. This facilitates the binding of the LPS/LBP/CD14 complex to MD-2, which is located on the concave surface of TLR4 (Tobias et al., 1986). Lastly, the formation of the LPS/LBP/CD14/MD-2/TLR4 complex leads to dimerization of TLR4. This subsequently initiates a signal transduction cascade in the cytoplasmic space (Lu et al., 2008).

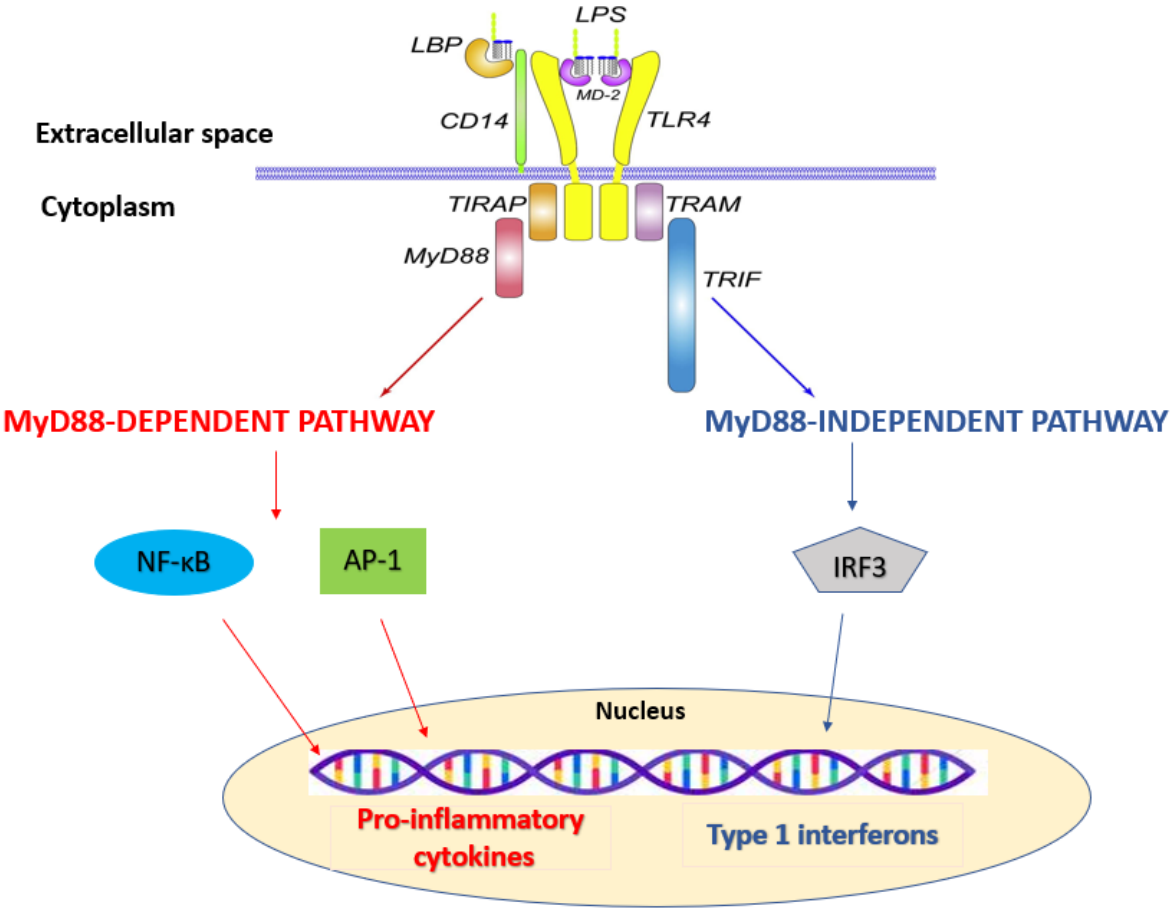

Figure 1.4: LPS-stimulated TLR4 signalling pathways.
The formation of the LPS/LBP/CD14/MD-2/TLR4 complex on the cell surface induces dimerization with another TLR4 monomer. This dimerization is mediated by a homotypic association of the TIR domains of the TLR4 monomers. These events propagate a signal that can be propelled via two cell signalling pathways, namely the MyD88-dependent or the MyD88-independent pathways. In the MyD88-dependent pathway the signalling cascade is mediated by two adapter proteins, TIRAP and MyD88, which associate via a homotypic association of their TIR domains. This signalling cascade leads to translocation of the transcription factors, AP-1 and NF-κB, from the cytosol to the nucleus where they activate the transcription of genes that encode for pro-inflammatory cytokines and proteins. By contrast, signalling in the MyD88-independent pathway is mediated by adaptor proteins, TRAM and TRIF. This pathway leads to the translocation of IFR3, which promotes the transcription of Type 1 interferons. Adapted (Lu et al., 2008).

As illustrated in **Figure 1.4**, following the formation of the LPS-induced TLR4 complex on the cell surface, a signalling cascade is initiated in the cytoplasm. To achieve this, TLR4 signalling involves four adapter proteins, namely the TIR domain-containing adapter protein (TIRAP), the TIR domain-containing adapter inducing interferon β

(TRIF), the TRIF-related adapter molecule (TRAM), and the myeloid differentiation factor 88 (MyD88) (Lu et al., 2008). MyD88 consists of an N-terminal death domain (DD) and a C-terminal TIR domain (Bonnert et al., 1997, Ohnishi et al., 2009), whereas TRIF consists of an N-terminal protease-resistant domain and a TIR domain flanked by a disordered region on the C terminus (Mahita and Sowdhamini, 2017).

By contrast, TIRAP and TRAM can be described as bridging adaptor proteins, as they specifically facilitate the recruitment of MyD88 and TRIF, respectively, towards the plasma membrane, where they can be activated (Sampaio et al., 2018). TIRAP contains an N-terminal phosphatidylinositol 4,5-biphosphate (PIP_2) binding site, whereas TRAM contains an N-terminal myristoylation site. These sites localise TIRAP and TRAM to the plasma membrane (Kagan and Medzhitov, 2006, Rowe et al., 2006).

Figure 1.4 shows that the signal can be propelled from the plasma membrane and through the cytoplasm along two pathways, namely the MyD88-dependent pathway and the MyD88-independent pathway (Lu et al., 2008). In the early stages of both pathways, the TIR domains of dimerised TLR4 receptors form a homotypic association in the cytoplasmic space. Similarly, the adaptor proteins, TIRAP and TRAM, form homotypic interactions with TLR4 through their TIR domains (Lu et al., 2008, Medzhitov et al., 1998).

Signal transduction via the MyD88-independent pathway, which is shown in blue, is mediated by homotypic binding of the TIR domains of TRAM to TLR4 in the cytoplasmic space. Similarly, TRAM then recruits and binds TRIF through TIR-TIR interactions. The signalling cascade that ensues continues through the cytoplasmic space, where it causes Interferon regulatory factor 3 (IRF3) to translocate to the nucleus. As a result, genes encoding Type 1 IFNs are activated for transcription (Lu et al., 2008).

In the MyD88-dependent pathway, TIRAP, also known as Mal, binds to the TIR domain of TLR4 through a homotypic association. TIRAP then recruits MyD88 to form a homotypic association with TIRAP through the TIR domain, leaving the DD of MyD88 exposed. In a similar manner, the unbound DD of MyD88 then recruits and binds an IL-1 receptor associated kinase (IRAK), which also contains a DD (Lu et al., 2008, Medzhitov et al., 1998).

Thereafter, the signal is progressively propelled through the cytoplasm via the MyD88-dependent pathway. This signalling cascades leads two transcription factors, activator protein 1 (AP-1) and nuclear factor kappa-light-chain-enhancer of activated B cells (NF-κB), to translocate from the cytoplasm to the nucleus, as illustrated in red in **Figure 1.4**. Here, these transcription factors promote transcription of genes that encode pro-inflammatory cytokines (Lu et al., 2008). The present study focused on the MyD88-dependent pathway.

1.1.1.6. The role of inflammation in innate immunity

Inflammation is an innate host immune response to pathogenic infection, toxic compounds, injury or irradiation (Medzhitov, 2010). Inflammation is typically characterised by swelling, a sensation of heat, redness and pain, which are usually caused by blood vessels undergoing changes at the site of the infection or injury. These localised physiological events isolate the infection, stifle replication of the pathogen and prevent rapid dissemination to other host tissues. Fever may also develop to suppress the metabolic function of the pathogen until a more targeted assault can be mounted by the host immune system against the pathogen (Chen et al., 2017, Medzhitov, 2010).

The permeability of blood vessels to fluids improves during inflammation, as the blood vessels dilate to accommodate increased blood circulation to the affected area. The rapid influx of blood causes redness and produces the sensation of heat. This also leads to accumulation of cells and signalling molecules at the site of infection, thereby causing swelling. Consequently, cell adhesion proteins are expressed from the endothelial cells lining local blood vessels to anchor the immune cells in the blood at the site of infection, where they are required to execute their functions (Ricciotti and Fitzgerald Garret, 2011). The accompanying sensation of pain is attributed to the effects of prostaglandin E_2 (PGE_2) on peripheral sensory neurons and central sites in the brain and spinal cord (Funk, 2001).

During inflammation, immune cells localised to the afflicted site release a myriad of pro-inflammatory mediators. These including vasoactive amines (e.g. histamines and serotonin), eicosanoids (e.g. prostaglandins, thromboxane and leukotrienes), reactive

oxygen/nitrogen species (ROS/RNS) and cytokines such as tumour necrosis factors (TNFs) and interleukins (ILs) (Abdulkhaleq et al., 2018, Graves, 2012). ROS and RNS have been identified as key role players in the activation mechanisms of redox-regulated transcription factors and kinases. As major modulators of the redox state of the cytoplasmic space, excessive production of these reactive species in activated phagocytes can induce oxidative or nitrosative stress. This can lead to apoptosis and tissue damage (Kolb and Kolb-Bachofen, 1998).

The two transcription factors, AP-1 and NF-κB, are redox-sensitive molecules whose activity is regulated by changes in the cellular redox environment. Upon activation, these transcription factors translocate from the cytosol into the nucleus, where they up-regulate transcription of genes encoding proteins such as cyclo-oxygenase (COX) 2 and inducible nitric oxide synthase (iNOS). The former is responsible for catalysing the formation of prostaglandins, whereas the latter plays a crucial role in the production of nitric oxide (NO) in response extracellular stimuli such as LPS (Kamata and Hirata, 1999, Mann et al., 2005).

1.1.1.7. Nitric oxide: an important signalling molecule in inflammation

NO is an important signalling molecule that exists constitutively at relatively low concentrations throughout the body. With a half-life of six seconds, NO is rapidly oxidised to more stable nitrate compounds, hence the effects of NO are often limited to cells and tissues at the site of production (Ignarro, 1989, Ignarro et al., 1993, Kelm et al., 1991). Although it plays an anti-inflammatory role under normal physiological conditions, NO can assume the role of a pro-inflammatory mediator when the host is threatened with pathogenic infection, as NO production is up-regulated (Sharma et al., 2007). Other than iNOS, there are two known isoforms of NO synthase (NOS), namely nNOS (neuronal NOS) and eNOS (endothelial NOS). NO produced by nNOS exhibits neurotoxic effects, whereas eNOS-derived NO serves an important role in protection against neurotoxicity (Kolb-Bachofen et al., 2006, Sharma et al., 2007). Nonetheless, evidence suggests that NO may be involved in the pathogenesis of some neurodegenerative diseases and that its presence may accelerate brain damage associated with ischaemia. Additionally, eNOS-derived NO primarily serves as a vasodilator during inflammation and other physiological processes (Nagai et al., 2002).

1.1.1.8. When inflammation goes wrong

Although inflammation is an intrinsically beneficial process that promotes wound-healing, chronic inflammation leads to progressive tissue damage. Chronic inflammation is linked to several diseases, including asthma, cancer, cardiovascular disease, atherosclerosis, stroke and some neurodegenerative diseases (Duan et al., 2019, Rottem and Shoenfeld, 2003). Studies have linked many autoimmune diseases such as rheumatoid arthritis, gout, diabetes, inflammatory bowel disease (IBD) and systemic lupus erythematosus (SLE) to chronic inflammation (Duan et al., 2019, Rottem and Shoenfeld, 2003). Furthermore, enhanced iNOS expression was identified in celiac disease patients, and those suffering from Crohn's disease and ulcerative colitis (Guslandi, 1998, Van Straaten et al., 1999). With much of the pathophysiology of NOS being attributed to iNOS-derived NO, which is produced in most organs, studies into the pharmacological suppression of iNOS could uncover new avenues for drug discovery against inflammatory disorders.

1.1.1.9. Currently available treatments for inflammatory diseases

Components of the TLR4 signalling pathway, which include TLR4, IRAK proteins and adaptor proteins among others, are good potential drug targets in the development of new therapeutic strategies for treating inflammatory diseases since the role of TLR4 signalling in inflammation is well-understood (Montero Vega and De Andrés Martín, 2008). Meanwhile, non-steroidal anti-inflammatory drugs (NSAIDs) are among the most common drugs used to treat inflammatory diseases. Other treatment strategies include corticosteroids to inhibit inflammation and relieve pain, disease-modifying antirheumatic drugs (DMARDs) to manage and reduce tissue and organ damage, and anti-TNF biologics (Li et al., 2017, Wong, 2019). However, despite the presence of these drugs, several challenges still exist between patients and safe long-term relief from chronic inflammatory diseases.

The anti-inflammatory effects of NSAIDs are attributed to their propensity to bind and inhibit the functions of COX enzymes, namely COX-1 and COX-2 (Wong, 2019). These enzymes are responsible for the synthesis of biomolecular mediators of pain signals known as prostaglandins, that play a critical role in orchestrating pro-

inflammatory responses (Li et al., 2017, Wong, 2019). However, the inhibitory activity of NSAIDs causes adverse side effects, since *COX-1* is normally expressed constitutively to perform crucial functions in other physiological processes (Antman et al., 2007, Li et al., 2017). Likewise, the expression of *COX-2* is also important for the normal functioning of inflammation. Moreover, the inhibition of COX-1 by some NSAIDs has been shown to have side effects such as gastrointestinal toxicity (Li et al., 2017). Other side effects include ulcers, haemorrhaging, acute myocardial faction, congestive heart failure, renal toxicity and renal failure (Li et al., 2017, Wong, 2019). Sudden death may also occur (Li et al., 2017).

Other currently available treatments for chronic inflammation are also tainted with adverse side effects. These include long-term bone damage, gastrointestinal ulcers and immunosuppression in the case of glucocorticoids, reversible and irreversible renal disease, and toxicity in the case of many DMARDs. Moreover, while some patients are unresponsive to anti-TNF biologics, some of these treatments are prohibitively expensive. This continuously stifles progress towards the sustainable treatment of inflammatory disease (Li et al., 2017); hence, there is a growing need for the discovery of new anti-inflammatory drug candidates. In this study, the potential anti-inflammatory activity of a tea compound known as epigallocatechin gallate (EGCG) was investigated.

1.1.2. The search for new anti-inflammatory drug candidates

The search for new anti-inflammatory drug candidates has taken us back in time to the realms of indigenous knowledge systems, where herbs and plants formed the basis of indigenous medicine. Among the indigenous herbaceous preparations used for medicinal purposes, tea has been a popular method of administering the curative power of herbs to patients for various ailments (Chacko et al., 2010). The leaves of *Camellia sinensis* (the tea bush) are popular medicinal herbs from which tonics and teas such as green tea, black tea and oolong tea have been derived. Among these teas, green tea reportedly confers the best health benefits (Chacko et al., 2010).

1.1.2.1. Green tea (*Camellia sinensis*)

The history of green tea can be traced back to India, from where it was subsequently exported to Japan in the 1600s and spread throughout Asia and into China (Chacko et al., 2010). Although green tea, oolong tea and black tea emanate from *C. sinensis*, the key distinguishing factor between these teas lie in the fermentation of *C. sinensis* leaves during the manufacturing process (Chacko et al., 2010). A crucial step that involves steaming freshly harvested leaves to prevent fermentation inactivates crucial enzymes that are responsible for degrading the colour pigments in the leaves. This preserves the characteristic green colour of green tea throughout further processing steps (rolling and drying) during green tea preparation. Oolong tea is the product of fermented tea leaves, and prolonged fermentation of these tea leaves produces black tea (Chacko et al., 2010).

The chemical composition of tea is highly dependent on factors such as the nutrient availability during plant growth, climate, horticultural practices and preparation methods (Sinija and Mishra, 2008). A good example of this is demonstrated in **Table 1.2**, which compares the composition of green tea to that of black tea. Most notably, this table illustrates the vast difference in the phenolic contents of green tea and black tea, which is mainly attributed to oxidation during fermentation of tea leaves to produce black tea (Chacko et al., 2010).

Phenolic compounds are chemical compounds which are characterised by the presence of an aromatic ring attached to at least one hydroxyl group (Ferrazzano et al., 2011). Three main classes of phenolic compounds are recognised, namely tannins, flavonoids and polyphenolic acids. They are commonly found in flowers, vegetative organs and fruits such as apples. Phenolic compounds have been identified as secondary metabolites that are associated with plant chemical defences and plant-plant interactions (Ferrazzano et al., 2011, Williamson, 2017).

Table 1.2: A comparison of the chemical composition of green tea and black tea.
The major constituents of green tea and black tea, and their percentage compositions in tea leaves. Adapted (Chacko et al., 2010)

Compound	**% Composition (dry weight of tea leaves)**	
	Green tea *****	Black tea *****
Phenolic compounds	30	5
Fibre	26	26
Protein	15	15
Lipids	7	7
*Other carbohydrates (e.g. cellulose, pectin, fructose, glucose, sucrose)	7	7
Minerals (e.g. calcium, magnesium, zinc, selenium, chromium etc.)	5	5
Amino acids	4	4
Pigments	2	2
Oxidized phenolic compounds	0	25
Total	96	96

***** Percentages represent % dry weight of *C. sinensis* leaves.

Table 1.2 shows that phenolic compounds in green tea constitute up to 30% of the dry weight of young tea leaves. Catechins, which are a class of flavonoids, are the most abundant phenolic compounds found in green tea (Chacko et al., 2010). Green tea comprises five major catechins, namely catechin (C), epicatechin (EC), epicatechin gallate (ECG), epigallocatechin (EGC) and epigallocatechin gallate (EGCG). It has been shown that green tea has a higher catechin content compared to oolong tea and black tea (Khokhar and Magnusdottir, 2002). Alkaloids such as caffeine, theobromine and theophylline are also found in green tea (Chacko et al., 2010, Sano et al., 2001). It is reported that, on average, black tea contains 3.23% caffeine, which is slightly higher than in green tea, which contains 2.69% caffeine (Astill et al., 2001). Several factors such as the original leaf size, preparation and processing methods impact the quality and quantity of all the constituents of the final tea product. Consequently, significant differences in catechin concentrations have been observed between

complete leaf extracts, from which the absolute concentrations can be determined, and fresh tea extracts (Chacko et al., 2010).

Commercial tea products are mainly derived from the processing of shoots, young leaves and mature leaves of *C. sinensis* (Fung et al., 1999, Zhang et al., 2019). Reports indicate that common green tea products consist of 15 - 20% phenolic compounds by dry weight, making green tea a rich source of flavonoids such as catechins (Lin et al., 2008, Quan et al., 2007). Out of 360 foods tested, green tea was found to be one of the few foods that could supply consumers with more than 250 mg of flavonoids per cup of tea (i.e. 250 mL infusion from 2 – 3 g of green tea) (Lin et al., 2008). Moreover, the study showed that the average tea consumer's daily total flavonoid intake is 40 – 60% higher than that of non-consumers (Lin et al., 2008). In the present study, we endeavoured to compare the total phenolic content of three green tea brands available on the South African market to get an indication of which green tea brand could be most beneficial for consumers.

Throughout history *C. sinensis* leaves have been used for the relief of asthma, peripheral vascular disease, angina pectoris, coronary artery diseases and other ailments (Graziose et al., 2010). With developments in research, more sophisticated applications of tea products in neurological, cardiovascular and chemotherapeutic disorders have emerged (Graziose et al., 2010). The phenolic compounds found in tea possess potent anti-oxidative properties, which make them scavengers of free radicals. Due to their high affinity for metal ions, these anti-oxidants can prevent metal ion-induced formation of ROS (Yang et al., 2014). More interestingly, a study into the cytotoxicity of NO found green tea powder to be a better scavenger of NO than black tea powder (Paquay et al., 2000).

Since EGCG is more abundant in green tea, it is plausible that this polyphenol may be responsible for the enhanced NO-scavenging activity of green tea compared to black tea. As such, EGCG may elicit anti-inflammatory activity by disrupting pro-inflammatory processes mediated by NO. Importantly, there is a growing body of research that has linked EGCG to the suppression of TLR4 signalling activity (Bao et al., 2015, Hong Byun et al., 2010, Wang et al., 2019). However, the *in vivo* mechanism of action of EGCG has yet to be fully understood.

1.1.2.2. EGCG as a potential drug candidate

The chemical structure of EGCG consists of galloyl moieties, which are believed to be critically involved in lipolytic effects and angiogenesis (Chu et al., 2017). EGCG is a hydrophilic molecule, owing to numerous hydroxyl groups that are abundantly distributed around its chemical backbone. This can become a barrier in the drug discovery stage as it decreases lipid solubility, which is an important aspect of cellular absorption and bioavailability in drug discovery. However, a study (Zhong et al., 2012) has shown that esterification of EGCG with docosapentaenoic acid (DPA) can overcome this problem. The chemical structures of several tea compounds, namely C, EC, ECG, EGC, EGCG, caffeine and gallic acid, are shown in **Figure 1.5**.

In the present study, we sought to extract and analyse phenolic compounds from commercial green tea sources using ultra-performance liquid chromatography (UPLC) and UPLC with mass spectrometry (UPLC-MS). We were interested in comparing the EGCG and caffeine contents of commercial green tea in the South African market. Additionally, we were also interested in measuring and comparing the total phenolic contents (TPCs) of commercial green tea using the Folin-Ciocalteu method. The pure compounds shown in **Figure 1.5** were used as tea standards throughout experimentation. The structures of mycophenolic acid, tryptamine and sulphanilamide are also included, as these compounds were used as internal standards for quality control purpose during this study.

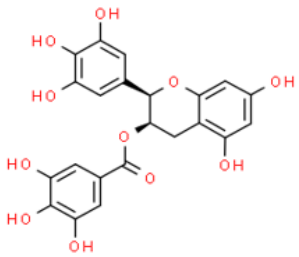

(A) Epigallocatechin gallate (EGCG)
458.37 g/mol

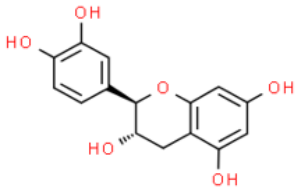

(B) Catechin
290.27 g/mol

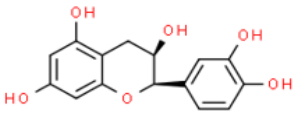

(C) Epicatechin (EC)
290.27 g/mol

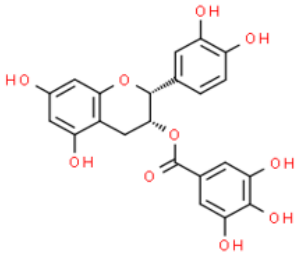

(D) Epicatechin gallate (ECG)
442.37 g/mol

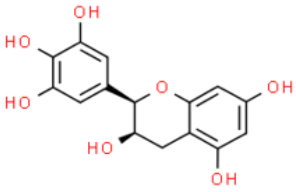

(E) Epigallocatechin (EGC)
306.27 g/mol

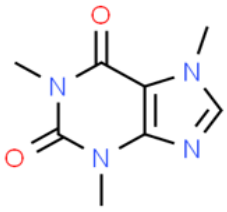

(F) Caffeine
194.19 g/mol

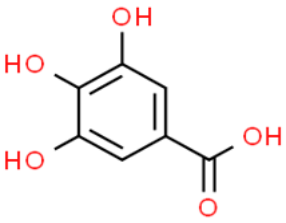

(G) Gallic acid
170.12 g/mol

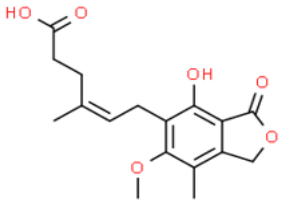

(H) Mycophenolic acid
320.13 g/mol

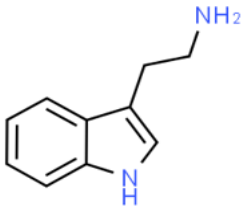

(I) Tryptamine
160.10 g/mol

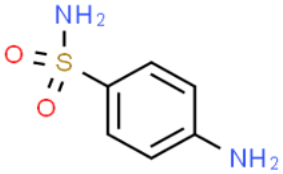

(J) Sulphanilamide
172.21 g/mol

Figure 1.5: Chemical structures of standards used for green tea analysis.
The chemical structures and monoisotopic masses of the major phenolic compounds found in green tea are shown in the following order; **(A)** EGCG, **(B)** catechin, **(C)** EC, **(D)** ECG, **(E)** EGC, **(F)** caffeine and **(G)** Gallic acid, which forms the galloyl moieties found in the catechins. Similarly, three internal standards that were used in this study, namely mycophenolic acid **(H)**, tryptamine **(I)** and sulphanilamide **(J)**, are also shown.

Rapid developments in the medical and pharmaceutical industries in the past century revolutionised the production processes of many drugs and pharmaceutical products. As a consequence of this, natural plant extracts were replaced by synthetic analogues of bioactive compounds from these extracts (Raskin et al., 2002). However, despite the great strides taken towards modernising the pharmaceutical industry, the application of synthetic biologics and compounds is still marred by controversy. The thalidomide disaster in the 1960s is a sobering example of the unparalleled complexity of natural products against the shortfalls of synthetic analogues, and the dangers of undermining this complexity (Lenz et al., 1962, Mcbride, 1961, Vargesson, 2015).

Although the present study included the extraction of EGCG from commercial green tea sources, pure EGCG was used in the mammalian cell experiments. This study is intended towards investigating the anti-inflammatory role of EGCG in TLR4 signalling and NO production using mammalian cell lines. This could be beneficial for drug discovery and design efforts geared towards exploring EGCG as a treatment strategy for inflammatory diseases in the future.

1.2. AIMS

1. To compare the EGCG content of three commercial green tea brands at the 95% level of confidence.
2. To determine the anti-inflammatory role of EGCG with respect to NO production and TLR4 signalling at the 95% level of confidence.

1.3. OBJECTIVES

1. Extract and quantify EGCG in three commercial green tea brands using methanol extraction, ultra-performance liquid chromatography (UPLC) and mass spectrometry (MS).
2. Determine NO production in cellular and acellular systems in response to treatment with EGCG using the Griess assay.
3. Determine the effects of EGCG on TLR4 signalling in LPS-stimulated HEK 293 cells and macrophages using a luciferase assay and ELISA, respectively.

1.4. HYPOTHESES

- $H1_0$: There is no statistically significant difference between the EGCG content of green tea brands at the 95% level of confidence.
- $H2_0$: EGCG does not significantly affect NO production in LPS-stimulated innate immune cells at the 95% level of confidence.
- $H3_0$: EGCG does not significantly affect TLR4 cell signalling at the 95% level of confidence.

CHAPTER 2: MATERIALS AND METHODS

2.1. INTRODUCTION

The details of the experimental work conducted in this study are documented in this chapter. Herein, descriptive lists of reagents, buffers and media used throughout the various experimental stages are provided to supplement the experimental procedures detailed in the Methods section. The Methods section is further divided into two sections to demonstrate the approaches used to achieve each of the aims if this study. Additionally, supplementary information such as plasmid DNA maps used in this study is provided.

2.2. REAGENTS AND BUFFERS

Table 2.1: Composition of chemical reagents and buffers used in this study

BUFFER/SOLUTION	BUFFER COMPOSITION
0.1 M PBS buffer pH 7.4	0.081 M Na_2HPO_4, 0.019 M $NaH_2PO_4 \cdot H_2O$, 0.15 M adjusted to pH 7.4 at room temperature.
SNP reagent	5 mM sodium nitroprusside in phosphate buffered saline (PBS buffer)
Griess reagent	2.5% (v/v) phosphoric acid, 1% (w/v) sulphanilamide, 0.1% (w/v) N-1-napthylethylenediamine dihydrochloride (NED)

Table 2.2: Composition of mammalian growth media buffers used in this study.

MEDIA	MEDIA COMPOSITION
RAW cell culture media	Dulbecco's modified eagle medium (DMEM), 10% foetal bovine serum (FBS), 1% (w/v) antibiotics (penicillin and streptomycin)
HEK cell complete media	DMEM, 10% FBS, 2 mM L-glutamine, 100 U/mL penicillin, 100 µg/mL streptomycin
HEK cell stimulation media	DMEM, 0.1% FBS, 2 mM L-glutamine, 100 U/mL penicillin, 100 µg/ml streptomycin
TE buffer pH 8.0	10 mM Tris, 1 mM ethylenediaminetetraacetic acid (EDTA)

2.3. METHODS

2.3.1. Chemical extraction and analysis of EGCG from green tea

2.3.1.1. Extraction of phenolic compounds and caffeine

The International Standards Organisation (ISO) method ISO 14502-2 (Iso, 2005) was used to extract phenolic compounds from tea samples. In summary, three commercial green tea brands (i.e. BST, Tetley and Lipton) were purchased (three batch numbers per brand). Green tea was liberated from tea bags and ground to a fine powder in a coffee grinder. The powdered green tea was then sifted through a 500 µm sieve. Thereafter, phenolic compounds were extracted from the powdered green tea samples by adding 5 mL of 70% methanol (Merck, South Africa) at 70ºC to 200±1 mg of powdered green tea in a glass test tube. The samples were vortex-mixed for approximately 5 s prior to being sealed loosely with a stopper and incubated at 70ºC for 5 min. The samples were then vortex-mixed and incubated at 70ºC for 5 min again as before. Thereafter, the samples were cooled at room temperature for 10 min, then centrifuged at 2000*g* for 10 min in a Heraeus Labofuge 300 centrifuge (Thermo Scientific, USA). The supernatant from each sample was decanted and collected into a separate 15 mL falcon tube, while the extraction procedure was repeated using the pelleted green tea samples. The resulting supernatant of each sample was then pooled with the respective supernatant collected in the first extraction step. Finally, each pooled supernatant sample was topped up to a final volume of 10 mL with 70% methanol at room temperature. Samples were stored at 4ºC until further use.

2.3.1.2. Ultra-performance liquid chromatography (UPLC)

In preparation for UPLC analysis, all green tea extracts and calibration curve standards were diluted (1:4) with stabilising solution containing 3 internal standards (mycophenolic acid, sulphanilamide and tryptamine) each at a final concentration of 0.05 mg/mL (Sigma Aldrich, South Africa). Each sample was then filtered separately through a 0.2 µm Minisart® RC4 syringe filter (Sartorius, South Africa) consisting of a solvent-resistant, hydrophilic regenerated cellulose membrane.

An ACQUITY UPLC H-class system (Waters, USA) fitted with a diode array detector (DAD), an autosampler, and a binary solvent delivery system controlled by Empower-3 software was used for UPLC analysis. Separation was achieved using an HSS T3 column (1.8 µm x 2.1 x 150 mm) (Waters, USA). UPLC analysis was performed using Solvent A (7% acetonitrile, 3% acetic acid in water) and Solvent B (80% acetonitrile, 3% acetic acid in water) with a gradient elution; 0 min (5% A), 0 – 21 min (5 - 20% A), 21 – 30 min (20 - 25% A), 30 – 32 min (25 - 100% A), 32 – 39 min (100 - 100% A), 39 – 40 min (100 – 5% A), 40 – 45 min (5 - 5% A). The column temperature was maintained at 40ºC and UV/Vis spectra were captured from 254 – 400 nm every 20 s. An injection volume of 5 µL and a flow rate of 0.3 mL/min were maintained throughout analysis.

2.3.1.3. UPLC mass spectrometry (UPLC-MS)

Six tea standards (C, EC, ECG, EGC, EGCG and caffeine) were prepared individually in 70% methanol, each at a stock concentration of 20 mg/mL. These standards were also combined in equal ratios to form cocktails of varying final concentrations (0.1 - 10 mg/mL). Green tea extracts from the three commercial brands were also diluted (1 in 100) with 70% methanol. The 70% methanol was also used as a blank. Each sample was filtered through a 0.2 µm Minisart® RC4 syringe filter consisting of a solvent-resistant, hydrophilic regenerated cellulose membrane.

A Waters UPLC system hyphenated to a Waters Synapt G2 QTOF (Waters, USA) instrument equipped with an autosampler and a binary solvent delivery system controlled by MassLynx v4.1 software was used for UPLC-MS analysis. Samples were analysed in the ES- and ES+ ionisation modes and separation was achieved using an HSS T3 column (same as above) and an injection volume of 5 µL. Analysis was performed using Solvent A (0.1% formic acid in water) and Solvent B (0.1% formic acid in acetonitrile) with a gradient elution; 0 min (0% B), 0 – 22 min (0 - 28% B), 22 – 24 min (28 - 100% B), 24 – 30 min (100 - 0% B).

2.3.1.4. Moisture content determination

Moisture content was determined using the standardised ISO 1573 method (Iso, 1980). The accurate masses of nine crucibles were determined by incubating the closed crucibles at 103ºC overnight. Each crucible was then cooled to room temperature and accurately weighed. Thereafter, each crucible was filled with 200 ±1 mg of the commercial green tea samples from three different brands (each with 3 biological repeats) and incubated again at 103ºC overnight to dehydrate the green tea samples. The filled crucibles were cooled as previously and accurately weighed.

2.3.1.5. Total phenolic content determination

The ISO 14502-1 (Iso, 2005) protocol was used to determine the total phenolic content of three green tea brands in this study. The Folin-Ciocalteu (FC) assay was used to determine the total phenolic content in green tea extracts. Green tea extracts were diluted (1 in 100) with dddH_2O. Thereafter, 1000 µL of 10% (v/v) FC phenol reagent was added to 200 µL of each green tea extract and vortexed briefly to mix (prepared in duplicate). The samples were kept at room temperature for 10 min before 800 µL of 7,5% (w/v) sodium carbonate was added, and the samples were vortexed briefly again. Gallic acid standard samples of varying concentrations (0 - 60 ppm) were prepared similarly. All samples were kept at room temperature for 60 min, after which the absorbance of each sample was determined spectrophotometrically at a wavelength of 765 nm. The following formula was used to calculate the average %TPC of each tea, which is expressed as % dry weight:

$$\%TPC = \frac{(OD_{sample} - OD_{intercept}) \times V \times d \times 100}{Slope_{std} \times M_{sample} \times 10\,000 \times DM}$$

Where:

- OD_{sample} is the optical density of the sample
- $OD_{intercept}$ is the y-intercept of the linear trendline
- V is the total extraction volume
- d is the dilution factor
- $Slope_{std}$ is the gradient of the linear trendline
- M_{sample} is the mass of tea from which extraction was performed
- DM is the % dry mass of tea (calculated from moisture content determination)

2.3.2. Determining the anti-inflammatory properties of EGCG

2.3.2.1. Acellular Griess assay

An adaptation of an established protocol (Jagetia and Baliga, 2004) was used to determine the NO-scavenging potential of EGCG. Initially, NO was produced from 5 mM sodium nitroprusside (SNP) prepared in phosphate-buffered saline (PBS) buffer and incubated at room temperature for 1 h under natural light. Ten EGCG concentrations of 0.01 mM, 0.025 mM, 0.05 mM, 0.1 mM, 0.25 mM, 0.5 mM, 1 mM, 2 mM, 4 mM and 8 mM were prepared by dissolving EGCG (Sigma-Aldrich, South Africa) in ddH_2O and mixing briefly by vortex. The SNP reagent was then mixed in a 1:1 ratio with the ten EGCG samples of varying concentrations (in triplicate) on a 96-well plate and incubated at room temperature in the dark for 1 h. An untreated control was prepared by mixing the SNP reagent in a 1:1 ratio with ddH_2O. A standard curve was prepared using a $NaNO_2$ concentration range of 0 mM, 0.005 mM, 0.01 mM, 0.02, 0.03 mM, 0.04 mM and 0.05 mM (in triplicate). Thereafter, the ten EGCG/SNP samples and the $NaNO_2$ standards were each mixed in a 1:1 ratio with the Griess reagent. The absorbance readings were determined at a wavelength of 570 nm using a FLUOstar Omega plate reader (BMG Labtech, Germany).

2.3.2.2. Cellular Griess assay

NO production in RAW 264.7 macrophages was determined using the Griess assay. Sterile 96-well plates were seeded with 1.25 x 10^6 cells/well in RAW cell culture media. Some cells were only treated with different final concentrations of EGCG of 1 μM, 2.5 μM, 5 μM, 10 μM, 25 μM, 50 μM, 100 μM, 200 μM, 400 μM and 800 μM, while others were stimulated with 100 ng/mL LPS and treated similarly with EGCG. Additionally, three controls were set up; RAW cell culture media, untreated unstimulated cells in RAW cell culture media, and LPS-stimulated cells in RAW cell culture media. Samples were then incubated for 24 h at 37ºC with 5% CO_2. All experiments and controls were made up to a final volume of 100 μL and performed in duplicate. Thereafter, 50 μL of each sample was carefully transferred (without dislodging the semi-adherent cells from the well surface) to a new 96-well plate and combined with 50 μL of Griess reagent

and analysed on a FLUOstar Omega plate reader (BMG Labtech, Germany) at 570 nm. A $NaNO_2$ standard curve was plotted as before.

2.3.2.3. Cell viability assay

Following the 24 h incubation of samples which was performed during the cellular Griess assay (in section **2.3.2.2**), 3-[4,5-dimethylthiazole-2-yl]-2,5-diphenyltetrazolium bromide (MTT) (Sigma-Aldrich, South Africa) was added to each of the remaining 50 µL samples to a final concentration of 0.1 mg/mL. The samples were incubated at 37ºC with their lids on for 3 h before the lids were removed to desiccate the samples. Thereafter, the dried sample residues were resuspended in a 100 µL solution of 25% dimethyl sulfoxide (DMSO) in ethanol and analysed spectrophotometrically at 570 nm using a FLUOstar Omega plate reader (BMG Labtech, Germany).

2.3.2.4. Culture and transfection of HEK 293 cells

Cryopreserved HEK 293 cell cultures were thawed. Once thawed, 1 mL of the HEK 293 stock culture was added to 5 mL of pre-warmed HEK cell complete media at 37ºC in a falcon tube and centrifuged for 5 min at 180*g*. The supernatant was decanted, and the pellet was resuspended in 12 mL of pre-warmed HEK cell complete media. The cells were then transferred into a 75 mL tissue culture flask and spread evenly across the surface of the flask. The cells were then incubated at 37ºC in the presence of 5% CO_2 for 72 h to allow the cells to adhere to the surface of the flask and grow. The media was then carefully decanted and replaced with 10 mL of pre-warmed HEK cell complete media at 37ºC. The tissue culture flask was gently swirled to evenly distribute the media, then the cells were incubated further at 37ºC in the presence of 5% CO_2 for 48 h. Again, the media was decanted and replaced as previously, then the cells were incubated at 48 h. The cells were then seeded into sterile 96-well plates at a concentration of 3×10^4 cells/well and incubated at 37ºC with 5% CO_2 for 48 h. Lastly, the cells were then transfected with a DNA mix consisting of expression vectors in the combination depicted in **Table 2.3**. The maps of these plasmid vectors are depicted in **Figure 2.1** and **Figure 2.2**.

Table 2.3: Components used to transfect HEK 293 cells

Component	Volume (µL)
pcDNA3-*hTLR4* (10 ng/mL)	1
pcDNA3-*MD-2* (10 ng/mL)	1
pcDNA3-*CD14* (10 ng/mL)	1
pNF-κB-luc (10 ng/mL)	10
hRG-TK (10 ng/ml)	5
pcDNA3 (100 ng/mL)	8.2
10X TE buffer	2.62
150 mM NaCl	21.18
TOTAL VOLUME	50

For cell transfection, the jetPEI reagent was prepared by making a 1 in 25 dilution of jetPEI (Polyplus-transfection SA, France) in 150 mM NaCl. The jetPEI reagent was then mixed in a 1:1 ratio with the DNA prepared as per **Table 2.3** and incubated at room temperature for 30 min. The DNA/jetPEI mix was further diluted (1 in 10) in HEK cell stimulation media. HEK cell complete media from the cells seeded previously in sterile 96-well plates were carefully decanted and replaced with 100 µL/well of the DNA/jetPEI/media mix. Cells were then incubated at 37ºC with 5% CO_2 for 48 h and then stimulated with 10 ng/mL LPS for 8 h. Unstimulated cells were used as a control.

2.3.2.5. TLR4 signalling assay in transfected HEK 293 cells.

Unstimulated cells and cells stimulated with an LPS concentration of 10 ng/mL for 8 h were exposed to various concentrations of EGCG (i.e. 0.1 µM, 1 µM and 10 µM) in triplicate for 4 h. After aspirating the media, the cells were gently washed with PBS before 50 µL of 1X Passive lysis buffer (Promega, USA) was added to the cells. Cells were then stored at -20ºC overnight. Luminescence was determined using a CLARIOstar microplate reader (BMG Labtech, Germany) which was programmed to 40 µL of luciferase substrate (luciferin) prior to reading.

2.3.2.6. Enzyme-linked immunosorbent assay (ELISA)

The ELISA was performed in duplicate on murine iBMDMs using a Mouse TNF-alpha DuoSet ELISA kit #DY410 (R&D systems, USA) as per the manufacturer's instructions. Briefly, a 96 well microplate was coated with 100 μL of the Capture Antibody solution in each well. The plate was then sealed and stored at room temperature overnight. Then the wells were aspirated, and each well was washed with 400 μL Wash Buffer three times. After the last wash, the plate was blotted gently on clean paper towel to remove excess Wash Buffer. Thereafter, 300 μL Reagent Diluent was added to each well for blocking at room temperature for a minimum of 1 h. The wells were then washed as previously. In preparation for ELISA, 100 μL of cell lysate from LPS-stimulated iBMDMs treated with EGCG (0.1 μM, 1 μM and 10 μM) and from untreated control cells was added into different wells in duplicate. The samples were covered with an adhesive strip and stored at room temperature for 2 h. The wells were aspirated and washed as previously. Thereafter, 100 μL of Detection Antibody solution was added to the samples, which were then covered and stored at room temperature for 2 h. The samples were washed again as previously. A volume of 100 μL of Streptavidin-HRP solution was then added to the samples and the plate was covered and stored at room temperature in the dark for 20 min. The samples were washed as previously. Then a volume of 100 μL of Substrate solution was added to each sample, followed by storage at room temperature for 20 min in the dark. Lastly, 50 μL of Stop solution was added to each reaction, followed by gentle mixing. Then the optical density was determined at 450 nm and 570 nm. To correct for optical imperfections in the plate, the readings at 570 nm were subtracted from the readings at 450 nm.

2.3.2.7. Statistical analyses

The means and Student's t-tests were calculated in Excel 2016. Data analysis was performed on GraphPad Prism 7.03 software to determine the normality of the data using the D'Agostino-Pearson test and the Shapiro-Wilks test. Depending on the normality of data, further analysis was performed to determine any statistically significant differences (at the 95% level of confidence) between EGCG concentrations using a one-way ANOVA. Then post-hoc analysis was performed using Tukey's test

for normally distributed data, or the Kruskal-Wallis test with post-hoc analysis using Dunn’s multiple test for skewed data.

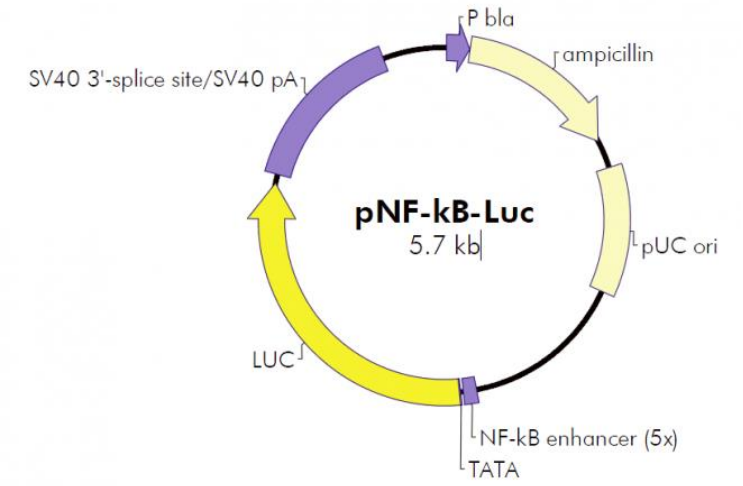

Figure 2.1: Map of the pNF-κB-Luc reporter vector.
NF-κB expression in LPS-stimulated HEK 293 cells was monitored using firefly luciferase activity as reported by the pNF-κB-Luc reporter vector.

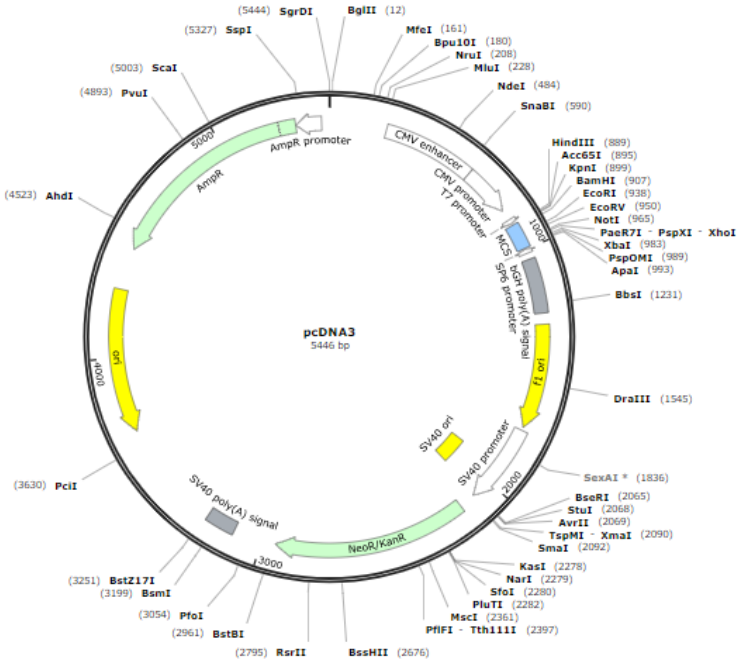

Figure 2.2: Map of the pcDNA3 plasmid vector.
The *hTLR4* template used in this study was cloned into the pcDNA3 plasmid vector at the University of Cambridge, UK. CMV forward and BGH reverse primers were used to sequence the gene. The *Amp*^{R} gene codes for ampicillin resistance.

CHAPTER 3: RESULTS

3.1. BACKGROUND

With a surge in the exploration of complementary and alternative medicine inspired by indigenous medicinal wisdom, an increasing number of plant-derived bioactive compounds are infiltrating the clinical research barrier (Roychoudhury and Bhowmik, 2020). EGCG, a polyphenol found in *C. sinensis* leaves, has been a consistent feature in indigenous medicine (Chacko et al., 2010, Singh et al., 2010). It is the prominent polyphenol found in green tea (Lambert and Elias, 2010). Tea polyphenols such as EGCG are known for their bioactive properties against free radical-induced oxidation and inflammation (Mao et al., 2017) among other things. Hence in this study, which sought to investigate the anti-inflammatory role of EGCG, different commercial green tea extracts were chemically analysed to compare the relative quantities of EGCG and the total phenolic contents of each tea brand. Furthermore, the anti-inflammatory activity of pure EGCG was investigated in a chemical system and in three cell lines, namely RAW 264.7 (murine macrophages), HEK 293 cells and murine immortalised bone marrow-derived macrophages (iBMDMs).

3.2. RESULTS

This section is divided into three sub-sections, with each focusing on a different aspect of this study. The first sub-section is focused on chemical analysis of three commercial green tea brands to compare the total phenolic contents and EGCG quantities between the three brands. The second sub-section is focused on investigating the NO-scavenging potential of EGCG in a chemical system and *in vitro*. Lastly, the third sub-section is focused on investigating the effects of EGCG on TLR4 signalling.

3.2.1. Investigating the phenolic composition of green tea

In this section, we assess the relative phenolic contents of commercial green tea to test our hypothesis that there is no significant difference in the EGCG contents of three commercial green tea brands. The green tea samples used in this study were obtained commercially. Three popular green tea brands, namely BST, Lipton and Tetley, that are available in South Africa were chosen. For each tea brand, three samples from different batches were selected to represent biological repeats for statistical significance. In these studies, the ISO 14502-2 (Iso, 2005) extraction method was used to extract phenolic compounds from the tea samples in preparation for analysis. However, before the phenolic compounds in the teas can be quantified, they must be identified first.

3.2.1.1. Detection and identification of phenolic compounds in green tea using UPLC-MS

UPLC-MS was used to detect and identify the major tea phenolic compounds, namely C, EC, ECG, EGC and EGCG. These phenolic compounds are polar in nature and they are further classified as catechins. Cocktail samples consisting of all these catechin standards were prepared at different concentrations to generate standard curves for the compounds. This was used as a guide when analysing the green tea extracts from BST, Tetley and Lipton. Caffeine, a compound commonly found in tea,

was also added in the cocktail samples as a control standard during this experiment. A blank sample was prepared using 70% methanol since this was the common solvent in all the above-mentioned samples.

Fresh green tea extracts, the blank, and the standard cocktail samples of known concentrations were analysed in two subsequent steps; UPLC then MS. In the first step, separation was achieved through liquid chromatography using the non-polar HSS T3 column (1.8 µm x 2.1 x 150 mm) at ultra-high pressure. After elution, separated compounds from the extracts were then subjected to MS, where they were ionised and projected towards a detector that detects ions in both the negative (ES-) and the positive (ES+) ionisation states. It was then possible to determine the concentration of any of the compounds from the area beneath the peak, with the aid of a standard curve.

UPLC-MS analysis of the blank in the ES- ion mode produced a prominent cluster of peaks with retention times of ~24 – 26 min, as shown in **Figure 3.1 (Neg)**. These peaks emanate from contaminants bound to the column that elute at high solvent strength. Notably, the results from the UPLC-MS analysis of the blank in the ES+ ion mode produced a cluster of peaks with similar retention times to those of the ES- ion mode, as shown in **Figure 3.1 (Pos)**. However, despite this similarity, the retention profiles displayed by the peaks were not identical, as shown by these two chromatograms.

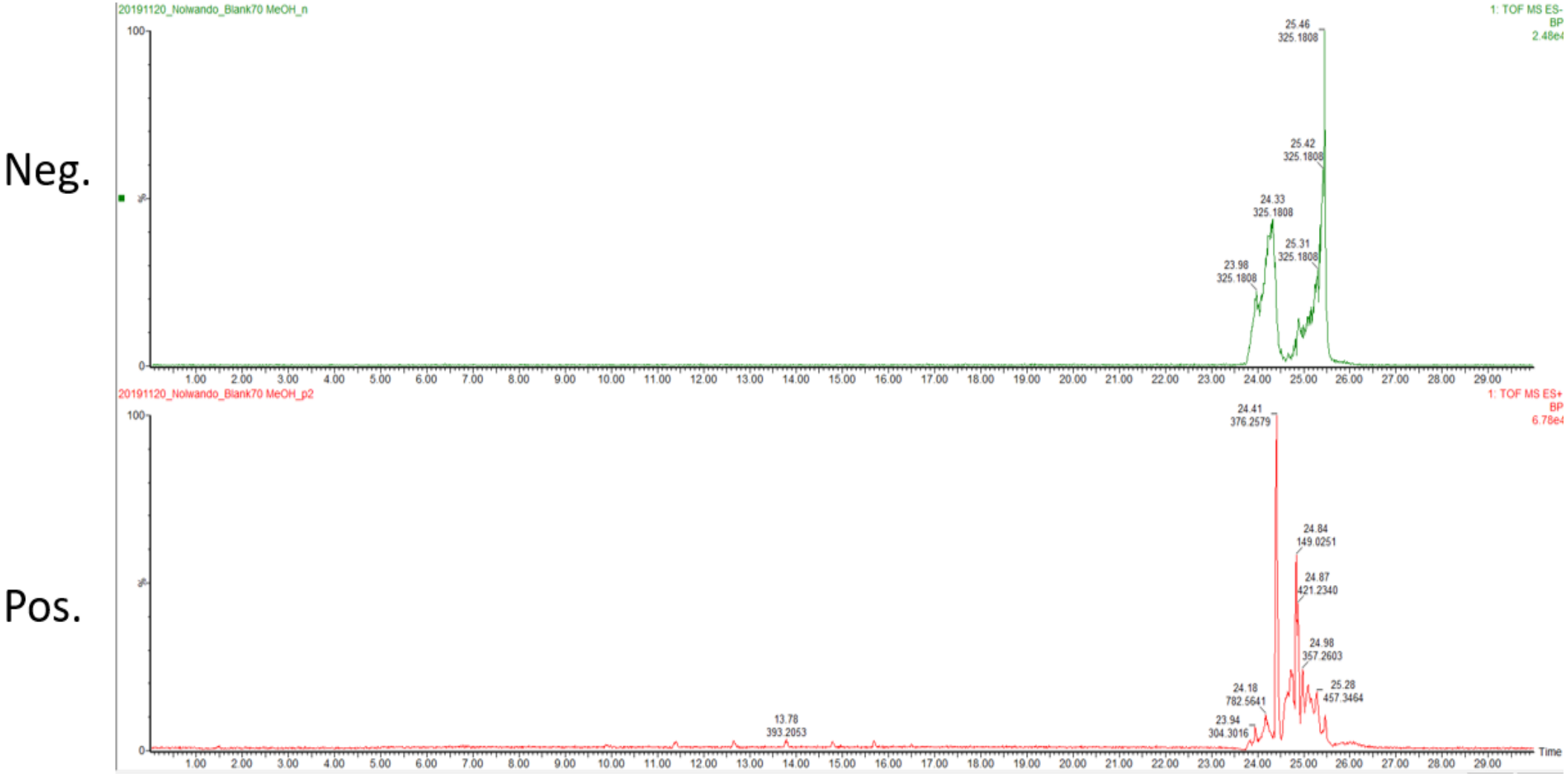

Figure 3.1: UPLC-MS analysis of the blank (70% methanol).
UPLC-MS analysis of methanol in the ES- and ES+ modes, which was used as the common solvent for all standards and tea test samples. The ES- ionisation mode chromatogram is labelled as "**Neg.**" and the ES+ ionisation chromatogram is labelled as "**Pos.**". The % intensity of the signal is shown on the y-axis, while retention time is shown on the x-axis. The chromatograms show a cluster of peaks with a similar retention time range of ~24 – 26 min in both the ES- and ES+ ionisation modes. Despite this, the retention profiles are non-identical between these two ionization modes.

Next, the catechin cocktail samples of varying concentrations from 0.005 – 1 mg/mL were analysed. All five catechins were detected in the ES- ion mode at concentrations of 1 mg/mL and 0.5 mg/mL as shown in **Figure 3.2(A)** and **Figure 3.2(B)** respectively. The eluted catechins are represented by peaks on the chromatograms and they are each recognisable by their molecular weights, which are displayed above each peak. As expected, the retention profiles of the catechins remained consistent throughout the cocktail samples where the catechins were detected. The data shows that they were eluted in the following order; EGC (305 g/mol), C and/or EC (both 289 g/mol), EGCG (457 g/mol), and ECG (441 g/mol). Notably, our catechin of interest, EGCG, was consistently eluted at ~14.9 min with the lowest % intensity among the catechins. Very small peaks were observed on the chromatogram for the cocktail sample with the lowest concentration, 0.005 mg/mL, as seen in **Figure 3.2(C)**. The only peaks that were observed on this chromatogram were those which were consistent with the blank, which consisted of 70% methanol. These peaks were expected to appear in all the samples since the samples were all prepared in the same solvent and analysed on the same column. However, caffeine was not detected in any of the cocktail samples in the ES- ion mode although it was added to all the cocktail samples.

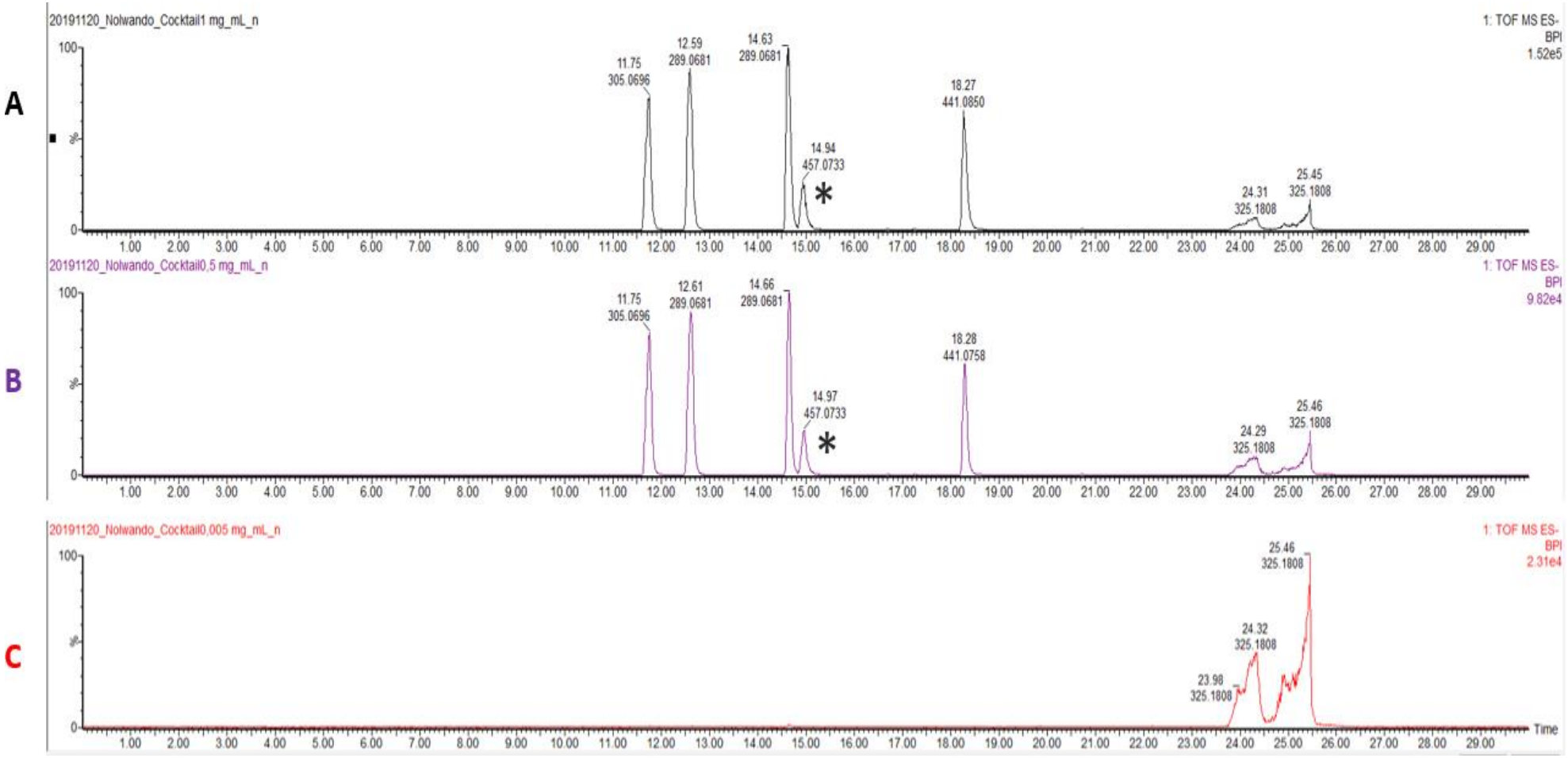

Figure 3.2: UPLC-MS analysis (ES- ionisation mode) of catechins and caffeine cocktail samples of various concentrations.
Three samples consisting of a cocktail of five tea catechin standards (C, EC, ECG, EGC, EGCG) and caffeine at different final concentrations were analysed using UPLC-MS. The chromatograms of the cocktail samples prepared at 1 mg/mL, 0.5 mg/mL and 0.005 mg/mL are represented as **A**, **B** and **C** respectively. The % intensity is shown on the y-axis, while retention time is shown on the x-axis. All samples were prepared with 70% methanol. The peaks representing EGCG are each identified with a black Asterix. In all three chromatograms, a cluster of peaks were observed at a retention time range of ~24 – 26 min owing to the solvent. More importantly, peaks corresponding to the five tea catechin standards, EGC (305 g/mol), C and EC (both 289 g/mol), EGCG (457 g/mol), and ECG (441 g/mol) were detected in the ES- ionisation mode, as expected. Caffeine was not detected in the ES- ion mode.

By contrast, a peak corresponding to caffeine (195 g/mol) was detected in the ES+ ion mode analysis with a retention time of ~12.5 min, as shown in **Figure 3.3(A)** and **Figure 3.3(B)**. As in the ES- ion mode analysis, very small peaks were observed on the chromatogram for the sample with the lowest concentration, 0.005 mg/mL, as seen in **Figure 3.3(C)**. One of the small peaks appears to have a retention time that is consistent with that of caffeine. Notably, none of the catechins were detected in the ES+ ion mode analysis of the cocktail samples at any of the concentrations tested. However, the cluster of peaks attributed to the contaminant in the column was observed consistently in the ES- ion mode analysis too, which was expected.

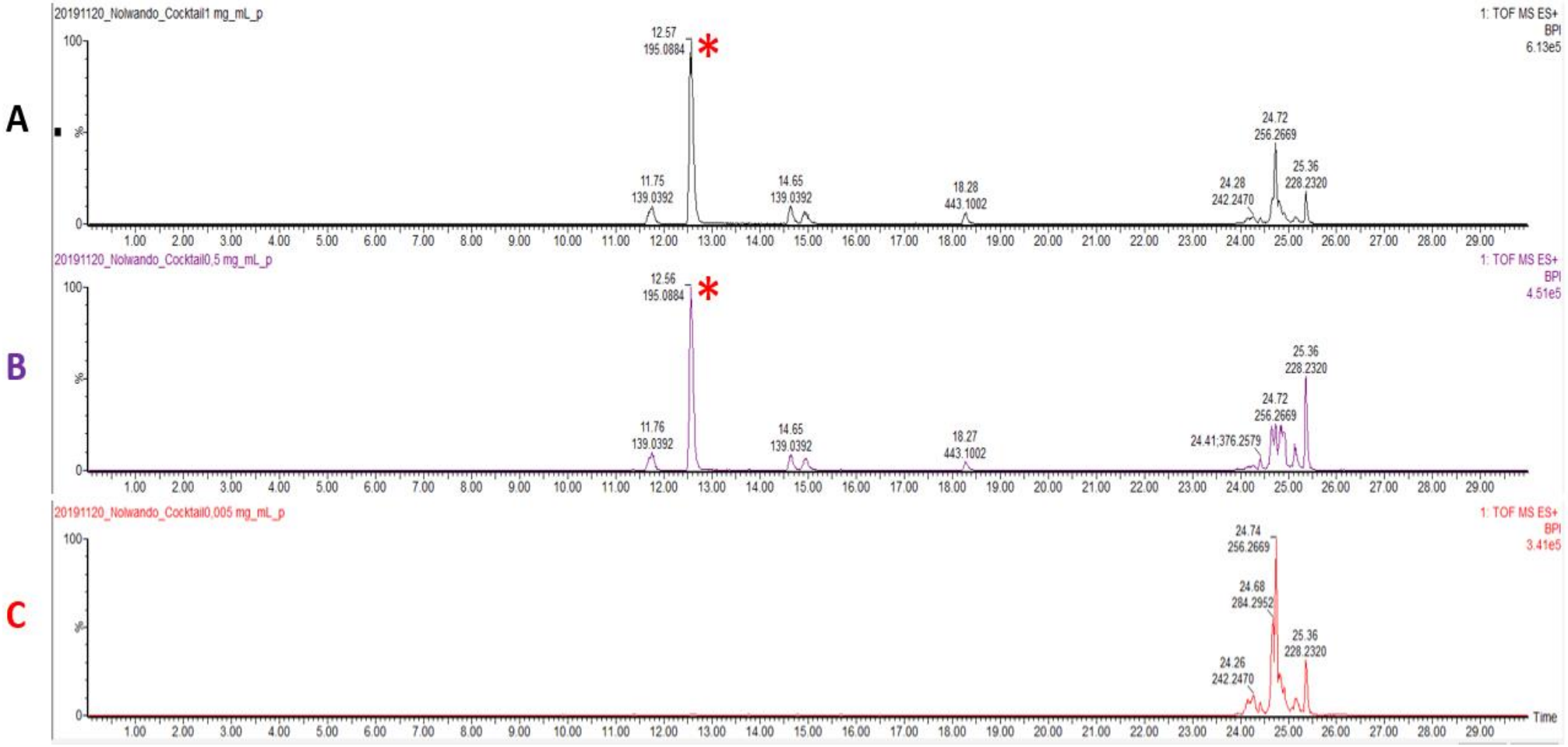

Figure 3.3: UPLC-MS analysis (ES+ ionisation mode) of catechins and caffeine cocktail samples of various concentrations.
Three samples consisting of a cocktail of five tea catechins standards (C, EC, ECG, EGC, EGCG) and caffeine at different final concentrations were analysed using UPLC-MS. The chromatograms of the cocktail samples prepared at concentrations of 1 mg/mL, 0.5 mg/mL and 0.005 mg/mL, are represented as **A**, **B** and **C** respectively. The % intensity is shown on the y-axis, while retention time is shown on the x-axis. All samples were prepared with 70% methanol. In all three chromatograms, a cluster of peaks is observed at a retention time range of ~24 – 26 min owing to the solvent. More importantly, peaks corresponding to caffeine (195 g/mol) were identified in the ES+ ionisation mode in **A** and **B**, as expected, where they are represented with red Asterixis. None of the tea standards were detected in **C** where the concentrations of the compounds may have been too low for detection. Moreover, none of the catechins were detected in the ES+ ion mode at any of the concentrations tested.

The data collected from the UPLC-MS analyses of the blank and the cocktail samples consisting of the tea standards gave us a glimpse into the retention characteristics and ionisation patterns of these compounds. From this data, we were able to build a basic profile of each of the standards that was used as a reference point when analysing the tea extracts from BST, Lipton and Tetley. This information provided a blueprint that allowed us to identify the peaks corresponding to each of the tea compounds in the analyses of the green tea extracts.

When analysing the extracts from Lipton (Lip), Tetley (Tet) and BST, the tea compounds were identified based on their molecular weights and retention times. This was achieved with the aid of the data collected from the tea standards. In the ES- ion mode analysis, shown in **Figure 3.4**, four of the five catechins were positively detected and identified at their expected molecular weights and retention times in all three tea extracts. EGC (305 g/mol), C and/or EC (both 289 g/mol), and ECG (441 g/mol) were identified in Lipton, Tetley and BST. The retention times of these catechins remained consistent with those that were determined during the analysis of the tea standards. Furthermore, the expected cluster of peaks attributed to the solvent were consistently observed in all tea samples. Interestingly, the chromatograms of the three green tea brands show many similarities, suggesting that the three tea brands share similar, but non-identical, chemical composition.

Notably, there was a peak with a retention time of ~14.9 min that was observed where we expected to find EGCG in all the green tea samples in **Figure 3.4**. However, the molecular weight of this peak was found to be 169 g/mol, which is different from the expected molecular weight of EGCG (457 g/mol). Hence, at first glance, these results seemed to suggest that none of the three green tea brands contained EGCG. However, careful study of the literature (Venzie et al., 2007) indicated that the 169 g/mol peak observed at a retention time of ~14.9 min represented one of the primary fragments of EGCG that can form during ionisation.

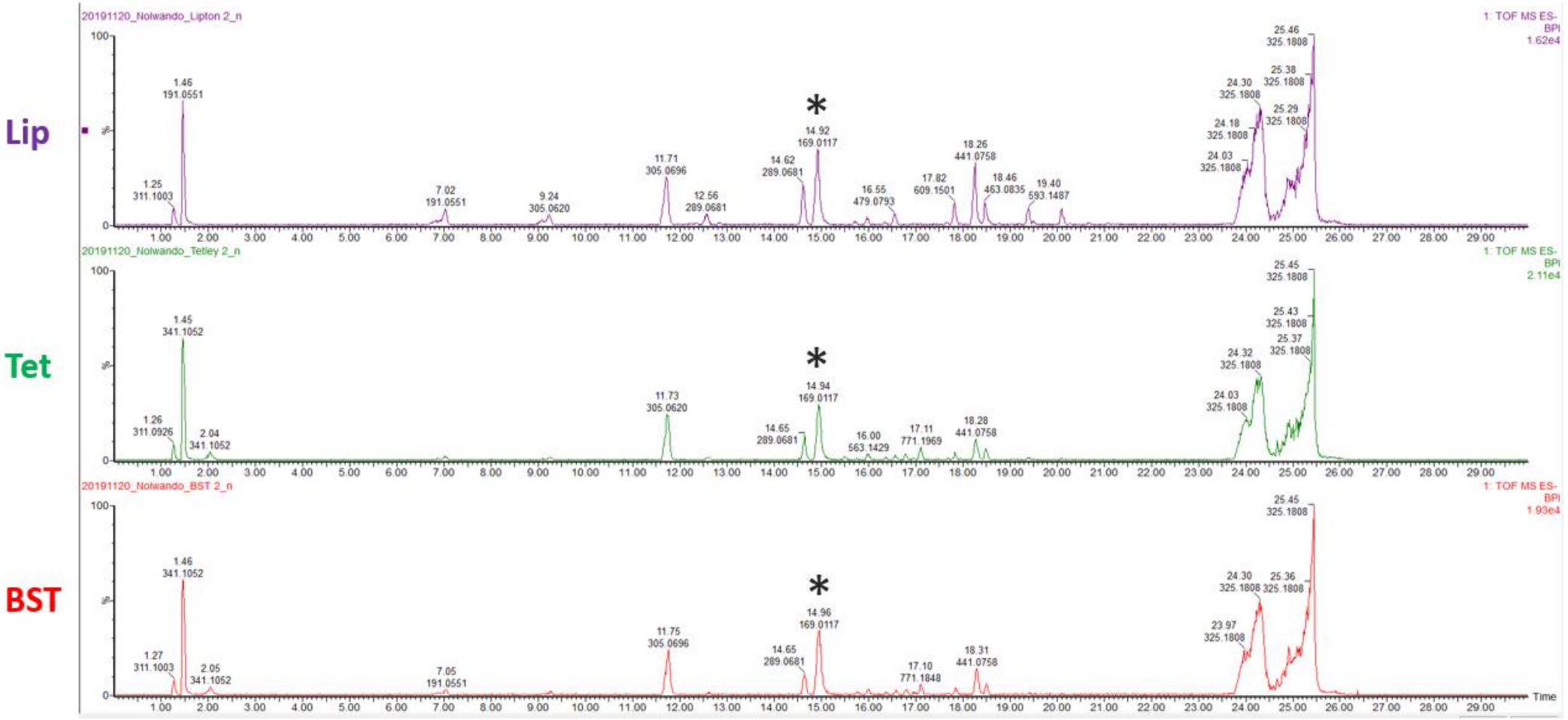

Figure 3.4: UPLC-MS analysis (ES- ionisation mode) of three commercial green tea brands.

Extracts from three commercial green tea brands, Lipton (Lip), Tetley (Tet) and BST were sampled for UPLC-MS analysis. Waters UPLC system hyphenated to Waters Synapt G2 QTOF instrument equipped with an autosampler and a binary solvent delivery system controlled by MassLynx v4.1 software was used. Separation was achieved using a Waters HSS T3 column (1.8 µm x 2.1 x 150 mm) with a gradient elution. In these chromatograms, retention time is displayed on the x-axis and % intensity of the signal is recorded on the y-axis. Peaks corresponding to four of the tea catechins, EGC (305 g/mol), C and EC (both 289 g/mol), and ECG (441 g/mol) were positively identified at the expected retention times in all three tea brands. However, EGCG was not observed at the expected molecular weight of 457 g/mol. Instead, one of its primary fragments (169 g/mol) was detected at the expected retention time of ~14.9 min. These peaks are represented with a black Asterix. A cluster of peaks at a retention time range of ~24 – 26 min was also observed, owing to the solvent.

By contrast, the ES+ ion mode analysis of Lipton, Tetley and BST tea extracts produced the expected result, as caffeine was detected at the correct molecular weight (195 g/mol) and retention time (~12.5 min) in all samples. The peaks representing caffeine in these chromatograms are shown in **Figure 3.5** alongside the cluster of peaks corresponding to the blank. Again, the chromatograms of the three green tea brands show many similarities, suggesting that the three tea brands share similar, but non-identical, chemical composition.

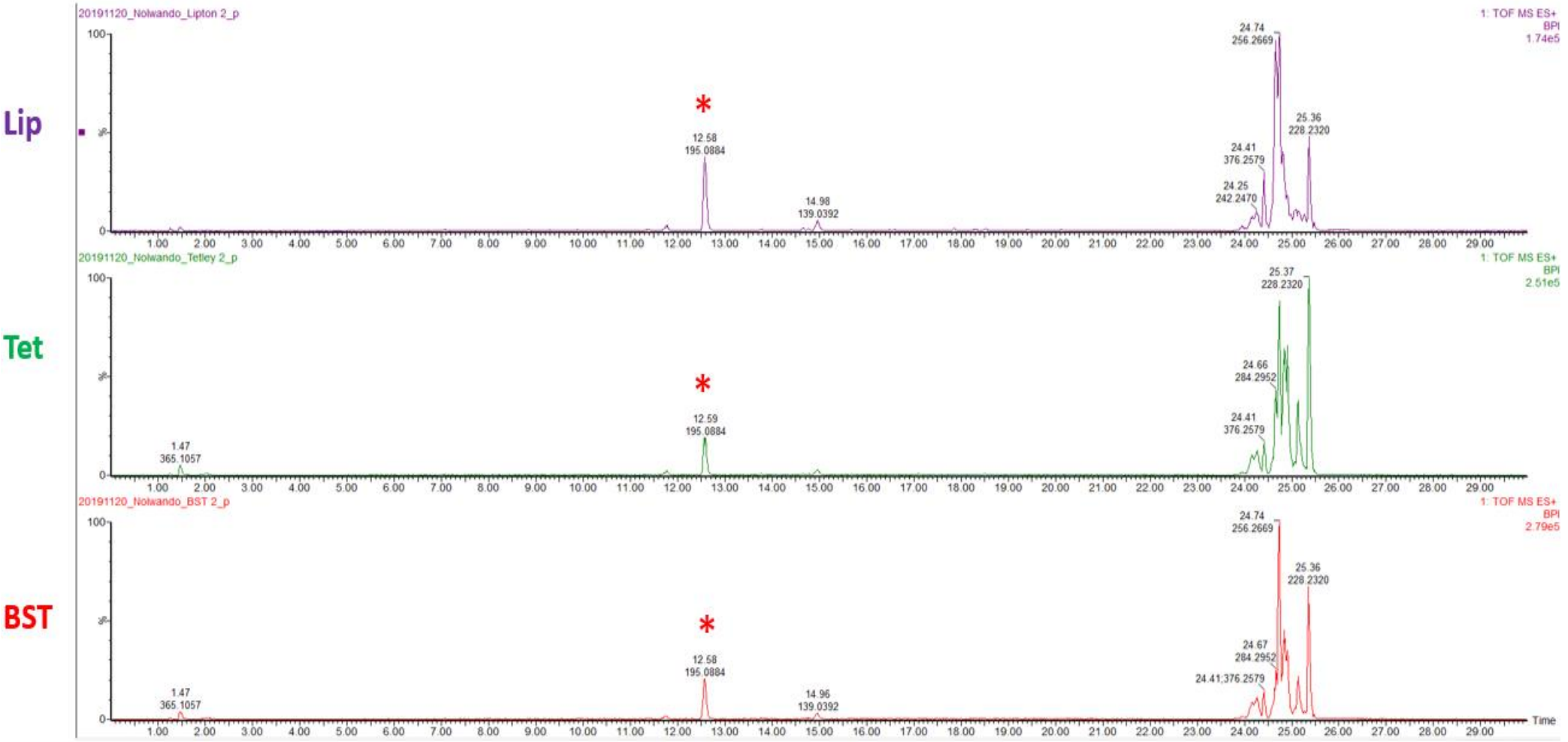

Figure 3.5: UPLC-MS analysis (ES+ ionisation mode) of three commercial green tea brands.

Extracts from three commercial green tea brands, Lipton (Lip), Tetley (Tet) and BST were sampled for UPLC-MS analysis. Waters UPLC system hyphenated to Waters Synapt G2 QTOF instrument equipped with an autosampler and a binary solvent delivery system controlled by MassLynx v4.1 software was used. Separation was achieved using a Waters HSS T3 column (1.8 µm x 2.1 x 150 mm) with a gradient elution. In these chromatograms, retention time is displayed on the x-axis and % intensity is recorded on the y-axis. A peak corresponding to caffeine (195 g/mol) was positively identified at consistent retention times in all three tea brands tested. The peaks representing caffeine is identified with a red Asterix. A cluster of peaks at a retention time range of ~24 – 26 min is also observed, owing to the solvent.

With the UPLC-MS analysis complete, we were able to identify most of the known tea catechins in Lipton, Tetley and BST green tea brands at the expected molecular weights and retention times. However, it was noted that UPLC-MS analysis of EGCG, our catechin of interest, in these tea extracts did not produce the expected results. We found that the ionisation pattern of EGCG observed from the tea extracts in the ES- ion mode was not consistent with that which was observed from the cocktail standards. Therefore, to validate the presence of EGCG in the green tea extracts, we resolved to try a different approach that omitted the ionisation process. Hence, we performed UPLC without MS.

3.2.1.2. Detection and identification of phenolic compounds in green tea using UPLC

The principles of UPLC in this experiment are based on separation of analytes based on polarity using ultra-high pressure, as previously described. As in the UPLC-MS experiment, the aim of this experiment was to quantify and compare EGCG in Lipton, Tetley and BST green tea extracts with the aid of a standard curve. The area of the EGCG peak was to be used as a proxy to calculate the concentration of EGCG in each of the green tea extracts. Caffeine was used as a control throughout this experiment. Additionally, mycophenolic acid, sulphanilamide, and tryptamine were used as internal standards in all the samples for quality control purposes.

Firstly, pure samples of EGCG and caffeine were analysed separately to generate a chromatographic blueprint of the retention patterns of each of these compounds from UPLC. To validate this data, a cocktail sample consisting of a 1:1 ratio of EGCG and caffeine was also similarly analysed using UPLC. Lastly, samples of green tea extracts from Lipton, Tetley and BST were analysed using UPLC.

Individual UPLC analysis of the pure caffeine standard sample produced a high-intensity peak with a retention time of ~10.0 min, as shown in **Figure 3.6(a)**. This peak was attributed to caffeine, which was the analyte with the highest concentration in this sample. As expected, another peak was observed at a retention time of ~31.5 min, which was attributed to mycophenolic acid (based on data from similar experiments, which is not shown). However, there were no peaks observed for the other internal standards, sulphanilamide and tryptamine, which were expected to elute after ~2.5 min and ~8.0 min respectively. Nonetheless, this does not conclusively indicate that these internal standards were not present in this sample, as their peaks may have been too small

to be seen due to the scale of this chromatogram. By contrast, a peak attributed to EGCG was observed from the analysis of the pure EGCG standard, as shown in **Figure 3.6(b)**. The retention time of this peak was ~10.5 min. Peaks corresponding to the three internal standards were observed at the expected retention times. Finally, analysis of the cocktail sample containing EGCG and caffeine, shown in **Figure 3.6(c)**, also confirmed the retention patterns shown by the EGCG and caffeine standard samples. Again, three peaks corresponding to the internal standards were also observed in this sample.

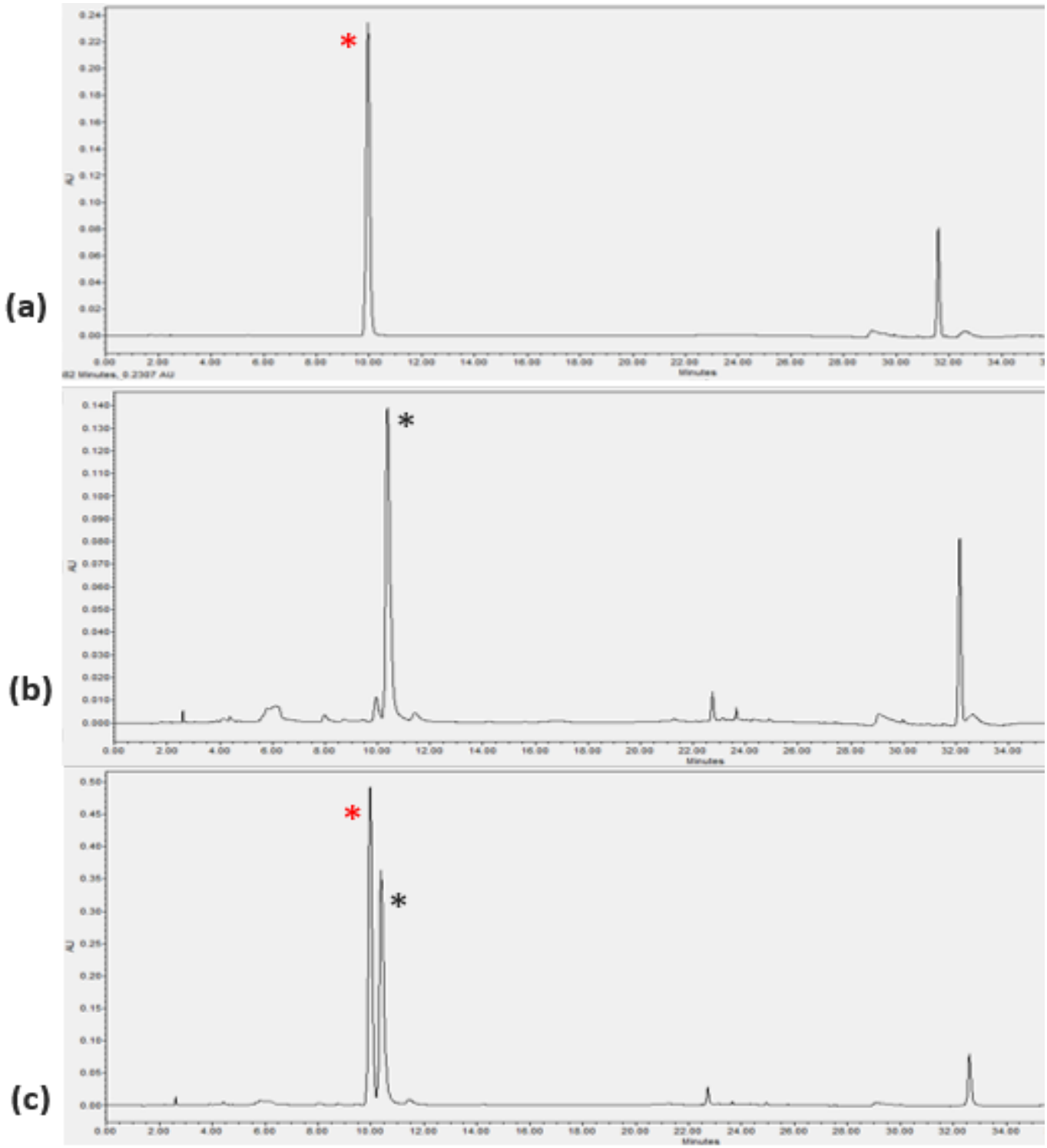

Figure 3.6: UPLC analysis of caffeine and EGCG standards.
Pure samples of caffeine **(a)** and EGCG **(b)** standards were analysed using UPLC to determine the retention profile of each compound. A cocktail sample consisting of both standards in a 1:1 ratio was also analysed in **(c)**. An ACQUITY UPLC H-class system fitted with a DAD, an autosampler, and a binary solvent delivery system controlled by Empower-3 software was used for UPLC analysis. Separation was achieved using an HSS T3 column (1.8 µm x 2.1 x 150 mm). UV/Vis spectra were captured from 254 – 400 nm. All samples were diluted with stabilising solution containing three internal standards. Peaks representing caffeine, which has a retention time of ~10.0 min, are identified with a red Asterix. Similarly, peaks representing EGCG, which has a retention time of ~10.5 min, are identified with a black Asterix. Peaks corresponding to the three internal standards were also observed with retention times of ~2.5 min for sulphanilamide, ~8.0 min for tryptamine and ~31.5 min for mycophenolic acid

Lastly, the green tea extracts from Lipton (Lip), Tetley (Tet) and BST were analysed using UPLC. In this instance, the results of two technical repeats (labelled A and B) for each tea brand are superimposed, as shown in **Figure 3.7**. The technical repeats shown in this experiment were performed on the same day. Comparing the chromatograms from technical repeats can be used as a measure of consistency throughout the extraction process. Theoretically, the chromatograms are expected to superimpose perfectly if there is consistency during the extraction process. Practically, however, this is not always achievable when human error is a factor, as evidenced by the results in **Figure 3.7**.

UPLC analysis of the tea extracts showed that EGCG and caffeine were present in all three of the green tea brands, as shown in **Figure 3.7**. This is evidenced by the presence of peaks with retention characteristics that are consistent with those of caffeine (~10.0 min) and EGCG (~10.5 min) with reference to the standards analysed earlier (shown in **Figure 3.6**). Furthermore, the similarities between the chromatographic profiles of Lipton, Tetley and BST indicate that these green tea brands have very similar chemical compositions. This may suggest that the manufacturing processes that create these green tea products may also be similar.

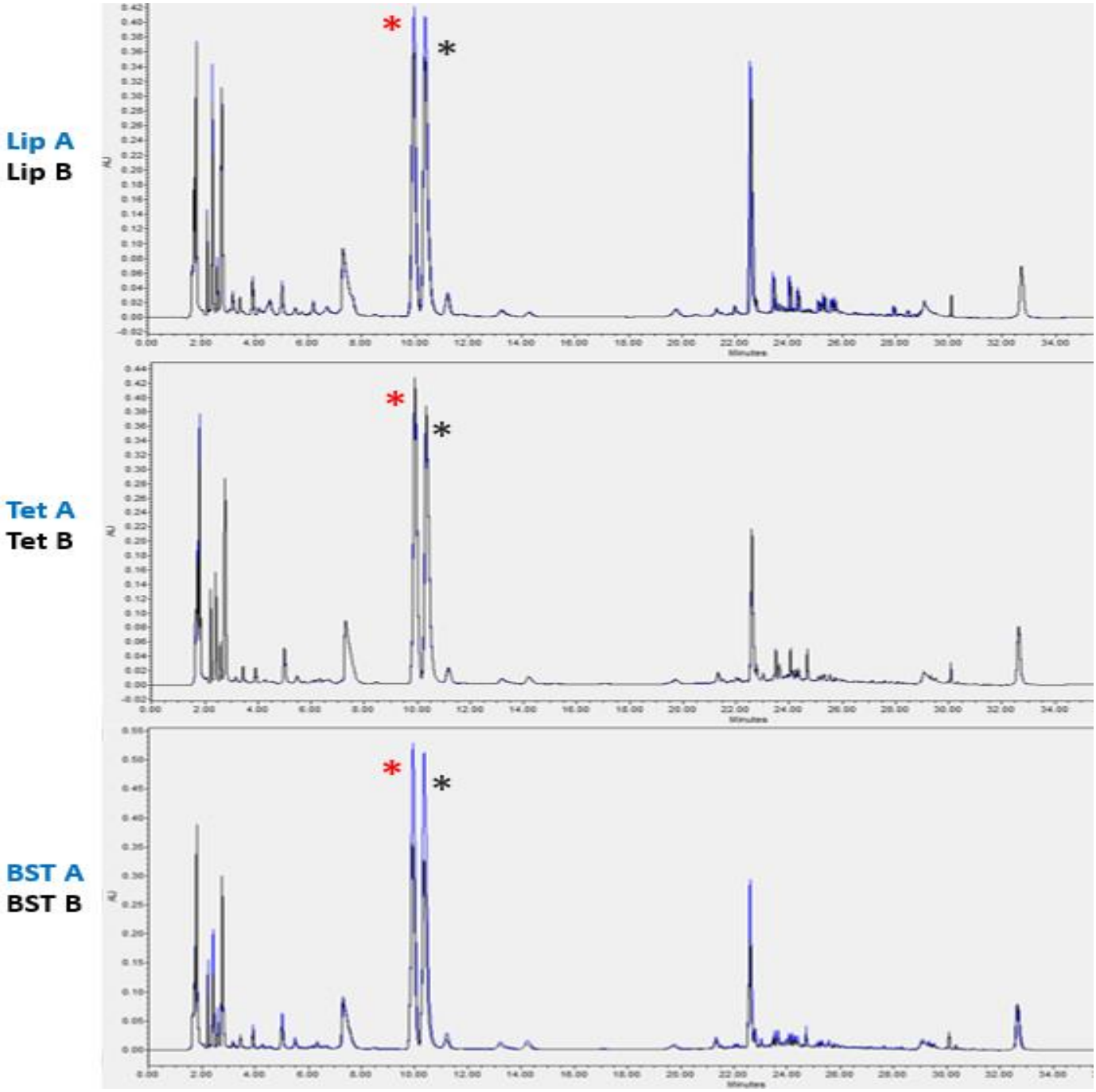

Figure 3.7: UPLC analysis of extracts from three commercial green tea brands.
Three commercial green tea brands, namely Lipton (Lip), Tetley (Tet) and BST were subjected to UPLC analysis to identify and quantify EGCG and caffeine. An ACQUITY UPLC H-class system fitted with a DAD, an autosampler, and a binary solvent delivery system controlled by Empower-3 software was used for UPLC analysis. Separation was achieved using an HSS T3 column (1.8 µm x 2.1 x 150 mm). UV/Vis spectra were captured from 254 – 400 nm. The UPLC chromatograms from two technical repeats that were prepared on the same day, labelled A (blue) and B (black), have been superimposed for each of the tea brands tested. Retention time (in min) is shown on the x-axis, while absorbance (in AU) is measured on the y-axis. Peaks corresponding to caffeine, identified with red Asterixis, were observed in all tea brands with a retention time ~10.5 min. Similarly, the peaks corresponding to EGCG were identified with a black Asterixis in all three green tea brands with the expected retention time of ~10.5 min.

Therefore, we succeeded in detecting and identifying EGCG and caffeine in Lipton, Tetley and BST green tea extracts using UPLC at their expected retention times. The results of the UPLC analysis verified the findings of the UPLC-MS analysis, which indicated that both EGCG and caffeine were present in all three green tea brands. With all the data collected, it was then possible to determine the concentration of EGCG and caffeine in the extracts from all three green tea brands. This was achieved with the aid of caffeine and EGCG standard curves. These standard curves were generated by analysing the cocktail sample containing both compounds in a 1:1 ratio using UPLC with a DAD at a UV/Vis spectrum of 254 – 400 nm. Finally, from this information, the quantities of EGCG and caffeine in Lipton, Tetley and BST were then calculated and compared.

3.2.1.3. Determining the polyphenol contents of commercial green tea brands

We were interested in determining the phenolic composition of commercial green tea. For this purpose, we chose Lipton, Tetley and BST because they are popular green tea brands in the South African market. Since it has been established that phenolic compounds found in tea have bioactive properties against inflammation, among other things, this information may be useful to consumers suffering from inflammatory illnesses.

Firstly, the total phenolic content (TPC) of each green tea brand was determined using the Folin-Ciocalteu (FC) assay. Briefly, the ISO 14502-1 (Iso, 2005) method was used to extract phenolic compounds from green tea samples from the three brands. The samples were then treated with FC reagent, which contains sodium molybdate and sodium tungstate among other things. When reacting with phenolic compounds, the FC reagent undergoes a colour change from yellow to blue, which absorbs light at a wavelength of 765 nm. The intensity of this colorimetric absorbance can be quantified using a spectrophotometer to determine the concentration of phenolic compounds in a sample with the aid of a gallic acid standard curve. Gallic acid is chosen for this purpose because it is a stable phenolic compound also found in green tea. Then the

UPLC data was also used to quantify and compare EGCG and caffeine in these tea brands.

To determine the concentrations of EGCG and caffeine, and the TPC of Lipton, Tetley and BST, standard curves were generated. The EGCG and caffeine standard curves shown in **Figure 3.8** were developed from UPLC analysis of the cocktail sample consisting of pure EGCG and caffeine in a 1:1 ratio. These standard curves report the concentration of EGCG and caffeine as a function of the area of the respective peak. Additionally, the gallic acid standard curve shown in **Figure 3.9** reports the concentration of gallic acid as a function of absorbance at 765 nm.

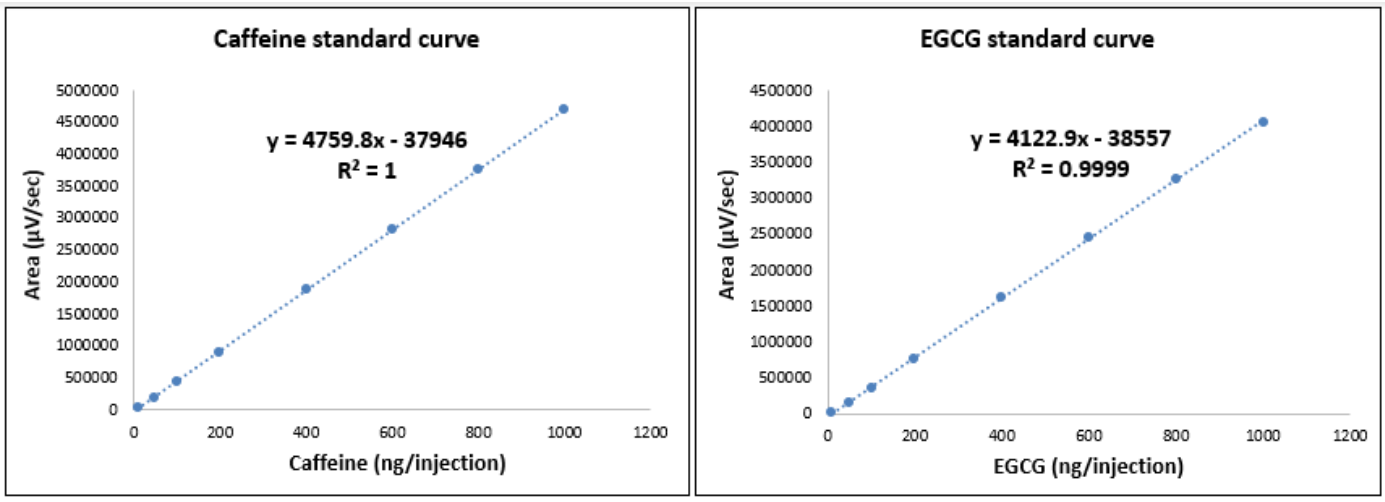

Figure 3.8: Standard curves used to determine relative EGCG and caffeine contents of three commercial green tea brands.
Caffeine and EGCG standard curves were generated by analysing the cocktail sample containing both compounds in a 1:1 ratio using UPLC with a DAD at a UV/Vis spectrum of 254 – 400 nm. The area (in µV/sec) of each peak was plotted against the quantity of caffeine or EGCG (in ng/injection) to form a linear trend, which was used to quantify these compounds in green tea extracts. The regression model of the linear trend is described by the R^2 value in each of the standard curves.

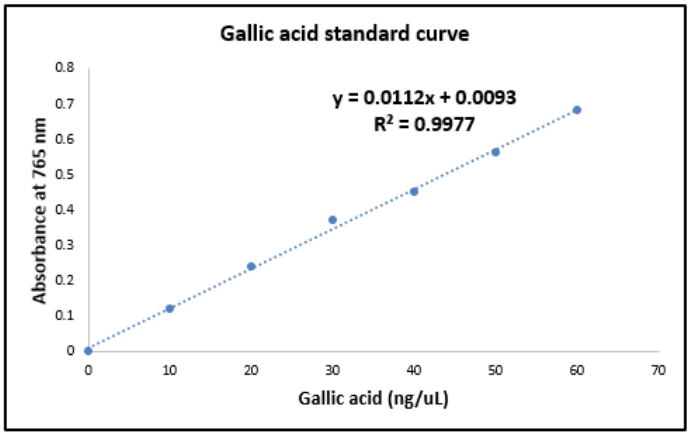

Figure 3.9: Gallic acid standard curve used to determine total polyphenol contents of three commercial green tea brands.
A gallic acid standard curve was used to determine the total phenolic contents of the green tea samples using the Folin-Ciocalteu (FC) assay. The regression model of the linear trend is described by the R^2 value in each of the standard curves.

With the aid of the gallic acid standard curve, we determined that Lipton had the highest TPC among the three brands, with an TPC of 23%, as shown in **Figure 3.10**. BST was found to possess the second highest TPC at 16%, while Tetley had a TPC of 15%. However, statistical analysis of this data revealed that the difference between the TPCs of Tetley and BST was insignificant. This means that, statistically, they are equal. However, the %TPC of Lipton was found to be statistically higher than that of Tetley and BST. Collectively, this study showed that Lipton, Tetley and BST have an average total phenolic content of 18%.

With previous literature data (Lambert and Elias, 2010) suggesting that EGCG is the most abundant phenolic compound in green tea, we went further to determine the EGCG contents of Lipton, Tetley and BST. This was achieved using the EGCG standard curve. For quality control purpose, caffeine was also quantified similarly, using the caffeine standard curve. Our findings showed that all three green tea brands contained ~1% of EGCG with no statistically significant difference between them, as shown in **Figure 3.10**. Similarly, all samples were found to contain between 0.8 - 0.9% of caffeine with no statistically significant difference between the three green tea brands, as seen in **Figure 3.10**.

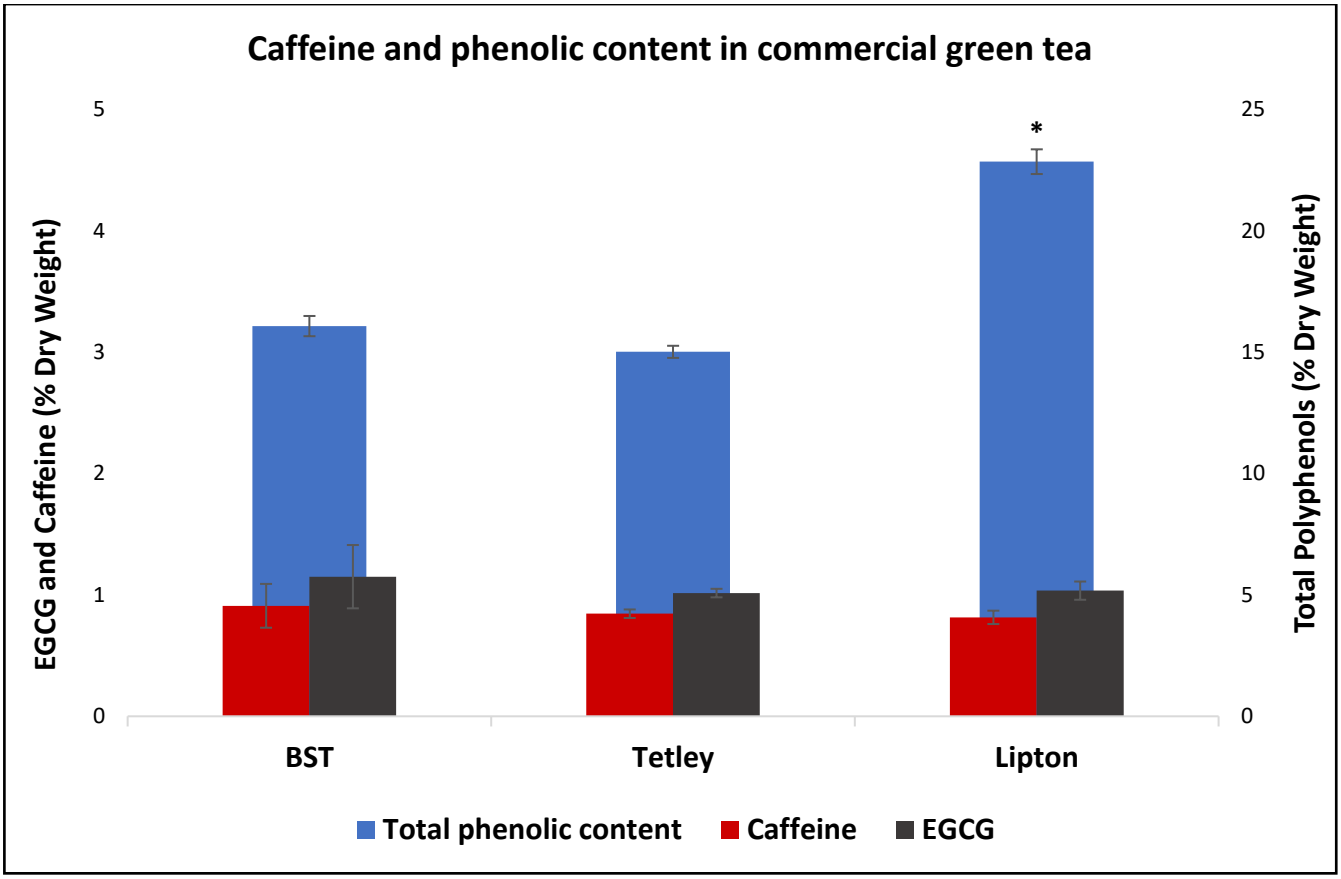

Figure 3.10: Comparing the relative amounts of phenolic compounds and caffeine found in three commercial green tea brands.
The Folin-Ciocalteu (FC) assay was used to determine the % total phenolic contents (blue) of three commercial green tea brands, namely BST, Tetley and Lipton. The % total phenolic content (%TPC) is reported on the primary y-axis (right-hand side), which has a range of 0 – 25% Dry Weight. UPLC analysis was then used to determine the caffeine (red) and EGCG (black) contents of the same green tea brands. The EGCG and caffeine contents are reported on the secondary y-axis (left-hand side), which has a range of 0 – 5% Dry Weight. Error bars represent the standard error of the mean for n = 3 experiments. Statistical significance at the 95% level of confidence is specified with an Asterix where applicable. EGCG accounted for ~1% of the dry weight of each tea brands, while caffeine accounted for between 0.8 – 0.9% of the dry weight of the three green tea brands.

3.2.2. Investigating the NO-scavenging potential of EGCG

This section documents the results of the first of two parts of our investigation into the hypothesis that EGCG, the prominent polyphenol in green tea, possesses anti-inflammatory activity. In this section, this hypothesis was investigated specifically in the context of NO, a free radical that plays a crucial mediatory role in inflammation (Radi, 2018). Although NO is constitutively present in small amounts in many tissues across the body, excessive NO production is associated with many rheumatic diseases where inflammation is improperly regulated (Clancy et al., 1998). We also investigate the cytotoxicity of EGCG.

3.2.2.1. NO-scavenging potential of EGCG in an acellular system

We assayed the NO-scavenging potential of EGCG at different concentrations in an acellular system using a chemical Griess assay. In this experiment, a stock solution of NO was initially generated from a solution of 5 mM SNP ($Na_2[Fe(CN)_5NO]$), which is a nitrosating agent, prepared in PBS buffer. This was achieved by exposing the SNP solution to natural light for 1 h, thereby photodegrading the compound and releasing NO. The NO resulting from this process was considered as the starting NO concentration throughout the experiment. During experimentation, the starting NO concentration was exposed to different concentrations of EGCG (0.01 – 8 mM) for 1 hour. This was done in the dark to maintain the starting NO concentration by preventing further photodegradation of SNP. Importantly, since NO is highly unstable, it is rapidly converted into the more stable nitrite (NO_2^{-1}) form. As such, NO remaining in each sample after exposure to EGCG was quantified as a function of nitrite equivalence.

As a quality control measure, we also tested the same concentrations of EGCG (0.01 – 8 mM) with PBS to determine if the combination PBS and EGCG had any unintended effect of NO concentration. Lastly, NO concentration in the controls and test samples was determined using the Griess reagent, which consists of sulphanilamide, NED and phosphoric acid. The sulphanilamide in the Griess reagent reacts with nitrite ions to form a diazonium salt, which reacts with NED to produce a pink colour, as shown in **Figure 3.11(a)**. The intensity of this colour can be analysed spectrophotometrically to

determine the concentration of NO (as NO_2^{-1} equivalence) remaining after each reaction. A NO_2^{-1} standard curve is required to do this, which is shown in **Figure 3.11(b)**. In this case, NO_2^{-1} ions were released from the dissolution of $NaNO_2$ in water. The Griess reagent was also added to these standard samples, which results in a concentration-dependent colorimetric shift to form the standard curve.

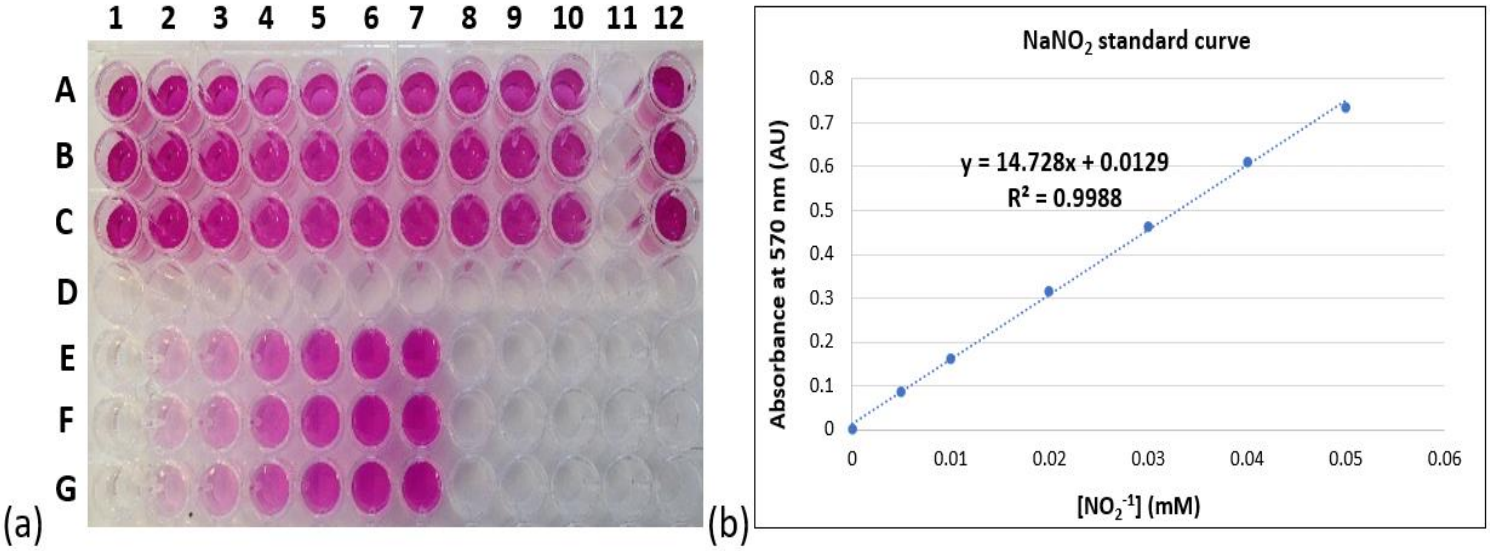

Figure 3.11: Calorimetric determination of nitrite concentration using an acellular Griess assay.

NO_2^{-1} concentration was determined as a proxy for NO concentration. The concentration of NO_2^{-1} was determined spectrophotometrically based on a colorimetric shift induced by the reaction of the Griess reagent with nitrite ions present in a solution. In **(a)** the reactions of EGCG samples of increasing initial concentration (i.e. 0.01 mM, 0.025 mM, 0.05 mM, 0.1 mM, 0.25 mM, 0.5 mM, 1 mM, 2 mM, 4 mM and 8 mM) with the SNP reagent and the Griess reagent are shown in triplicate (rows A, B and C) from columns 1 to 10. Column 11 is empty, while column 12 rows A, B and C similarly represent the triplicate blank samples (i.e. 0 mM EGCG). The $NaNO_2$ standard curve samples are depicted similarly in rows E, F and G in the order of increasing final concentration (i.e. 0 mM, 0.005 mM, 0.01 mM, 0.02, 0.03 mM, 0.04 mM and 0.05 mM). In **(b)** the $NaNO_2$ standard curve is shown, depicting the linear relationship between nitrite concentration (in mM) and the absorbance at 570 nm in arbitrary units (AU), which is defined by a linear function. The regression model of the linear trend is described by the R^2 value.

Since PBS buffer was used as the solvent in the SNP reagent, pure PBS buffer was used a negative control in the experiment to determine if its interaction with EGCG has any effect on NO concentration in this study. The data showed no statistically significant difference in the NO production of samples containing PBS and EGCG in comparison to the PBS-only control, as shown in **Figure 3.12**. This means that the interaction between PBS buffer and EGCG had no significant impact on NO production, which was expected. These results from the negative control experiment strengthen the validity of the results from the test experiment since they rule out unintended interference from the PBS as a solvent in this experiment.

By contrast, the results from the test samples are reported with reference to the SNP positive control. This control represents the starting NO concentration in the experiment, which is considered as the 100% NO production standard. The results indicate that below a concentration of 0.05 mM EGCG had no significant effect on the concentration of NO in comparison to the SNP standard. However, at higher concentrations of EGCG (≥0.05 mM) the % NO produced decreased significantly, as shown in **Figure 3.12**. This means that EGCG is a scavenger of NO at these concentrations, although this scavenging activity does not occur in a linear fashion as to be expected.

Interestingly, the greatest reduction in NO was observed in the sample treated with 0.1 mM of EGCG, where % NO produced was determined to be 44.2%. This may suggest that EGCG exhibits the best NO-scavenging activity at a concentration of 0.1 mM; however, further statistical analysis showed that this is not the case. This is because there was statistically significant difference between the % NO produced in this samples compared to the other samples that were exposed to higher concentrations (0.25 – 8 mM) of EGCG.

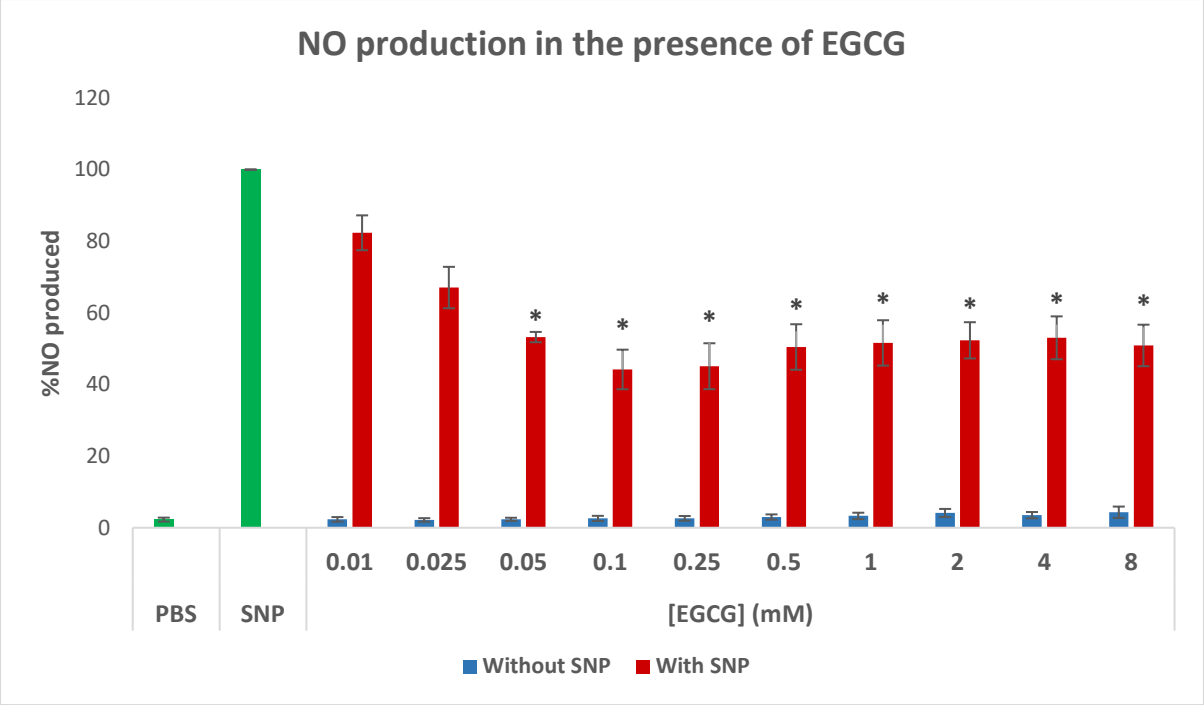

Figure 3.12: Effects of EGCG on NO production in an acellular system.
The % NO produced is depicted as a function of EGCG concentration (in mM) based on data generated from a chemical Griess assay. These results were determined using the absorbance data (recorded at 570 nm) obtained from the acellular Griess assay, where the Griess reagent produced a concentration-dependent colorimetric shift in SNP samples containing nitrite ions after treatment with EGCG to determine the NO-scavenging potential of EGCG after 1 h of incubation in the dark. Error bars represent the standard error of the mean for n = 3 experiments. Statistical significance at CI= 95% for the data in the absence of SNP relative to the "PBS" control is indicated with a hash sign (#), whereas the statistical significance of the data in the presence of SNP relative to the "SNP" control is indicated with an Asterix (*). According to the data, EGCG exhibits significant NO-scavenging activity at concentrations from 0.05 – 8 mM in comparison to the SNP control. Moreover, PBS and EGCG together have no significant impact of NO concentration, as shown by the blue graphs, when compared to the "PBS" control.

From the data of the acellular NO tests, one can get a broad understanding of the chemical characteristics of EGCG. From this data, it is evident that EGCG scavenges NO in a concentration-dependent manner. However, due to the complexity and sensitivity of biological systems, it would be unwise to assume that this observation holds the same relevance physiologically. Therefore, we deemed it necessary to test the NO-scavenging potential of EGCG *in vitro* using macrophages, which are innate immune cells. Importantly, due to the sensitivity of biological cell systems, we decided

to perform this experiment at a lower concentration range than that previously tested in the chemical system.

3.2.2.2. NO-scavenging potential of EGCG in a cellular system

The NO-scavenging potential of EGCG *in vitro* was tested on murine macrophages known as RAW 264.7 cells using the Griess assay as before. Since RAW 264.7 are adherent cells, they remain attached to the surface of the wells of the 96-well plate. As such, in the cellular experiment, the Griess assay is performed using samples of the cell culture media, and not directly on the cells. Contrary to the chemical Griess assay that was performed previously, NO was initially generated biologically by the cells. To do this, the cells were exposed to LPS, which is the known ligand for TLR4. Exposure to LPS stimulates a pro-inflammatory response that triggers NO production in the cells.

LPS-stimulated cells were treated with varying concentrations of EGCG (1 – 800 μM) to determine the effects of EGCG on NO production in these immune cells. LPS-stimulated cells not treated with EGCG were used as a positive control that was considered as the 100% NO production standard. In addition, resting cells (unstimulated and untreated) were used as a negative control, which accounted for any NO that was produced constitutively in the cells. Cell culture medium (DMEM) alone was also tested as a control to determine if the culture media had any effect on NO concentration in the experiment. Lastly, unstimulated cells treated with 1 – 800 μM EGCG were tested to determine if EGCG had any effect on NO production in the absence of LPS-stimulation.

As expected, a high-intensity pink colour was observed from the LPS-stimulated untreated cells (used as the 100% NO production standard) upon addition of the Griess reagent, as shown in **Figure 3.13(a)**. This indicates that the sample contained a high concentration of NO_2^{-1} ions, which were used as a proxy to measure concentration of the highly unstable NO ions. In comparison to this sample, however, all the unstimulated samples still exhibited a colour that resembled the culture media after addition of the Griess reagent. This indicates that there was low NO production

in these samples, which is the expected outcome since a pro-inflammatory response was not stimulated. Moreover, this result also observed and expected from the unstimulated cells treated with EGCG, as it suggested that there was little, or no, NO production attributed specifically to EGCG. Importantly, these visual results could only be verified after quantitative data analysis involving a standard curve. The NaNO standard curve used to calculate the concentration of NO in the samples is shown in **Figure 3.13(b)**.

Notably, a brown colour was observed in all samples that were treated with higher concentrations of EGCG (i.e. 400 – 800 μM) after incubation, regardless of LPS-stimulation. This browning can be seen in wells A12, C1, 9E and 10E, and their duplicates. This phenomenon was observed consistently with several repeats of this experiment, and we postulate that it may be due to oxidation of EGCG during the incubation period.

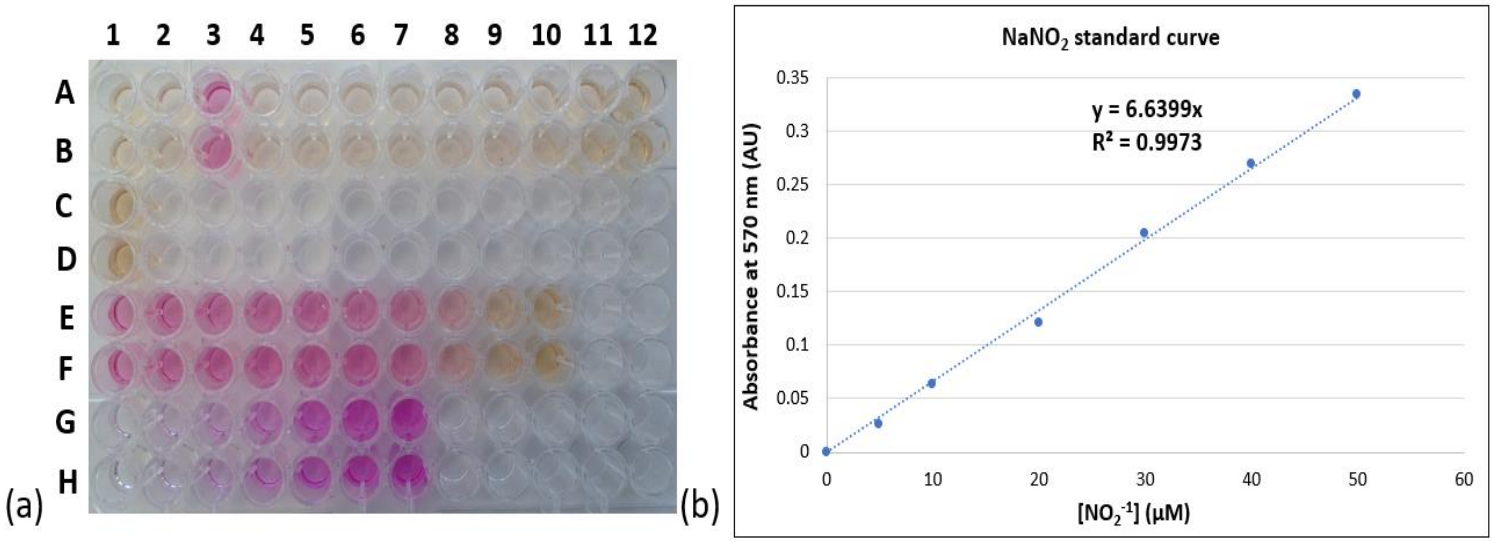

Figure 3.13: Calorimetric determination of nitrite concentration using a cellular Griess assay.

NO_2^{-1} concentration was determined as a proxy for NO concentration. NO_2^{-1} concentration was determined spectrophotometrically based on a concentration-dependent colorimetric shift caused by the reaction of the Griess reagent and nitrite ions produced by unstimulated and LPS-stimulated (100 ng/mL) RAW 264.7 cells (1.25 x 10^6 cells/well) incubated for 24 h in DMEM at 37ºC in the presence of 4.6% CO_2. In **(a)** The three controls (i.e. DMEM, cells in DMEM and LPS-stimulated cells) are shown in wells A1, A2 and A3 (respectively), with their duplicates below each of them in row B in a 1:1 ratio with Griess reagent. Similarly, the unstimulated cells were exposed to varying final concentrations of EGCG (i.e. 1 µM, 2.5 µM, 5 µM, 10 µM, 25 µM, 50 µM, 100 µM, 200 µM and 400 µM) in wells A4 to A12 (duplicates below in row B). The 800 µM duplicates are shown in wells C1 and D1. The ten LPS-stimulated samples exposed to the EGCG samples (i.e. 1 µM, 2.5 µM, 5 µM, 10 µM, 25 µM, 50 µM, 100 µM, 200 µM, 400 µM and 800 µM) are shown in row E (duplicated in row F) in order of increasing final concentration. Lastly, the seven Na_2NO standard curve samples (i.e. 0 µM, 5 µM, 10 µM, 20 µM, 30 µM, 40 µM and 50 µM) are shown in duplicate in rows G and H. Samples containing nitrite ions can be identified by the development of a pink colour. Lastly, the linear $NaNO_2$ standard curve is shown in **(b)**. The regression model of the linear trend is described by the R^2 value.

Although the visual analysis of the Griess assay results suggested that there was little, or no, NO production attributed specifically to EGCG in unstimulated cells, the quantitative data analysis proved otherwise. The data shown in **Figure 3.14** showed that NO production in unstimulated cells treated with higher concentrations of EGCG (200 – 800 µM) was significantly higher than that of resting cells. This finding suggests that EGCG at higher concentrations may possess pro-oxidant activity in unstimulated

cells. As such, EGCG may act as a pro-inflammatory agent in these cells at higher concentrations.

By contrast, it was found that treating LPS-stimulated cells with lower concentrations of EGCG (1 – 100 μM) had no significant impact in NO production compared to the LPS-stimulated untreated control. However, at concentrations between 200 – 400 μM, EGCG significantly decreased the concentration of NO relative to the same control, as shown in **Figure 3.14**. Interestingly, at a concentration of 800 μM, treatment with EGCG showed no significant impact on the NO concentration when compared to the LPS-stimulated untreated control.

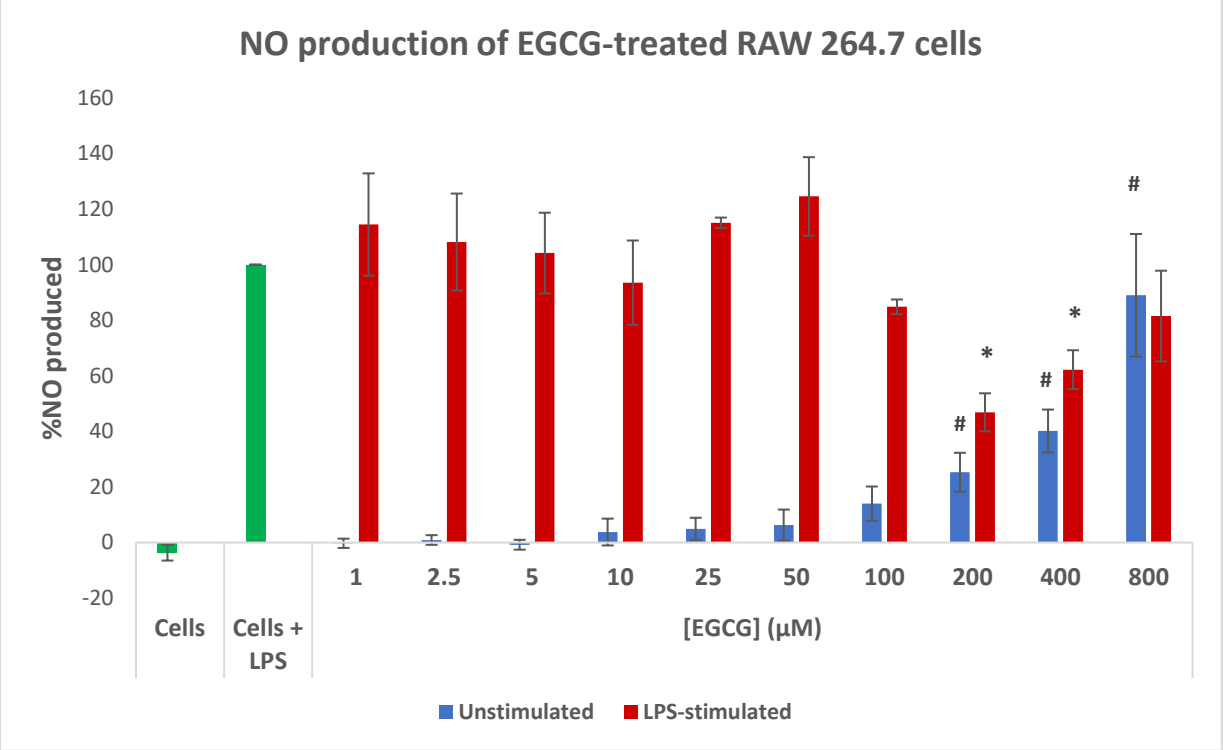

Figure 3.14: Effects of EGCG on NO production in stimulated and unstimulated macrophages.
Untreated unstimulated RAW 264.7 cells (denoted as "Cells") and untreated LPS-stimulated RAW 264.7 cells (denoted as "Cells + LPS") were used as controls (shown in green) in this experiment. Experimental samples consisted of RAW 264.7 cells (stimulated and unstimulated) treated with varying final concentrations of EGCG (1 – 800 µM). Unstimulated cells treated with EGCG are shown in blue, while LPS-stimulated cells treated with EGCG are indicated in red. Error bars represent the standard error of the mean for n = 3 experiments. The statistical significance of the unstimulated cells data relative to the "Cells" control (where the concentration of EGCG is 0 mM) at a 95% confident interval, is indicated with a hash sign (#), whereas the statistical significance of the data relative to the "Cells +LPS" control is indicated with an Asterix (*). According to this data, treating LPS-stimulated cells with 200 µM and 400 µM EGCG significantly reduced NO production in LPS-stimulated cells with reference to untreated LPS-stimulated control cells. Furthermore, treating unstimulated cells with 200 – 800 µM EGCG significantly increased NO production in comparison to resting cells.

From this data, it seems that EGCG exhibits the best NO-scavenging activity at a concentration of 200 µM, where little or no browning (a sign of oxidation) was observed in RAW 264.7 cells. However, despite the evidence collected thus far, we were still unable to draw any valid conclusions as there was another important variable to eliminate in this study. It was still unclear what effect the exposure to EGCG may have had on the integrity of the cells during the experiment. As such, the validity of these

results remained questionable. Hence, the MTT assay was performed using the same cell cultures used during the Griess assay to determine the viability of the cells.

3.2.2.3. The cytotoxicity of EGCG

The cytotoxic effects of EGCG were investigated by determining the viability of RAW 264.7 cells exposed to EGCG for 24 h. Importantly, to ensure that the results of this experiment were effectively correlated to those of the cellular NO production experiment, the same set of cells had to be used for both experiments. Briefly, the MTT reagent was added to the remaining cell cultures from the previous experiment in a 1:1 ratio. Scientific evidence suggests that MTT, a yellow tetrazolium dye, readily crosses intact cell membranes and undergoes bioreduction by both the plasma membrane and intracellular reductase enzymes (Bernas and Dobrucki, 2000). During this process, metabolically active cells reduce MTT to a purple formazan. It is important to note that although MTT is cytotoxic, reducing cells can remain metabolically active and undamaged for at least 45 min. As such, the intensity of the purple colour can be quantified spectrophotometrically as a proxy for cell viability.

The resting cells, which were unstimulated and not treated with EGCG, were used as the standard for 100% cell viability. It was observed that the viability of LPS-stimulated untreated cells matched that of the resting cells, as shown in **Figure 3.15**. As expected, the results showed that the viability of unstimulated cells treated with EGCG was preserved throughout experimentation. This was determined through statistical analysis, which found that the difference observed between each of the unstimulated samples in comparison to the cell viability of controls was insignificant.

By contrast, similar findings were made from most of the LPS-stimulated cells treated with EGCG, as shown by the red bars in **Figure 3.15**. However, the LPS-stimulated cells treated with 800 μM EGCG exhibited ~68% cell viability, which was the lowest result in this study. This was found to be significantly lower than the resting cells control and the LPS-stimulated control. The data indicates that 800 μM EGCG was cytotoxic to LPS-stimulated mouse macrophages, as cell viability in this instance was below the acceptable threshold of 80%.

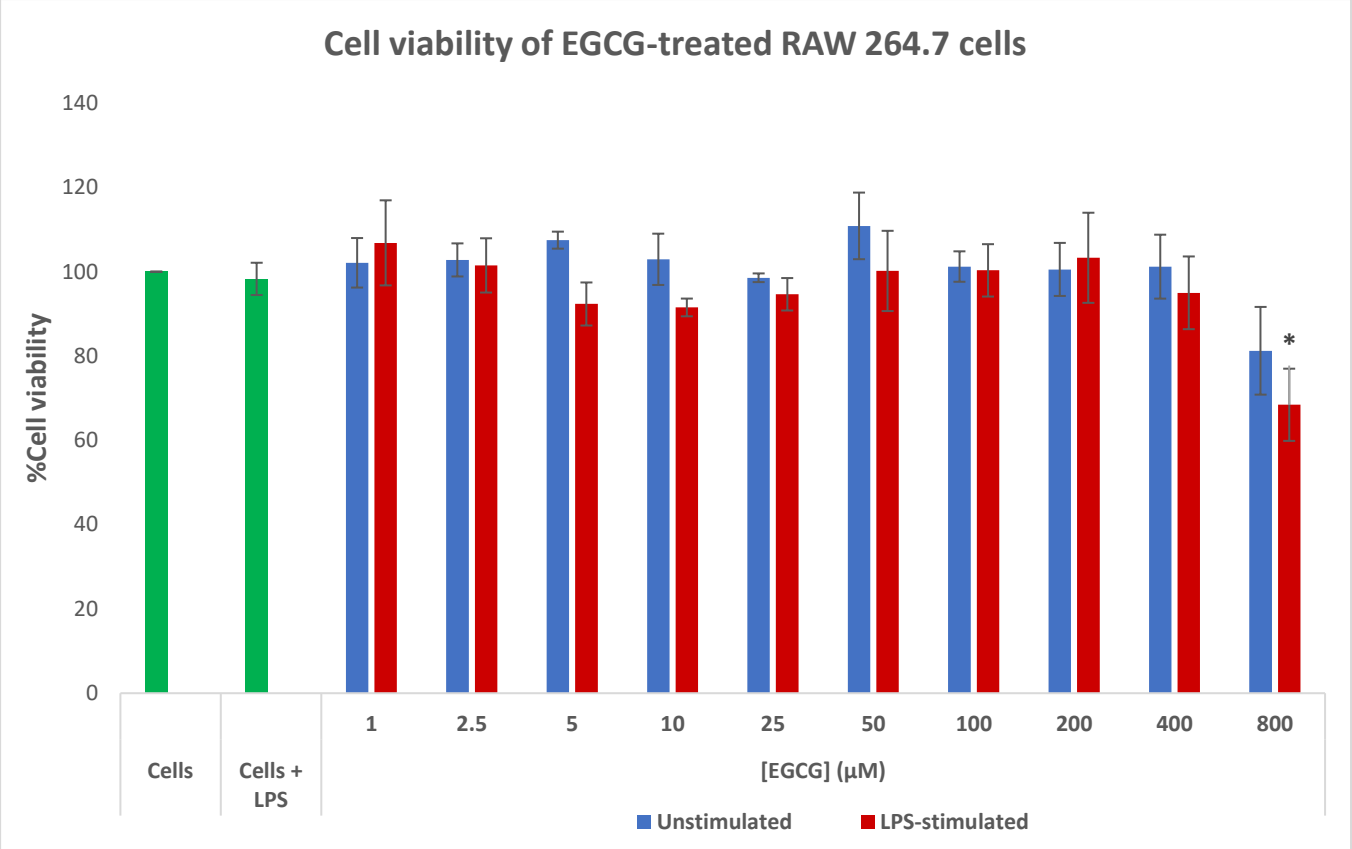

Figure 3.15: Cytotoxicity of EGCG on macrophages.
Untreated unstimulated RAW 264.7 cells (denoted as "Cells") and untreated LPS-stimulated RAW 264.7 cells (denoted as "Cells + LPS") were used as controls (shown in green) in this experiment. Experimental samples consisted of RAW 264.7 cells (stimulated and unstimulated) treated with varying final concentrations of EGCG (1 – 800 µM). Unstimulated cells treated with EGCG are shown in blue, while LPS-stimulated cells treated with EGCG are indicated in red. Error bars represent the standard error of the mean for n = 3 experiments. The statistical significance of each data point relative to the "Cells" control (where cell viability is considered to be 100% and the concentration of EGCG is 0 mM) at a 95% confident interval, is indicated with a hash sign (#), whereas the statistical significance of the data relative to the "Cells +LPS" control is denoted with an Asterix (*). A significant decrease in % cell viability is observed in LPS-stimulated cells treated with 800 µM EGCG in comparison to the controls. Moreover, % cell viability of this sample is below the satisfactory level of ≥80%, indicating that EGCG may be cytotoxic to these cells at higher concentrations.

In summary, we investigated the NO-scavenging potential of EGCG in a chemical system and a cellular system. Additionally, we investigated the cytotoxicity of EGCG in RAW 264.7 cells. The results of this study found that, although EGCG scavenges NO in a concentration-dependent manner, this scavenging activity did not follow a fixed linear trend, as it was expected for a chemical system. Instead, the results

indicate that NO-scavenging activity plateaus after reaching its peak at 0.1 mM in the chemical system. By contrast, EGCG exhibited no significant NO-scavenging activity at lower concentrations of EGCG (i.e. 1 – 100 μM), but higher concentrations (i.e. at 800 μM) were cytotoxic to RAW 264.7 cells. Ultimately, the data suggested that EGCG may exhibit the most potent anti-inflammatory activity, as it relates to NO-scavenging, at a concentration of 200 μM where the NO concentration was reduced to its lowest with no cytotoxicity. However, this data alone is not enough to draw a solid conclusion on the anti-inflammatory role of EGCG since NO production is only one of many components of the inflammatory response. Furthermore, in this study, LPS was used to stimulate cells and trigger a pro-inflammatory response. Since LPS specifically binds TLR4, we know that this inflammatory response is the result of TLR4 signalling. Therefore, as a follow-up to this study, we decided to investigate the anti-inflammatory role of EGCG in the context of TLR4 signalling.

3.2.3. Investigating the effects of EGCG on TLR4 signalling

As previously explained, TLR4 signalling can occur through two pathways; the MyD88-dependent and the MyD88-independent pathways. The MyD88-dependent pathway activates transcription factors, NF-κB and AP-1, which promote the transcription of pro-inflammatory cytokines such as TNFα. By contrast, the MyD88-independent pathway activates IRF3, which promotes the transcription of type 1 interferons (Akira and Takeda, 2004, Lu et al., 2008, O'neill, 2004).

In this study, the anti-inflammatory role of EGCG in TLR4 signalling was investigated in the context of the MyD88-dependent pathway. This was achieved by monitoring the expression of NF-κB in LPS-stimulated HEK 293 cells treated with EGCG. Secondly, the expression of TNFα was also monitored in LPS-stimulated iBMDMs after treatment with EGCG. These experiments were performed in collaboration with the University of Cambridge, United Kingdom.

3.2.3.1. The effects of EGCG on NF-κB expression

HEK 293 cells do not naturally express TLR4. Hence, the cells were transfected with individual pcDNA3 plasmid constructs containing genes encoding human TLR4, MD-2 and CD14. Additionally, the cells were transfected with a plasmid construct encoding firefly luciferase under the control of an NF-κB promoter. This gene was used as a reporter gene for NF-κB expression. This means that whenever the NF-κB promoter was activated through cell signalling events, the firefly luciferase gene was transcribed.

Importantly, we previously determined during the cellular NO study that EGCG exhibited optimum NO-scavenging activity in mouse macrophages at a concentration of 200 μM. However, published literature data showed that such a high concentration of EGCG was cytotoxic to human astrocytoma U373MG cells (Kim et al., 2007b). Based on this, we resolved to lower the concentration range in this study. Hence, a lower EGCG concentration range (0.1 – 10 μM) was tested on the cells in this study.

The transfected cells were stimulated with LPS for 8 h. The cells were then treated with 1 – 10 μM EGCG. Lastly, NF-κB expression in the cells was quantified using luciferase activity. To do this, the cells were lysed to release firefly luciferase. The substrate for firefly luciferase was then added to the cell lysate to facilitate the substrate-enzyme reaction which produces a luminescence signal. This signal was detected using a luminometer and its intensity was used to quantify firefly luciferase present in the cells. As such, the strength of the luminescence signal was used as a proxy for NF-κB expression in the cells. Untreated LPS-stimulated cells and unstimulated cells were used as controls in this study.

A luminescence signal of ~36 400 relative absorbance units (RAU) was detected from the resting cells (unstimulated and untreated), as shown in **Figure 3.16**. This indicates that resting cells do express low levels of NF-κB. Unstimulated treated cells exhibited similar levels of NF-κB expression, indicating that EGCG alone did not affect NF-κB expression. As expected, the LPS-stimulated untreated control exhibited much higher levels of NF-κB expression, indicating that TLR4 signalling was activated after stimulation with LPS. However, only the cells treated with 10 μM EGCG exhibited a significant decrease in NF-κB expression compared to the LPS-stimulated control. This suggests that at a concentration of 10 μM, EGCG significantly down-regulates TLR4 signalling through the MyD88-dependent pathway.

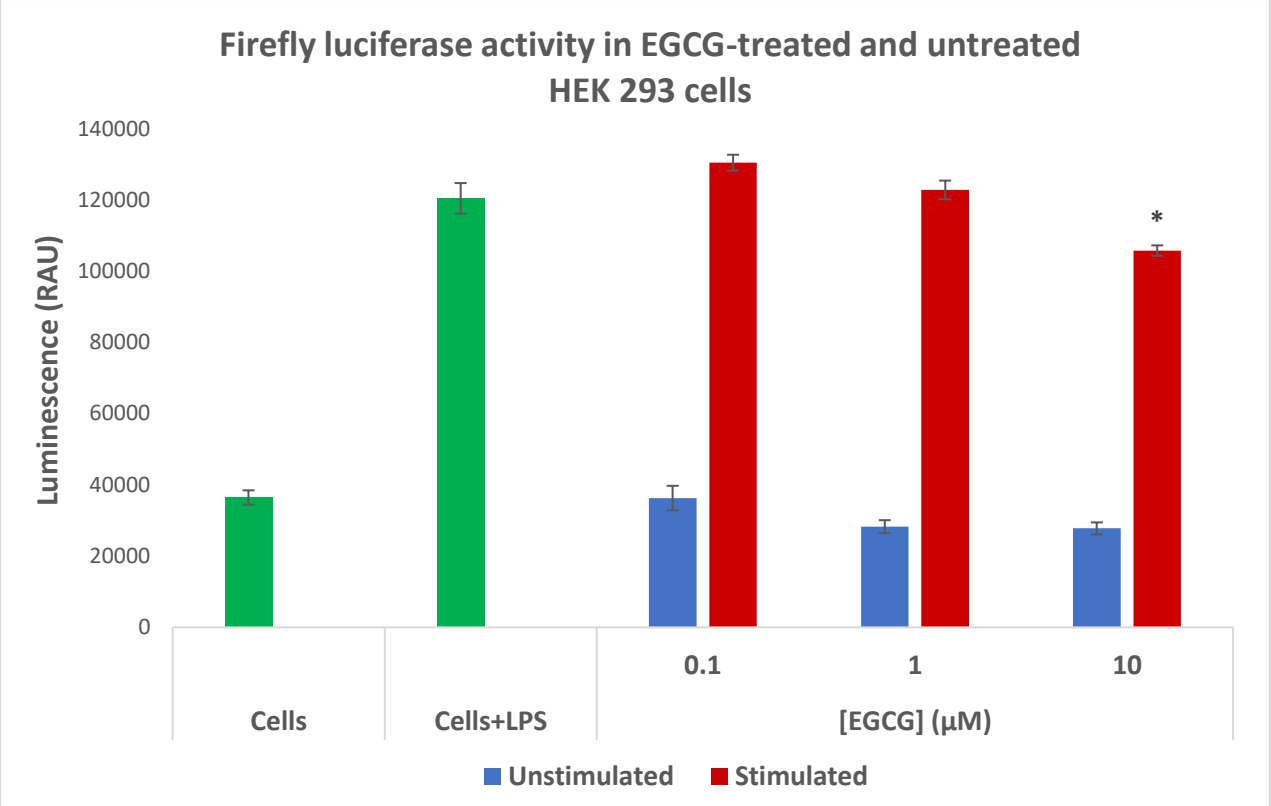

Figure 3.16: Effects of EGCG on NF-κB expression in HEK 293 cells.
HEK 293 cells transfected with plasmid constructs encoding luciferase (controlled by an NF-κB promotor), TLR4, MD-2 and CD-14 were stimulated with 10 ng/mL LPS. The firefly luciferase activity assay was then used to determine luminescence (as a proxy for NF-κB expression) in response to treatment or non-treatment with 0.1 – 10 µM EGCG. Two controls; the untreated unstimulated cells (labelled "Cells") and the LPS-stimulated cells (labelled "Cells+LPS") are shown in green. Treated unstimulated cells are shown in blue, and treated LPS-stimulated cells are shown in red. Error bars represent the standard error of the mean for n = 3 experiments. Statistical significance at a 95% confidence interval in luminescence data of LPS-stimulated cells relative to the LPS-stimulated control is indicated by an Asterix (*****). A significant reduction in NF-κB expression was observed in LPS-stimulated cells treated with 10 µM EGCG.

3.2.3.2. The effects of EGCG on TNFα expression

Murine iBMDMs were stimulated with LPS to trigger a pro-inflammatory response. The cells were then treated with varying concentrations of EGCG (0.1 μM, 1 μM and 10 μM). Thereafter, ELISA, which is an immunoassay, was used to determine the concentration of TNFα in the cells. LPS-stimulated untreated cells were used as a control in this experiment.

The control was found to have a concentration of ~3400 pg/mL of TNFα, as shown in **Figure 3.17**. TNFα concentrations of 2243 pg/mL, 3705 pg/mL and 3267 pg/mL were observed for samples treated with 0.1 μM, 1 μM and 10 μM EGCG respectively. However, although it seems that EGCG caused the greatest reduction in TNFα expression at a concentration of 0.1 μM, statistical analysis showed otherwise. It was found that EGCG in the range of 0.1 – 10 μM had no significant impact on TNFα in comparison to non-treatment. These findings suggest that, in this concentration range, EGCG has no effect TLR4 signalling, as it relates to the expression of TNFα.

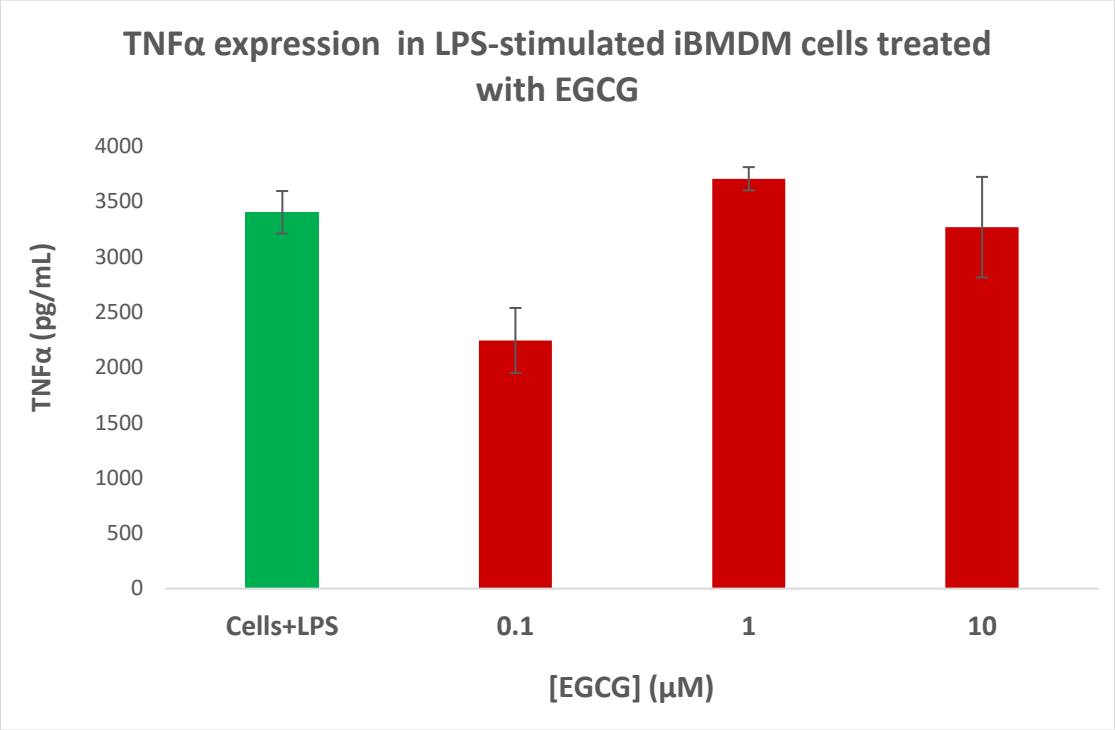

Figure 3.17: Effects of EGCG on TNFα expression in LPS-stimulated iBMDM cells. LPS-stimulated mouse iBMDM cells were treated with varying concentrations (0.1 - 10 µM) of EGCG. ELISA was used to assay the concentration of TNFα in the culture supernatant using a murine TNFα DuoSET ELISA kit. LPS-stimulated untreated cells (shown in green) were used as a control. Error bars represent the standard error of the mean for n = 3 experiments. Statistical significance of data at a 95% confidence interval relative to this control is indicated by an Asterix (*****). The data shows that treating LPS-stimulated iBMDMs with 0.1 – 10 µM EGCG has no significant impact on TNFα expression in comparison to non-treatment.

Our investigation into the effects of EGCG (0.1 – 10 µM) on TLR4 signalling in the context of NF-κB and TNFα expression produced contradictory results. Across this concentration range, the data suggested that EGCG significantly down-regulates TLR4 signalling in relation to NF-κB expression in LPS-stimulated cells. On the contrary, EGCG across the same concentration range showed no effect on TLR4 signalling in LPS-stimulated cells with respect to TNFα expression. However, the data presented in this section represents the early stages of an on-going study into the role of EGCG in TLR4 signalling as part of a larger investigation into the anti-inflammatory role of EGCG.

CHAPTER 4: DISCUSSION

In this section, we discuss the results presented in the previous chapter and their implications in our study to investigate the anti-inflammatory role of EGCG, which is abundantly found in green tea.

4.1. Comparing the phenolic composition of commercial green tea brands, Lipton, Tetley and BST.

Since green tea phenolic compounds are associated with health benefits, we were interested in the phenolic contents of three popular commercial green tea brands available in South Africa, namely Lipton, Tetley and BST. Through UPLC-MS analysis of tea extracts, we successfully identified four of the five major catechins, namely C, EC, ECG, and EGC, in all three green tea brands. Using this approach, tea compounds were identified based on their unique retention characteristics during liquid chromatography and their molecular weights, which can be determined from charge-to-mass ratios after mass spectrometry. Notably, we were unable to draw a clear distinction between peaks corresponding to C and EC from the UPLC-MS chromatograms because they share the same molecular weight of 289 g/mol. Although it would have been possible to resolve this experimentally, we did not pursue this matter further, as neither of these catechins were of specific interest in this study. The catechin of interest in this study was EGCG, the predominant phenolic compound in green tea (Shimamura et al., 2007).

In the present study, electrospray ionisation (ESI) was a critical part of MS that involved three steps; dispersal of a fine spray of highly charged droplets, then desolvation and finally, ejection of ions from the charged droplets (Ho et al., 2003). In the ES+ ion mode, the electrospray nozzle is maintained at positive potential, thus ionisation occurs through protonation. Conversely, charging in the ES- ion mode, where the electrospray nozzle is maintained at negative potential, occurs through deprotonation (Banerjee and Mazumdar, 2012). This phenomenon explains the discrepancy that was consistently observed between the known molecular weights of the compounds and the molecular weights reported from UPLC-MS analysis. For example, the known molecular weight of caffeine is ~194 g/mol, however the observed

molecular weight of caffeine throughout UPLC-MS ES+ analysis was 195 g/mol. Similarly, C and EC are both known to be 290 g/mol, yet they were reported to be 289 g/mol throughout UPLC-MS ES- analysis.

Generally, negatively charged ions including deprotonated organic acids and inorganic anions are analysed in the ES- ion mode. Positively charged ions such as protonated organic bases and inorganic cations are analysed in the ES+ ion mode (Cech and Enke, 2001). For this reason, tea catechins, which are highly populated with -OH functional groups on the surface, were consistently detected in the ES- ion mode in this study. Caffeine, which contains nitrogen atoms, was consistently detected in the ES+ ion mode.

We initially used UPLC-MS to analyse the green tea samples. During ESI, the sample is exposed to high voltage to create charged aerosols consisting of ionised species (Ho et al., 2003). These ionised species are referred to as parent ions and they may become labile during ionisation, which can cause them to fragment (Gabelica and Pauw, 2005). Notably, each compound has a distinctive fragmentation pattern and the extent of fragmentation varies depending on the amount of internal energy exerted on the sample in the source during MS (Gabelica and Pauw, 2005, Venzie et al., 2007). Literature data has shown that EGCG, which has a molecular weight of 458 g/mol, fragments into two primary fragments with molecular weights of 287 g/mol and 170 g/mol. Further fragmentation of these primary fragments forms secondary fragments with molecular weights of 139 g/mol and 153 g/mol respectively (Venzie et al., 2007).

In our analyses, all the catechins in the cocktail samples, including EGCG, were successfully detected in the ES- ion mode. This demonstrated that our instrument was indeed capable and adequately configured to do this. However, the peak corresponding to EGCG with a retention time of ~14.9 min in the ES- analysis did not present the expected molecular weight of 457 g/mol. Instead, a molecular weight of 169 g/mol was observed for this peak, which is consistent with the expected molecular weight that would be observed for one of the primary fragments of EGCG (i.e. the 170 g/mol primary fragment) in the ES- ion mode.

Importantly, it should be noted that our tea extracts from Lipton, Tetley and BST contained a variety of other compounds besides caffeine and catechins. In this study we did not determine the identities and concentrations of all the other compounds in

the extracts. However, it is known that analyte structure, conformation, and concentration in the spray solution are some of the critical factors that affect signal intensity during ESI-MS analysis (Banerjee and Mazumdar, 2012). Furthermore, ions generated from ESI are often multiply charged. In the case of multiply charged ions, some ions display a linear relationship between the concentration of the analyte in solution and the observed ion signal intensity up to a set concentration limit. Thereafter, signal intensity may decrease at very high analyte concentrations (Banerjee and Mazumdar, 2012). As such, this can present challenges when attempting to determine the quantity of highly concentrated compounds in a sample.

Our findings showed that Lipton possessed the highest total phenolic content among the three green tea brands. However, we found no evidence to show that any of these brands contained more EGCG than the others. In the present study, we also determined that the average %TPC of the three green tea brands was ~18%. This value falls in the range of ~15% (Quan et al., 2007) and 20% (Lin et al., 2008) which were previously reported in studies of green tea. However, another study conducted on different commercial green tea brands in the United Kingdom reported much lower %TPC values, which ranged from 8.7 – 10.6% (Khokhar and Magnusdottir, 2002). Ultimately, we intended to use our data from the comparative study to get an indication of the phenolic content of commercial green tea in South Africa as part of our larger study into the anti-inflammatory role of our polyphenol of interest, EGCG.

Our study also determined that the Lipton, Tetley and BST green tea brands each contained ~1% of EGCG, which is much lower than the average of ~3% reported in the study conducted in the United Kingdom (Khokhar and Magnusdottir, 2002). Furthermore, we found that these three green tea brands contained between 0.8 – 0.9% of caffeine, whereas the United Kingdom study reported this value to be between 1.1 – 2.0%. Seemingly, these discrepancies lend themselves as evidence to the fact that the chemical composition, and thus the nutritional value, of green tea is influenced by factors such as preparation methods, which often vary between manufacturers (Chacko et al., 2010, Sinija and Mishra, 2008). Nonetheless, it is worth noting that increasing the number of brands in this study may strengthen the validity of these results.

4.2. The effects of EGCG on the *in vitro* production of NO, a critical mediator of inflammation.

The bioactive properties of green tea phenolic compounds include anti-oxidant and anti-inflammatory activity (Yan et al., 2020). Since EGCG is the predominant phenolic compound in green tea, it is plausible that the bioactivity associated with green tea consumption may be largely due to EGCG. We tested the anti-oxidant activity of EGCG by studying its NO-scavenging potential, which could play a critical role in down-regulating pro-inflammatory responses that are mediated by NO. Although EGCG exhibited the best NO-scavenging activity with minimal cytotoxicity to mouse macrophages at a concentration of 200 μM, this concentration seemed to be rather high for safe human consumption. This view was justified by literature evidence showing that 200 μM EGCG was cytotoxic to human astrocytoma cells (Kim et al., 2007b).

Another interesting observation from the *in vitro* NO-scavenging tests was the development of a brown colour in both LPS-stimulated and unstimulated cells treated with 400 – 800 μM of EGCG. As literature data has shown, browning is a typical marker of oxidation of phenolic compounds (Sioumis et al., 2006). A similar phenomenon occurs when apple tissues that contain phenolic compounds turn brown after exposure to air, which is attributed to the action of an enzyme known as polyphenol oxidase (Deutch, 2018). Moreover, from our data, it seems that treating the cells with higher concentrations of EGCG promotes NO production in unstimulated cells and reduces the viability of LPS-stimulated cells. This observation leads us to believe that EGCG may possess both pro-oxidant and anti-oxidant activity in mouse macrophages, depending on the concentration. By applying this logic, we can postulate that EGCG plays a dual-natured role in inflammation with respect to NO, depending on the concentration. Moreover, there is literature data (Kim et al., 2014) to corroborate our theory of the dual-oxidant nature of EGCG. Despite this, it is worth noting that browning may have affected the results, since in the Griess assay the concentration of NO in each sample is determined based on a colour change. Nevertheless, further testing over an extended EGCG concentration range would have to be conducted to better understand these trends.

4.3. The effects of EGCG on TLR4 signalling

At the time of submitting this dissertation, we were still in the early stages of our study into the role of EGCG in TLR4 signalling. We found that, although the expression of NF-κB was slightly down-regulated in LPS-stimulated cells treated with 10 μM EGCG, TNFα expression remained unabated after treatment with any of the EGCG concentrations tested. Importantly, in the MyD88-dependent pathway, NF-κB is one of the transcription factors that translocate from the cytoplasm to the nucleus to promote the transcription of genes encoding pro-inflammatory cytokines such as TNFα (Lu et al., 2008). Therefore, we expected that an increase in the expression of NF-κB would correlate with an increase in the expression of TNFα, but this was contradicted by the observations made in this study. Thus, the data collected so far failed to provide convincing evidence to show that EGCG, at concentrations from 0.1 – 10 μM, possesses anti-inflammatory activity. However, another study (Singh et al., 2010) concluded that EGCG exhibits anti-inflammatory and anti-oxidant activity by inhibiting the activation of AP-1, NF-κB and MAPKs in different cell types. As such, more extensive experimentation is required to conclusively determine the effects of EGCG on TLR4 signalling and inflammation in general.

4.4. Prospects for the future of this study

Since the mechanism of action of EGCG was not determined in this study, the possibility of EGCG interacting directly with LPS cannot be excluded. Such an interaction could affect the activity of one or both molecules, thereby interfering with the results of this study. To investigate this possibility, future studies can include a *Limulus* amoebocyte lysate (LAL) assay using a quantitative chromogenic LAL kit. This experiment can be performed similarly to the one which was performed in a previous study (Malan et al., 2016). LAL is an aqueous extract of blood cells called amoebocytes that are found in the haemolymph of some *Limulus* species such as *L. polyphemus*. LAL contains granules of a substance that interacts with LPS to form a gel-like consistency (Webster, 1980). Using the quantitative chromogenic LAL assay, we can study the affinity of LPS for a competing substrate such as EGCG in the presence of LAL.

The NO production tests performed in the present study were based on a mouse macrophage cell line, namely RAW 264.7. However, since the greater goal would be to confer the anti-inflammatory properties of EGCG in humans, these studies could also be extended to human macrophage cell lines such as the U937 cell line. However, the mouse-derived data could still be used as a guide in animal trials.

Additionally, more data is required before the role of EGCG in TLR4 signalling can be conclusively defined in the context of the present study. With more time, the experiments we performed can be repeated to improve the statistical significance of the results and redesigned to improve robustness. Additionally, untreated controls and cytotoxicity studies of EGCG on HEK 293 cells and iBMDMs should be included in the TLR4 signalling assays, similarly to those which were performed on the RAW 264.7 cells in the NO production tests. Lastly, more comprehensive experiments are required, incorporating primary wild-type BMDMs and selected PRR knockouts with EGCG-treated and untreated controls.

CHAPTER 5: CONCLUSION

Based on the findings of this study, we conclude the following with respect to our hypotheses:

$H1_0$: There is no statistically significant difference between the EGCG content of green tea brands at the 95% level of confidence.
We accept this hypothesis based on our findings, which showed that there was no statistically significant difference between the EGCG contents of the three green tea brands, namely Lipton, Tetley and BST at the 95% level of confidence.

$H2_0$: EGCG does not significantly affect NO production in LPS-stimulated innate immune cells at the 95% level of confidence.
We reject this hypothesis based on our data, which showed that EGCG, at concentrations of 200 μM and 400 μM, significantly reduced NO production in LPS-stimulated RAW 264.7 macrophages at the 95% level of confidence.

$H3_0$: EGCG does not significantly affect TLR4 cell signalling at the 95% level of confidence.
We can neither accept nor reject this hypothesis based on our data from the NF-κB and TNFα expression tests. Since these tests produced contradictory results, a firm conclusion could not be reached regarding the effects of EGCG on TLR4 signalling. Hence, further testing is required.

REFERENCES

Abdulkhaleq, L. A., Assi, M. A., Abdullah, R., Zamri-Saad, M., Taufiq-Yap, Y. H. & Hezmee, M. N. M. 2018. The crucial roles of inflammatory mediators in inflammation: A review. *Veterinary world,* 11**,** 627-635.

Akira, S. & Takeda, K. 2004. Toll-like receptor signalling. *Nature Reviews Immunology,* 4**,** 499-511.

Akira, S., Uematsu, S. & Takeuchi, O. 2006. Pathogen Recognition and Innate Immunity. *Cell,* 124**,** 783-801.

Anderson, K. V., Bokla, L. & Nüsslein-Volhard, C. 1985. Establishment of dorsal-ventral polarity in the Drosophila embryo: the induction of polarity by the Toll gene product. *Cell,* 42**,** 791-798.

Antman, E. M., Bennett, J. S., Daugherty, A., Furberg, C., Roberts, H. & Taubert, K. A. 2007. Use of nonsteroidal antiinflammatory drugs: an update for clinicians: a scientific statement from the American Heart Association. *Circulation,* 115**,** 1634-1642.

Astill, C., Birch, M. R., Dacombe, C., Humphrey, P. G. & Martin, P. T. 2001. Factors affecting the caffeine and polyphenol contents of black and green tea infusions. *Journal of agricultural and food chemistry,* 49**,** 5340-5347.

Banerjee, S. & Mazumdar, S. 2012. Electrospray ionization mass spectrometry: a technique to access the information beyond the molecular weight of the analyte. *International journal of analytical chemistry,* 2012.

Bao, S., Cao, Y., Zhou, H., Sun, X., Shan, Z. & Teng, W. 2015. Epigallocatechin Gallate (EGCG) Suppresses Lipopolysaccharide-Induced Toll-like Receptor 4 (TLR4) Activity via 67 kDa Laminin Receptor (67LR) in 3T3-L1 Adipocytes. *Journal of Agricultural and Food Chemistry,* 63**,** 2811-2819.

Bella, J., Hindle, K. L., Mcewan, P. A. & Lovell, S. C. 2008. The leucine-rich repeat structure. *Cellular and Molecular Life Sciences,* 65**,** 2307-2333.

Bernas, T. & Dobrucki, J. W. 2000. The Role of Plasma Membrane in Bioreduction of Two Tetrazolium Salts, MTT, and CTC. *Archives of Biochemistry and Biophysics,* 380**,** 108-116.

Beutler, B. & Rietschel, E. T. 2003. Innate immune sensing and its roots: the story of endotoxin. *Nature Reviews Immunology,* 3**,** 169-176.

Bonnert, T. P., Garka, K. E., Parnet, P., Sonoda, G., Testa, J. R. & Sims, J. E. 1997. The cloning and characterization of human MyD88: a member of an IL-1 receptor related family 1The nucleotide sequences reported in this paper have been submitted to the Genbank/EMBL Data Bank with accession numbers U84408 and U84409.1. *FEBS Letters,* 402**,** 81-84.

Botos, I., Segal, D. M. & Davies, D. R. 2011. The structural biology of Toll-like receptors. *Structure (London, England : 1993),* 19**,** 447-459.

Cech, N. B. & Enke, C. G. 2001. Practical implications of some recent studies in electrospray ionization fundamentals. *Mass spectrometry reviews,* 20**,** 362-387.

Chacko, S. M., Thambi, P. T., Kuttan, R. & Nishigaki, I. 2010. Beneficial effects of green tea: a literature review. *Chinese medicine,* 5**,** 13-13.

Chen, L., Deng, H., Cui, H., Fang, J., Zuo, Z., Deng, J., Li, Y., Wang, X. & Zhao, L. 2017. Inflammatory responses and inflammation-associated diseases in organs. *Oncotarget,* 9**,** 7204-7218.

Chu, C., Deng, J., Man, Y. & Qu, Y. 2017. Green Tea Extracts Epigallocatechin-3-gallate for Different Treatments. *BioMed Research International,* 2017**,** 9.

Clancy, R. M., Amin, A. R. & Abramson, S. B. 1998. The role of nitric oxide in inflammation and immunity. *Arthritis & Rheumatism,* 41**,** 1141-1151.

Deutch, C. E. 2018. Browning in apples: Exploring the biochemical basis of an easily-observable phenotype. *Biochemistry and Molecular Biology Education,* 46**,** 76-82.

Duan, L., Rao, X. & Sigdel, K. R. 2019. Regulation of Inflammation in Autoimmune Disease. *Journal of Immunology Research,* 2019**,** 2.

El-Zayat, S. R., Sibaii, H. & Mannaa, F. A. 2019. Toll-like receptors activation, signaling, and targeting: an overview. *Bulletin of the National Research Centre,* 43**,** 187.

Ferrazzano, G. F., Amato, I., Ingenito, A., Zarrelli, A., Pinto, G. & Pollio, A. 2011. Plant polyphenols and their anti-cariogenic properties: a review. *Molecules (Basel, Switzerland),* 16**,** 1486-1507.

Flajnik, M. F. & Kasahara, M. 2010. Origin and evolution of the adaptive immune system: genetic events and selective pressures. *Nature reviews. Genetics,* 11**,** 47-59.

Fuchs, K., Cardona Gloria, Y., Wolz, O. O., Herster, F., Sharma, L., Dillen, C. A., Täumer, C., Dickhöfer, S., Bittner, Z., Dang, T. M., Singh, A., Haischer, D., Schlöffel, M. A., Koymans, K. J., Sanmuganantham, T., Krach, M., Roger, T., Le Roy, D., Schilling, N. A., Frauhammer, F., Miller, L. S., Nürnberger, T., Leibundgut-Landmann, S., Gust, A. A., Macek, B., Frank, M., Gouttefangeas, C., Dela Cruz, C. S., Hartl, D. & Weber, A. N. R. 2018. The fungal ligand chitin directly binds TLR2 and triggers inflammation dependent on oligomer size. *EMBO reports,* 19**,** e46065.

Fung, K. F., Zhang, Z. Q., Wong, J. W. C. & Wong, M. H. 1999. Fluoride contents in tea and soil from tea plantations and the release of fluoride into tea liquor during infusion. *Environmental Pollution,* 104**,** 197-205.

Funk, C. D. 2001. Prostaglandins and Leukotrienes: Advances in Eicosanoid Biology. *Science,* 294**,** 1871.

Gabelica, V. & Pauw, E. D. 2005. Internal energy and fragmentation of ions produced in electrospray sources. *Mass Spectrometry Reviews,* 24**,** 566-587.

Gay, N. J. & Gangloff, M. 2007. Structure and Function of Toll Receptors and Their Ligands. *Annual Review of Biochemistry,* 76**,** 141-165.

Gay, N. J., Symmons, M. F., Gangloff, M. & Bryant, C. E. 2014. Assembly and localization of Toll-like receptor signalling complexes. *Nature Reviews Immunology,* 14**,** 546.

Graves, D. B. 2012. The emerging role of reactive oxygen and nitrogen species in redox biology and some implications for plasma applications to medicine and biology. *Journal of Physics D: Applied Physics,* 45**,** 263001.

Graziose, R., Lila, M. A. & Raskin, I. 2010. Merging traditional Chinese medicine with modern drug discovery technologies to find novel drugs and functional foods. *Current drug discovery technologies,* 7**,** 2-12.

Guslandi 1998. Nitric oxide and inflammatory bowel diseases. *European Journal of Clinical Investigation,* 28**,** 904-907.

Ho, C. S., Lam, C. W. K., Chan, M. H. M., Cheung, R. C. K., Law, L. K., Lit, L. C. W., Ng, K. F., Suen, M. W. M. & Tai, H. L. 2003. Electrospray ionisation mass spectrometry: principles and clinical applications. *The Clinical biochemist. Reviews,* 24**,** 3-12.

Hong Byun, E., Fujimura, Y., Yamada, K. & Tachibana, H. 2010. TLR4 Signaling Inhibitory Pathway Induced by Green Tea Polyphenol Epigallocatechin-3-

Gallate through 67-kDa Laminin Receptor. *The Journal of Immunology,* 185**,** 33.
Hoving, J. C., Wilson, G. J. & Brown, G. D. 2014. Signalling C-type lectin receptors, microbial recognition and immunity. *Cellular microbiology,* 16**,** 185-194.
Ignarro, L. J. 1989. Biological actions and properties of endothelium-derived nitric oxide formed and released from artery and vein. *Circulation Research,* 65**,** 1-21.
Ignarro, L. J., Fukuto, J. M., Griscavage, J. M., Rogers, N. E. & Byrns, R. E. 1993. Oxidation of nitric oxide in aqueous solution to nitrite but not nitrate: comparison with enzymatically formed nitric oxide from L-arginine. *Proceedings of the National Academy of Sciences of the United States of America,* 90**,** 8103-8107.
Iso 1980. ISO 1573: tea: determination of loss in massa at 103° C. ISO Geneva.
Iso 2005. ISO 14502-1: 2005, Determination of substances characteristic of green and black tea—Part 1: Content of total polyphenols in tea-colorimetric method using Folin-Ciocalteu reagent. *ISO 14502-1 International Standardization.* International Organization for Standardization Switzerland.
Jagetia, G. C. & Baliga, M. S. 2004. The Evaluation of Nitric Oxide Scavenging Activity of Certain Indian Medicinal Plants In Vitro: A Preliminary Study. *Journal of Medicinal Food,* 7**,** 343-348.
Jiang, S., Li, X., Hess, N. J., Guan, Y. & Tapping, R. I. 2016. TLR10 Is a Negative Regulator of Both MyD88-Dependent and -Independent TLR Signaling. *Journal of immunology (Baltimore, Md. : 1950),* 196**,** 3834-3841.
Jin, M. S., Kim, S. E., Heo, J. Y., Lee, M. E., Kim, H. M., Paik, S.-G., Lee, H. & Lee, J.-O. 2007. Crystal Structure of the TLR1-TLR2 Heterodimer Induced by Binding of a Tri-Acylated Lipopeptide. *Cell,* 130**,** 1071-1082.
Kagan, J. C. & Medzhitov, R. 2006. Phosphoinositide-mediated adaptor recruitment controls Toll-like receptor signaling. *Cell,* 125**,** 943-955.
Kajava, A. V. 1998. Structural diversity of leucine-rich repeat proteins11Edited by F. Cohen. *Journal of Molecular Biology,* 277**,** 519-527.
Kajiwara, Y., Schiff, T., Voloudakis, G., Gama Sosa, M. A., Elder, G., Bozdagi, O. & Buxbaum, J. D. 2014. A critical role for human caspase-4 in endotoxin sensitivity. *Journal of immunology (Baltimore, Md. : 1950),* 193**,** 335-343.
Kamata, H. & Hirata, H. 1999. Redox Regulation of Cellular Signalling. *Cellular Signalling,* 11**,** 1-14.
Kawai, T. & Akira, S. 2010. The role of pattern-recognition receptors in innate immunity: update on Toll-like receptors. *Nature Immunology,* 11**,** 373.
Kawasaki, T. & Kawai, T. 2014. Toll-like receptor signaling pathways. *Frontiers in immunology,* 5**,** 461-461.
Kelm, M., Feelisch, M., Deuen, A., Schrader, J. & Strauer, B. E. 1991. The Role of Nitric Oxide in the Control of Coronary Vascular Tone in Relation to Partial Oxygen Pressure, Perfusion Pressure, and Flow. *Journal of Cardiovascular Pharmacology,* 17**,** S95-S99.
Khokhar, S. & Magnusdottir, S. G. M. 2002. Total Phenol, Catechin, and Caffeine Contents of Teas Commonly Consumed in the United Kingdom. *Journal of Agricultural and Food Chemistry,* 50**,** 565-570.
Kim, H.-S., Quon, M. J. & Kim, J.-A. 2014. New insights into the mechanisms of polyphenols beyond antioxidant properties; lessons from the green tea polyphenol, epigallocatechin 3-gallate. *Redox biology,* 2**,** 187-195.
Kim, H. M., Oh, S. C., Lim, K. J., Kasamatsu, J., Heo, J. Y., Park, B. S., Lee, H., Yoo, O. J., Kasahara, M. & Lee, J.-O. 2007a. Structural diversity of the hagfish

variable lymphocyte receptors. *Journal of Biological Chemistry,* 282**,** 6726-6732.
Kim, S.-J., Jeong, H.-J., Lee, K.-M., Myung, N.-Y., An, N.-H., Mo Yang, W., Kyu Park, S., Lee, H.-J., Hong, S.-H., Kim, H.-M. & Um, J.-Y. 2007b. Epigallocatechin-3-gallate suppresses NF-κB activation and phosphorylation of p38 MAPK and JNK in human astrocytoma U373MG cells. *The Journal of Nutritional Biochemistry,* 18**,** 587-596.
Kindt, T. J., Goldsby, R. A., Osborne, B. A. & Kuby, J. 2007. *Kuby Immunology*, W. H. Freeman.
Kolb-Bachofen, V., Kuhn, A. & Suschek, C. V. 2006. The role of nitric oxide. *Rheumatology,* 45**,** iii17-iii19.
Kolb, H. & Kolb-Bachofen, V. 1998. Nitric oxide in autoimmune disease: cytotoxic or regulatory mediator? *Immunology Today,* 19**,** 556-561.
Kumar, H., Kawai, T. & Akira, S. 2011. Pathogen Recognition by the Innate Immune System. *International Reviews of Immunology,* 30**,** 16-34.
Lambert, J. D. & Elias, R. J. 2010. The antioxidant and pro-oxidant activities of green tea polyphenols: a role in cancer prevention. *Archives of biochemistry and biophysics,* 501**,** 65-72.
Latz, E., Verma, A., Visintin, A., Gong, M., Sirois, C. M., Klein, D. C. G., Monks, B. G., Mcknight, C. J., Lamphier, M. S., Duprex, W. P., Espevik, T. & Golenbock, D. T. 2007. Ligand-induced conformational changes allosterically activate Toll-like receptor 9. *Nature Immunology,* 8**,** 772.
Lemaitre, B., Nicolas, E., Michaut, L., Reichhart, J.-M. & Hoffmann, J. A. 1996. The Dorsoventral Regulatory Gene Cassette spätzle/Toll/cactus Controls the Potent Antifungal Response in Drosophila Adults. *Cell,* 86**,** 973-983.
Lenz, W., Pfeiffer, R. A., Kosenow, W. & Hayman, D. J. 1962. THALIDOMIDE AND CONGENITAL ABNORMALITIES. *The Lancet,* 279**,** 45-46.
Li, P., Zheng, Y. & Chen, X. 2017. Drugs for Autoimmune Inflammatory Diseases: From Small Molecule Compounds to Anti-TNF Biologics. *Frontiers in pharmacology,* 8**,** 460-460.
Lin, L.-Z., Chen, P. & Harnly, J. M. 2008. New Phenolic Components and Chromatographic Profiles of Green and Fermented Teas. *Journal of Agricultural and Food Chemistry,* 56**,** 8130-8140.
Lu, Y.-C., Yeh, W.-C. & Ohashi, P. S. 2008. LPS/TLR4 signal transduction pathway. *Cytokine,* 42**,** 145-151.
Mahita, J. & Sowdhamini, R. 2017. Integrative modelling of TIR domain-containing adaptor molecule inducing interferon-β (TRIF) provides insights into its autoinhibited state. *Biology direct,* 12**,** 9-9.
Malan, M., Serem, J. C., Bester, M. J., Neitz, A. W. & Gaspar, A. R. 2016. Anti-inflammatory and anti-endotoxin properties of peptides derived from the carboxy-terminal region of a defensin from the tick Ornithodoros savignyi. *Journal of Peptide Science,* 22**,** 43-51.
Mann, J. R., Backlund, M. G. & Dubois, R. N. 2005. Mechanisms of Disease: inflammatory mediators and cancer prevention. *Nature Clinical Practice Oncology,* 2**,** 202-210.
Mao, X., Gu, C., Chen, D., Yu, B. & He, J. 2017. Oxidative stress-induced diseases and tea polyphenols. *Oncotarget,* 8**,** 81649-81661.
Matsushima, N., Miyashita, H., Mikami, T. & Kuroki, Y. 2010. A nested leucine rich repeat (LRR) domain: the precursor of LRRs is a ten or eleven residue motif. *BMC microbiology,* 10**,** 235-235.

Mcbride, W. G. 1961. THALIDOMIDE AND CONGENITAL ABNORMALITIES. *The Lancet,* 278**,** 1358.

Medzhitov, R. 2001. Toll-like receptors and innate immunity. *Nature Reviews Immunology,* 1**,** 135-145.

Medzhitov, R. 2010. Inflammation 2010: New Adventures of an Old Flame. *Cell,* 140**,** 771-776.

Medzhitov, R., Preston-Hurlburt, P., Kopp, E., Stadlen, A., Chen, C., Ghosh, S. & Janeway, C. A., Jr. 1998. MyD88 Is an Adaptor Protein in the hToll/IL-1 Receptor Family Signaling Pathways. *Molecular Cell,* 2**,** 253-258.

Montero Vega, M. T. & De Andrés Martín, A. 2008. Toll-like receptors: a family of innate sensors of danger that alert and drive immunity. *Allergologia et Immunopathologia,* 36**,** 347-357.

Nagai, K., Jiang, M. H., Hada, J., Nagata, T., Yajima, Y., Yamamoto, S. & Nishizaki, T. 2002. (−)-Epigallocatechin gallate protects against NO stress-induced neuronal damage after ischemia by acting as an anti-oxidant. *Brain Research,* 956**,** 319-322.

Netea, M. G., Gow, N. a. R., Munro, C. A., Bates, S., Collins, C., Ferwerda, G., Hobson, R. P., Bertram, G., Hughes, H. B., Jansen, T., Jacobs, L., Buurman, E. T., Gijzen, K., Williams, D. L., Torensma, R., Mckinnon, A., Maccallum, D. M., Odds, F. C., Van Der Meer, J. W. M., Brown, A. J. P. & Kullberg, B. J. 2006. Immune sensing of Candida albicans requires cooperative recognition of mannans and glucans by lectin and Toll-like receptors. *The Journal of clinical investigation,* 116**,** 1642-1650.

O'neill, L. a. J. 2004. TLRs: Professor Mechnikov, sit on your hat. *Trends in Immunology,* 25**,** 687-693.

O'neill, L. a. J. & Bowie, A. G. 2007. The family of five: TIR-domain-containing adaptors in Toll-like receptor signalling. *Nature Reviews Immunology,* 7**,** 353.

Ohnishi, H., Tochio, H., Kato, Z., Orii, K. E., Li, A., Kimura, T., Hiroaki, H., Kondo, N. & Shirakawa, M. 2009. Structural basis for the multiple interactions of the MyD88 TIR domain in TLR4 signaling. *Proceedings of the National Academy of Sciences of the United States of America,* 106**,** 10260-10265.

Ohto, U., Fukase, K., Miyake, K. & Shimizu, T. 2012. Structural basis of species-specific endotoxin sensing by innate immune receptor TLR4/MD-2. *Proceedings of the National Academy of Sciences,* 109**,** 7421.

Ohto, U. & Shimizu, T. 2016. Structural aspects of nucleic acid-sensing Toll-like receptors. *Biophysical reviews,* 8**,** 33-43.

Oosting, M., Cheng, S.-C., Bolscher, J. M., Vestering-Stenger, R., Plantinga, T. S., Verschueren, I. C., Arts, P., Garritsen, A., Van Eenennaam, H., Sturm, P., Kullberg, B.-J., Hoischen, A., Adema, G. J., Van Der Meer, J. W. M., Netea, M. G. & Joosten, L. a. B. 2014. Human TLR10 is an anti-inflammatory pattern-recognition receptor. *Proceedings of the National Academy of Sciences of the United States of America,* 111**,** E4478-E4484.

Pålsson-Mcdermott, E. M. & O'neill, L. a. J. 2007. Building an immune system from nine domains. *Biochemical Society Transactions,* 35**,** 1437.

Pancer, Z. & Cooper, M. D. 2006. The evolution of adaptive immunity. *Annu. Rev. Immunol.,* 24**,** 497-518.

Paquay, J. B. G., Haenen, G. R. M. M., Stender, G., Wiseman, S. A., Tijburg, L. B. M. & Bast, A. 2000. Protection against Nitric Oxide Toxicity by Tea. *Journal of Agricultural and Food Chemistry,* 48**,** 5768-5772.

Quan, P. T., Hang, T., Ha, N. H. & Glang, B. 2007. Total polyphenols, total catechin content and DPPH free radical scavenger activity of several types of Vietnam commercial green tea. *Science & Technology Development,* 10.

Radi, R. 2018. Oxygen radicals, nitric oxide, and peroxynitrite: Redox pathways in molecular medicine. *Proceedings of the National Academy of Sciences,* 115**,** 5839.

Raetz, C. R. H. & Whitfield, C. 2002. Lipopolysaccharide endotoxins. *Annual review of biochemistry,* 71**,** 635-700.

Raskin, I., Ribnicky, D. M., Komarnytsky, S., Ilic, N., Poulev, A., Borisjuk, N., Brinker, A., Moreno, D. A., Ripoll, C., Yakoby, N., O'neal, J. M., Cornwell, T., Pastor, I. & Fridlender, B. 2002. Plants and human health in the twenty-first century. *Trends in Biotechnology,* 20**,** 522-531.

Reuven, E. M., Fink, A. & Shai, Y. 2014. Regulation of innate immune responses by transmembrane interactions: Lessons from the TLR family. *Biochimica et Biophysica Acta (BBA) - Biomembranes,* 1838**,** 1586-1593.

Ricciotti, E. & Fitzgerald Garret, A. 2011. Prostaglandins and Inflammation. *Arteriosclerosis, Thrombosis, and Vascular Biology,* 31**,** 986-1000.

Rottem, M. & Shoenfeld, Y. 2003. Asthma as a Paradigm for Autoimmune Disease. *International Archives of Allergy and Immunology,* 132**,** 210-214.

Rowe, D. C., Mcgettrick, A. F., Latz, E., Monks, B. G., Gay, N. J., Yamamoto, M., Akira, S., O'neill, L. A., Fitzgerald, K. A. & Golenbock, D. T. 2006. The myristoylation of TRIF-related adaptor molecule is essential for Toll-like receptor 4 signal transduction. *Proceedings of the National Academy of Sciences of the United States of America,* 103**,** 6299-6304.

Roychoudhury, A. & Bhowmik, R. 2020. Health Benefits of Plant-Derived Bioactive Secondary Metabolites as Dietary Constituents. *SF J Clin Pharm Res.,* 2**,** 1002.

Sampaio, N. G., Kocan, M., Schofield, L., Pfleger, K. D. G. & Eriksson, E. M. 2018. Investigation of interactions between TLR2, MyD88 and TIRAP by bioluminescence resonance energy transfer is hampered by artefacts of protein overexpression. *PloS one,* 13**,** e0202408-e0202408.

Sano, M., Tabata, M., Suzuki, M., Degawa, M., Miyase, T. & Maeda-Yamamoto, M. 2001. Simultaneous determination of twelve tea catechins by high-performance liquid chromatography with electrochemical detection. *Analyst,* 126**,** 816-820.

Sharma, J. N., Al-Omran, A. & Parvathy, S. S. 2007. Role of nitric oxide in inflammatory diseases. *Inflammopharmacology,* 15**,** 252-259.

Shimamura, T., Zhao, W.-H. & Hu, Z.-Q. 2007. Mechanism of action and potential for use of tea catechin as an antiinfective agent. *Anti-Infective Agents in Medicinal Chemistry (Formerly Current Medicinal Chemistry-Anti-Infective Agents),* 6**,** 57-62.

Singh, R., Akhtar, N. & Haqqi, T. M. 2010. Green tea polyphenol epigallocatechi3-gallate: Inflammation and arthritis. *Life Sciences,* 86**,** 907-918.

Sinija, V. R. & Mishra, H. N. 2008. Green tea: Health benefits. *Journal of Nutritional & Environmental Medicine,* 17**,** 232-242.

Sioumis, N., Kallithraka, S., Makris, D. P. & Kefalas, P. 2006. Kinetics of browning onset in white wines: influence of principal redox-active polyphenols and impact on the reducing capacity. *Food chemistry,* 94**,** 98-104.

Swidergall, M. 2019. Candida albicans at Host Barrier Sites: Pattern Recognition Receptors and Beyond. *Pathogens,* 8.

Takeda, K. & Akira, S. 2004. TLR signaling pathways. *Seminars in Immunology,* 16**,** 3-9.

Tang, D., Kang, R., Coyne, C. B., Zeh, H. J. & Lotze, M. T. 2012. PAMPs and DAMPs: signal 0s that spur autophagy and immunity. *Immunological reviews,* 249**,** 158-175.

Tobias, P. S., Soldau, K. & Ulevitch, R. J. 1986. Isolation of a lipopolysaccharide-binding acute phase reactant from rabbit serum. *The Journal of experimental medicine,* 164**,** 777-793.

Turvey, S. E. & Broide, D. H. 2010. Innate immunity. *The Journal of allergy and clinical immunology,* 125**,** S24-S32.

Van Straaten, E. A., Koster-Kamphuis, L., Bovee-Oudenhoven, I. M., Van Der Meer, R. & Forget, P. P. 1999. Increased urinary nitric oxide oxidation products in children with active coeliac disease. *Acta Paediatrica,* 88**,** 528-531.

Vargesson, N. 2015. Thalidomide-induced teratogenesis: history and mechanisms. *Birth defects research. Part C, Embryo today : reviews,* 105**,** 140-156.

Venzie, J. L., Castro, J., Balarama Krishna, M. V., Nelson, D. M. & Marcus, R. K. 2007. Electron-impact and glow-discharge ionization LC–MS analysis of green tea tincture. *Analytical and Bioanalytical Chemistry,* 387**,** 321-333.

Wang, J., Fan, S. M. & Zhang, J. 2019. Epigallocatechin-3-gallate ameliorates lipopolysaccharide-induced acute lung injury by suppression of TLR4/NF-κB signaling activation. *Brazilian Journal of Medical and Biological Research,* 52.

Warrington, R., Watson, W., Kim, H. L. & Antonetti, F. R. 2011. An introduction to immunology and immunopathology. *Allergy, asthma, and clinical immunology : official journal of the Canadian Society of Allergy and Clinical Immunology,* 7 Suppl 1**,** S1-S1.

Webster, C. J. 1980. Principles of a quantitative assay for bacterial endotoxins in blood that uses Limulus lysate and a chromogenic substrate. *Journal of clinical microbiology,* 12**,** 644-650.

Wesselingh, R., Butzkueven, H., Buzzard, K., Tarlinton, D., O'brien, T. J. & Monif, M. 2019. Innate Immunity in the Central Nervous System: A Missing Piece of the Autoimmune Encephalitis Puzzle? *Frontiers in immunology,* 10**,** 2066-2066.

Williamson, G. 2017. The role of polyphenols in modern nutrition. *Nutrition bulletin,* 42**,** 226-235.

Wong, R. S. Y. 2019. Disease-Modifying Effects of Long-Term and Continuous Use of Nonsteroidal Anti-Inflammatory Drugs (NSAIDs) in Spondyloarthritis. *Advances in Pharmacological Sciences,* 2019**,** 6.

Yan, Z., Zhong, Y., Duan, Y., Chen, Q. & Li, F. 2020. Antioxidant mechanism of tea polyphenols and its impact on health benefits. *Animal nutrition (Zhongguo xu mu shou yi xue hui),* 6**,** 115-123.

Yang, C. S., Chen, G. & Wu, Q. 2014. Recent scientific studies of a traditional chinese medicine, tea, on prevention of chronic diseases. *Journal of traditional and complementary medicine,* 4**,** 17-23.

Zhang, L., Ho, C.-T., Zhou, J., Santos, J. S., Armstrong, L. & Granato, D. 2019. Chemistry and Biological Activities of Processed Camellia sinensis Teas: A Comprehensive Review. *Comprehensive Reviews in Food Science and Food Safety,* 18**,** 1474-1495.

Zhong, Y., Chiou, Y.-S., Pan, M.-H. & Shahidi, F. 2012. Anti-inflammatory activity of lipophilic epigallocatechin gallate (EGCG) derivatives in LPS-stimulated murine macrophages. *Food Chemistry,* 134**,** 742-748.